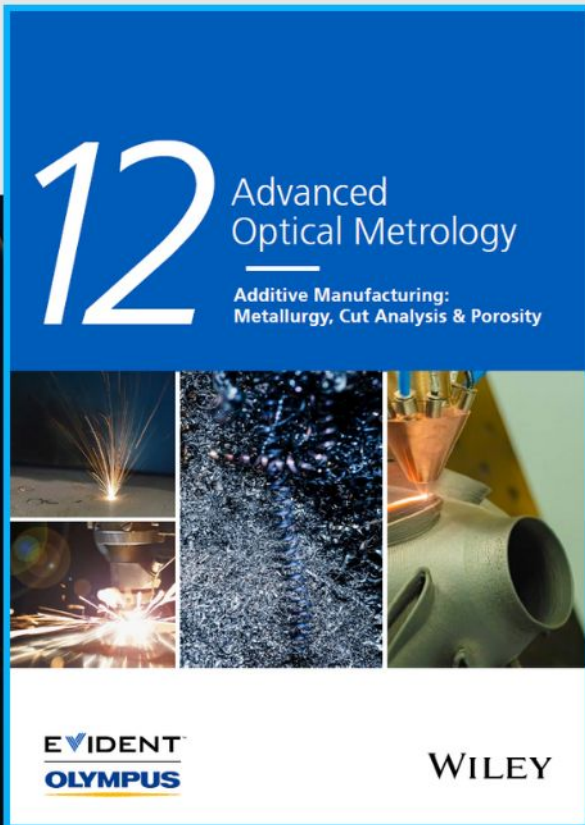




Additive Manufacturing: Metallurgy, Cut Analysis & Porosity



The latest eBook from
Advanced Optical Metrology.
Download for free.

In industry, sector after sector is moving away from conventional production methods to additive manufacturing, a technology that has been recommended for substantial research investment.

Download the latest eBook to read about the applications, trends, opportunities, and challenges around this process, and how it has been adapted to different industrial sectors.

EVIDENT™
OLYMPUS

WILEY

Microfluidic Nanoparticles for Drug Delivery

Yun Liu, Guangze Yang, Yue Hui, Supun Ranaweera, and Chun-Xia Zhao*

Nanoparticles (NPs) have attracted tremendous interest in drug delivery in the past decades. Microfluidics offers a promising strategy for making NPs for drug delivery due to its capability in precisely controlling NP properties. The recent success of mRNA vaccines using microfluidics represents a big milestone for microfluidic NPs for pharmaceutical applications, and its rapid scaling up demonstrates the feasibility of using microfluidics for industrial-scale manufacturing. This article provides a critical review of recent progress in microfluidic NPs for drug delivery. First, the synthesis of organic NPs using microfluidics focusing on typical microfluidic methods and their applications in making popular and clinically relevant NPs, such as liposomes, lipid NPs, and polymer NPs, as well as their synthesis mechanisms are summarized. Then, the microfluidic synthesis of several representative inorganic NPs (e.g., silica, metal, metal oxide, and quantum dots), and hybrid NPs is discussed. Lastly, the applications of microfluidic NPs for various drug delivery applications are presented.

1. Introduction

NPs have attracted significant interest in the past decades. Various NPs have been developed to address different drug delivery challenges, including poor drug solubility, poor bioavailability, intrinsic drug instability, serious adverse effects, and lack of targeted delivery.^[1,2] Traditionally, NPs are often fabricated using bulk methods. In comparison, microfluidics offers a new strategy for making NPs with controlled properties for various applications due to its unique capabilities such as in handling

samples of picoliter (or less) scale, fast mixing, rapid mass transfer, precise control over reaction conditions and the addition of reagent, cost-effectiveness, and short-production time.^[3] More importantly, NPs can be reproducibly synthesized in microfluidic devices with well controlled and tunable properties, such as size, shape, surface properties, structures, etc.^[4,5] The capability of microfluidic methods to provide homogeneous reaction environments along with fast mixing of reagents, to continuously adjust the reaction conditions, and to control the mixing sequence of reagents during the reaction process, makes it ideal for NP synthesis for drug delivery applications.^[6,7] Furthermore, it can be quickly scaled up via parallelization or numbering-up, making it viable for NPs manufacturing for practical applications.

These advantages have been well validated by the recent success of Pfizer's mRNA vaccine manufacturing.


mRNA vaccines produced by Pfizer are lipid NPs with mRNA encapsulated inside. The lipid NPs act not only as delivery vehicles for mRNA molecules but also as a nanocarrier protecting mRNA from degradation. To produce these mRNA-loaded lipid NPs, an impingement jet mixer (IJM) of a US quarter coin size, also known as the tea stirrer, was used. Basically, the lipid solvent solution is mixed with the mRNA solution by simply pumping lipids from one channel and mRNA from the other, forcing them to mix together with 400 pounds of pressure. To meet the large-scale production requirement, instead of going bigger and making a large-scale mixer to allow bigger volume to pass through, Pfizer replicated the quarter-sized mixers and achieved a parallelization (or numbering-up) of 100 static mixers, allowing the continuous synthesis and the increase of their vaccine productivity at the Kalamazoo (US) site to 100 million doses per month.^[8] To automate the process, a computer system was established to run the whole system that ensures the precise control over the flow rate and pressure. Although the IJM is small in size, it is able to be scaled up very rapidly based on the original design, which is the key for pharmaceutical manufacturing especially for pandemics like COVID-19.

The success of the Pfizer mRNA vaccine for COVID-19 represents a significant milestone not only for mRNA vaccines, but also for microfluidics and nanomedicines, and it has demonstrated the feasibility and versatility of microfluidics for making nanomaterials for drug delivery. Therefore, it is timely and important to review this field. In this review, we are not aiming to provide a comprehensive review of all the different microfluidic nanomaterials for drug delivery, we will focus on three types of NPs including typical organic NPs, inorganic

Y. Liu, G. Yang, S. Ranaweera, C.-X. Zhao
Australian Institute for Bioengineering and Nanotechnology
The University of Queensland
Brisbane, QLD 4072, Australia
E-mail: z.chunxia@uq.edu.au

Y. Hui
Institute of Advanced Technology
Westlake University
Hangzhou, Zhejiang 310024, China

C.-X. Zhao
School of Chemical Engineering and Advanced Materials
Faculty of Engineering
Computer and Mathematical Sciences
The University of Adelaide
Adelaide, SA 5005, Australia

 The ORCID identification number(s) for the author(s) of this article can be found under <https://doi.org/10.1002/smll.202106580>.

© 2022 The Authors. Small published by Wiley-VCH GmbH. This is an open access article under the terms of the Creative Commons Attribution License, which permits use, distribution and reproduction in any medium, provided the original work is properly cited.

DOI: 10.1002/smll.202106580

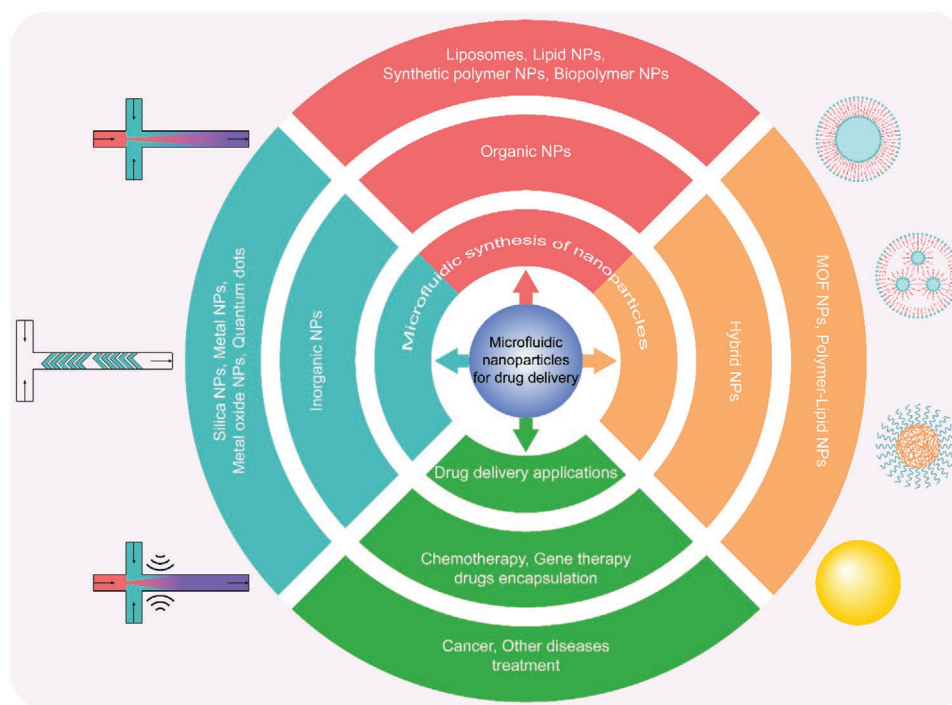


Figure 1. Overview of the structure of this review. This review summarizes the recent progress in microfluidic NPs for drug delivery (inner core), comprising of the microfluidic synthesis of various NPs (inner ring) including organic NPs, inorganic NPs, and hybrid NPs (middle ring; red, blue, and orange colors respectively) and their drug delivery applications (inner ring; green color). The applications of typical microfluidic methods such as the hydrodynamic flow-focusing, staggered herringbone micromixing, and acoustic micromixing (from top to bottom of the chip schematics) in making popular and clinically relevant NPs such as liposomes, lipid NPs, synthetic polymer NPs, silica NPs, etc. (outer ring; from top to bottom of the NP schematics) are explored in this review. Moreover, the drug encapsulation strategies (middle ring; green color), and cancer and other diseases treatment applications (outer ring; green color) of these NPs are reviewed.

NPs, and hybrid NPs, including their microfluidic synthesis methods, and their drug delivery applications (Figure 1). With the introduction of past research and the recent success of microfluidic NPs, more interests are expected to be drawn for this field not only in laboratory research but also in industrial-scale production.

2. Microfluidic Synthesis of Organic NPs

Microfluidics has been extensively used for making organic NPs including liposomes, lipids, or polymers. The principle of synthesizing such organic NPs is mainly based on a nanoprecipitation process. Basically, an organic precursor (e.g., lipid, polymers) dissolved in a solvent solution mixes with an antisolvent solution (water or buffer solution), then NPs are formed via a nanoprecipitation process. Traditionally, this nanoprecipitation process occurs in bulk solutions (in beakers or vials) via mixing, so mixing efficiency or mixing time plays a critical role in controlling NP properties. In this sense, microfluidics provides an ideal approach for making uniform organic NPs with tunable and controllable properties. This section starts with a brief introduction of several typical microfluidic methods for making organic NPs, then reviews different types of organic NPs synthesized using microfluidics. Lastly NP synthesis mechanisms are discussed providing valuable insights.

2.1. Different Microfluidic Methods

Traditional methods of synthesizing NPs, such as bulk extrusion, bulk mixing, suffer from limitations, such as less control over particle size and polydispersity (PDI), poor reproducibility from batch to batch, and difficulties in scaling-up production. Alternatively, microfluidics has been explored for producing nanomedicines of well-controlled properties and reproducibility.^[9] Consequently, it has grown in popularity over the last decade.

Microfluidic platforms for organic NP synthesis are often referred to as micromixers. Various mixing technologies including both passive mixing and active mixing have been comprehensively reviewed and discussed in several excellent review articles.^[10–14] Also, traditional microfluidic mixing designs focus on liquid–liquid mixing, but mixing-induced nanoprecipitation or self-assembly of NPs involves the formation of solid NPs, that is, liquid–liquid–solid, which could potentially lead to channel blockage. Therefore, microfluidic devices for making NPs should be carefully designed to ensure excellent mixing but minimum NP disposition. In this section, we mainly focused on the mixing technologies commonly used for the microfluidic synthesis of organic NPs for drug delivery applications. Two widely used microfluidic designs include hydrodynamic flow focusing^[15–20] and staggered herringbone micromixer designs (Figure 2).^[21–27] External fields could be included to enhance mixing (e.g., acoustofluidics).^[28–32]

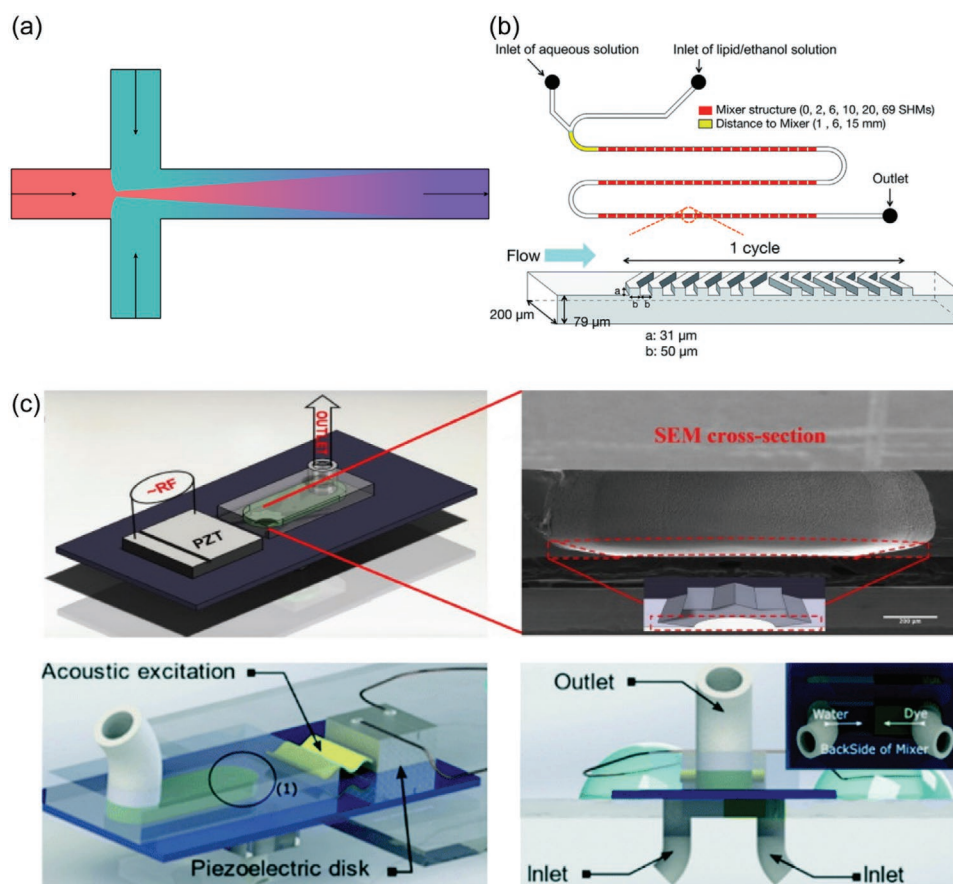


Figure 2. Different microfluidic methods. a) Schematic of the HFF method. b) Schematic of SHM. Reproduced with permission.^[33] Copyright 2015, The Royal Society of Chemistry. c) Acoustic micromixing devices using star-shaped oscillating plates: the assembled star-shaped microfluidic mixer (top) and the ultrafast star-shaped acoustic micromixer (bottom). (Top) Reproduced with permission.^[32] Copyright 2020, Elsevier Inc. (Bottom) Reproduced with permission.^[31] Copyright 2020, The Royal Society of Chemistry.

2.1.1. Hydrodynamic Flow Focusing (HFF)

HFF utilizes the laminar regime typically found within microfluidic platforms. In HFF, a narrow stream of fluid, typically lipid, polymer, or other NP precursor dissolved in a solvent flows in parallel with an antisolvent (e.g., water or buffer solution) from the two side channels (Figure 2a).^[17] Due to the laminar flow regime present within the device, rapid mixing occurs through diffusion. Mixing time correlates with several parameters following Equation (1):^[34]

$$t_{\text{mix}} \sim \frac{w_f^2}{4D} \approx \frac{w^2}{9D} \left(\frac{1}{(1+1/R)^2} \right) \quad (1)$$

where D is the diffusivity of the solvent, W_f is the width of the focused stream, W is the channel width, and R is the flow rate ratio of the middle stream to the flow rate of the sheath stream.

Based on Equation 1, mixing time correlates positively with the width of the central stream, but negatively with the diffusivity of the solvent. For example, for acetonitrile which has a diffusivity D of $10^{-9} \text{ m}^2 \text{ s}^{-1}$, with a central stream width W_f of $10 \text{ }\mu\text{m}$, the mixing time would be 2.5 ms , if the W_f decreases to $1 \text{ }\mu\text{m}$, the mixing time decreases to $25 \text{ }\mu\text{s}$ which is 100 times

reduction. As the W_f is dependent on both the width of the channel and the flow rate ratio, therefore, a smaller channel with bigger flow rates benefits shorter mixing time, thus smaller particle size and better uniformity. Therefore, the HFF allows for a greater degree of control over the NP synthesis compared to traditional methods.^[16] Also, by designing HFF with different channel widths and tuning the flow rate ratio, it can be used to produce highly tunable NPs with controlled size and size distribution.^[6] Furthermore, NPs with tunable surface properties (PEGylation, single targeting ligand, or dual ligands) can be fabricated using functionalized lipid or polymer precursors.^[35,36]

Most microfluidic HFF devices are made of polydimethylsiloxane (PDMS), as when cured it is transparent and can be patterned with high aspect ratio structures. However, HFF devices produced with PDMS suffer from poor solvent compatibility, channel fouling due to 2D flow geometries, and deformation during high-pressure operation, which can increase the maintenance required for these systems and limit the potential throughput.^[37] To counteract this, borosilicate glass capillary flow-focusing devices present the most promising avenue for the HFF devices. Borosilicate glass offers many advantages over PDMS such as being inert to most solvents, minimal deformation due to a high Young's modulus, leading to consistent

operating conditions and the ability to achieve 3D flow geometries, which reduce channel fouling and increases the interface between the solvent and the antisolvent. Borosilicate devices have been used to produce several different NPs including polymeric NPs and gold NPs (AuNPs).^[37–39]

Although many studies have utilized this method to produce various types of NPs/NMs, the HFF device relies on passive diffusive mixing of reagents. The controllable aspects of this device typically include flow rate ratio and channel dimensions.^[40] To make a smaller particle size, the dimension of this device needs to be small enough. Therefore, the throughput of this method is often very low. Consequently, it takes a long time to produce enough NP samples for further in vitro and in vivo biological experiments. A high flow rate ratio also leads to a very diluted NP solution at the outlet of the device.^[31] To overcome these limitations, the induction of turbulent flow to promote rapid mixing has been explored. First, through the implementation of additional features to existing passive micromixing designs, turbulent flow regimes can be induced in laminar flow systems, such as staggered herringbone micromixers, which can achieve quick mixing through the implementation of specific design elements to the microchannel.^[21] The second method to generate rapid micromixing is by using active micromixing such as acoustic micromixing, which allows for greater control of tunable properties with the addition of an external energy source.^[32]

2.1.2. Staggered Herringbone Micromixing

Unlike the HFF design, where micromixing is induced through diffusive forces between fluid streams, staggered herringbone micromixers (SHM) induce micromixing through chaotic advection, which allows for the mixing profile to become highly flexible through the channel cross-sectional area (Figure 2b). These herringbone structures are designed on the floor of the microchannel. Due to the induction of the chaotic advection mixing profile, smaller mixing times are achieved between fluids at lower flow rates, leading to less dilution and shorter processing times for synthesizing NPs.^[22] SHM micromixers have a suitable flow rate range (a range of Re numbers) to provide high mixing efficiency (i.e., $Re \approx 1$ to 100).^[33]

Six different geometric parameters affect the mixing efficiency of SHMs, including 1) the ratio of the channel width to the channel height (w/h), 2) the ratio of the groove depth to the channel height (dg/h), 3) the ratio of the groove width to the groove pitch (wg/k), 4) the asymmetry factor of the groove (b), 5) the angle of the groove (α), and 6) the numbers of grooves per half channel (Ng).^[34] Among these six parameters, the parameter wg/k plays the most significant role in the mixing performance (i.e., a high mixing performance with the lowest possible pressure drop). More specifically, the mixing performance increases with an increasing groove width. A higher dg/h results in an increased mixing index. Comparatively, the groove angle (h) has a more minor effect on the mixing performance.^[34] Several studies have used the SHM to synthesize different NPs/NMs. Lipid NPs were synthesized with a size of 100 nm, a narrow size distribution of 0.2, and a high doxorubicin encapsulation efficiency (EE) of greater than 80%.^[25] Hybrid PLGA–lipid NPs were also produced using a SHM

system with a desired size of 102.11 nm and a narrow size distribution of 0.126.^[24] A commercial microfluidic platform NanoAssemblr has been developed based on the staggered herringbone micromixing technology for lab scale and clinical scale NP manufacturing under cGMP conditions.^[41] The NanoAssemblr platform is a benchtop instrument integrating staggered herringbone microfluidic cartridges, syringe pumps, and computer software. The microfluidic cartridge consists of a Y-junction followed by a staggered herringbone mixing region. Several studies have utilized this platform to synthesize various NPs such as liposomes, LNPs, oil-in-water nanoemulsions, and unilamellar vesicles.^[42–45]

2.1.3. Acoustic Micromixing

Active micromixing is to utilize energy from an external source to enhance the mixing performance through disrupting the laminar flow regime and inducing faster homogenization, thus producing smaller NPs with a narrower size distribution (Figure 2c).^[31] They also allow for an additional layer of control, as these external energy sources show major influence on mixing time and mixing process, thereby decoupling it from flow rate, flow rate ratio, and the channel dimensions, allowing the optimization of each variable independently.^[32] Although many active micromixers exist, including using magnetic field forces and electrical actuation, the most promising system for producing NPs for biological applications is through acoustic actuation. In the past studies, ultrasound has been shown to increase the nucleation rate. Consequently, the mean size and polydispersity of NPs can be significantly reduced when compared to bulk synthesis.^[28,29,32]

Several studies have utilized acoustic micromixing to produce superior NPs with enhanced control in NPs size and polydispersity. Although the overall design and eventual application of each design differ significantly, the underlying principle remains the same. Typically, devices have an inlet for reagent perfusion, a transducer for generating the required frequency signal, an oscillating plate for generating the acoustic streaming field to perturb the laminar flow regime through actuation of the internal edges of the plate, and an outlet for harvesting the synthesized NPs/NMs.^[28–32] By controlling the oscillating plate design and the oscillation frequency, the NPs size can be tuned independently. The design of the oscillating plate and the optimization of the device operational parameters remain crucial in developing a reliable system for synthesizing monodisperse NPs.

Several studies implement acoustic actuation via a two-inlets-one-outlet device with an oscillating plate and piezoelectric transducer.^[31,32] The oscillating plate was designed in a star shape configuration with several sharp points which allow for the generation of the acoustic field stream. These devices have been used to produce various types of NPs including BCA-P114 NPs, Budesonide nanodrugs and DNA NPs with relatively low mixing times ranging from 4.1 to 6 ms.^[31,32] Huang et al. designed a piezoelectric actuator to induce the actuating frequency and to disrupt the laminar flow regime present. This creates rapid mixing of the two solutions and enhances NP formation through nanoprecipitation. The particle size correlates directly with the flow rate, but when the driving voltage increases from 20 to 55 Vpp, the particle size remains small

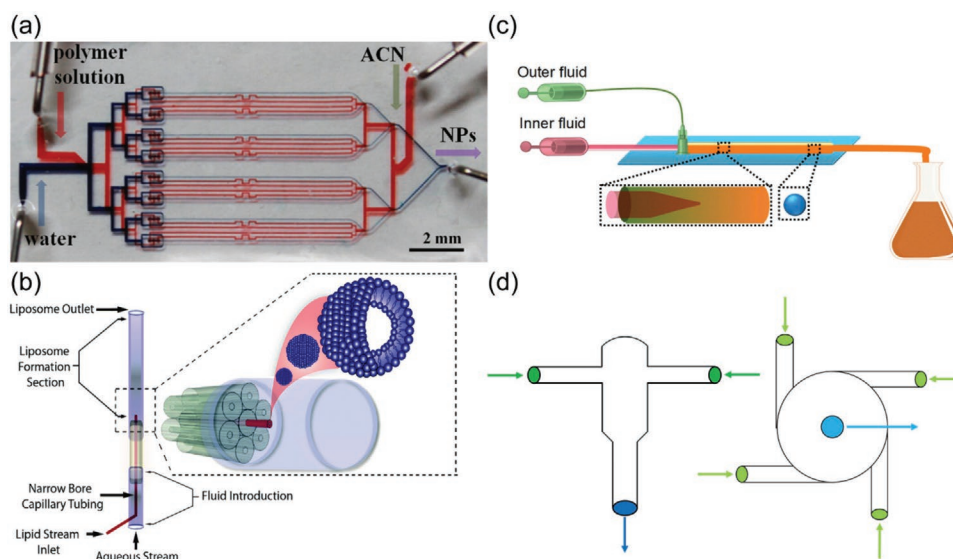


Figure 3. Devices for scale-up or scale-out production. a) Schematic of 3D HFF microfluidic device for parallel NP synthesis. Reproduced with permission.^[46] Copyright 2014, Elsevier Inc. b) Schematic of a 3D glass multicapillary array device. Reproduced with permission.^[48] Copyright 2014, The Royal Society of Chemistry. c) Schematic of a coaxial turbulent jet mixer. Reproduced with permission.^[49] Copyright 2019, Elsevier B.V. d) Schematic of the confined impinging jet (CIJ; left) and multiple inlet vortex micromixers (MIVM; right) to produce NPs through flash nanoprecipitation.

(68 nm) even at high total flow rates. The increase of total flow rates using such acoustic actuation allows much higher NP production throughput.^[29] Acoustofluidics has not only been utilized in microfluidic designs but also in millifluidic devices to increase the throughput for potential scale-up production, due to reduced fouling within the channel, easier maintenance of homogenous chemical environments and being simpler to manufacture, while producing tunable NPs with smaller size distributions when compared to bulk mixing methods.^[30]

2.1.4. Devices for Scale-Up or Scale-Out Production

One major limitation of synthesizing NPs using microfluidic platforms is their scale up for commercial relevance. As microfluidics typically deals with microscale variables using small volumes, this often means that the produced NPs are often on the milliliter scale per hour and are not commercially viable when considering large-scale production of NPs. Several approaches have been developed to increase production throughput. Parallel production of polymer NPs using a 3D HFF device can enhance the production rate without losing the advantages of robustness, controllability, and reproducibility. Karnik's group used a PDMS-based microfluidic system comprising of 8 parallel 3D HFF devices to reach the production rate of up to 84 mg h⁻¹ (Figure 3a).^[46] Another study used the 3D flash flow microreactor system to achieve the production rate of PEG-PLGA NPs at ≈10 g h⁻¹.^[47] Their device comprised eight sets of HFF units parallels with diverged inlets and a single converged outlet, which could sustain a high flow rate of the polymer due to its seven layers of the resistant PI polymer film and a following one-step adhesive bonding procedure.

In addition to the 3D HFF devices, glass capillary devices with other designs, coaxial turbulent jet mixers, multiple

inlet vortex mixers, and confined impinging jet mixers have also been developed for the continuous production of synthetic polymer NPs at high throughput (Figure 3b).^[50] Coaxial turbulent jet mixers (Figure 3c) are less difficult to fabricate than PDMS devices and achieve axisymmetric flow geometry, which reduces the fouling typically found within 2D HFF and SHM devices, increasing the reliability of the system for high throughput application.^[49] Coaxial turbulent jet mixers have been used successfully in the production of several stable NPs including NPs for diagnostics,^[37] and celecoxib NPs for anti-inflammatory medication.^[49] Coaxial turbulent jet mixer was found to be suitable for the large-scale production of synthetic polymer NPs as well as being simple to fabricate, and also showing improved robustness and solvent compatibility compared with 2D HFF device.^[51]

Confined impinging jet (Figure 3d) micromixing is a method of flash nanoprecipitation in which a drug and block copolymer are codissolved within an organic solvent, and then impinged at high velocities against an antisolvent, which induces turbulent mixing and high supersaturation.^[52] This results in coprecipitation of the drug and the block copolymer, leading to the formation of NPs. Confined impinging jet micromixing requires two equal momenta inlet streams, which imposes a limitation on the supersaturation levels that can be achieved.^[53] Thus, to overcome limitations imposed by confined impinging jet micromixing, multi-inlet vortex mixers (MIVM) (Figure 3d) were developed. Each stream momentum in MIVMs acts independently to induce the rapid mixing found within the device.^[54] Therefore, this allows for the possibility of differing flow rates to achieve tunable saturation levels and product formulation. MIVMs are designed with four independent streams which are organized as per Figure 3d (right). These are then fed into a central circularized chamber to induce rapid vortex micromixing within the chamber producing NPs through

nanoprecipitation. The final phase fluids of MIVMs are predominantly antisolvents (such as water), which lead to simpler postproduction processing and greater NP stability.^[53,54]

2.2. Different Organic NPs

2.2.1. Liposomes

Liposome is a lipid-based vesicular system consisting of a lipophilic lipid bilayer and an aqueous solution core. It has been widely used in drug delivery and medicines (Figure 4a). Liposomes are capable of encapsulating both hydrophobic and hydrophilic compounds in the lipid bilayer and aqueous core, respectively. Their surface can be modified with various ligands for immune evasion and targeted delivery. Therefore, liposome is the most widely studied and the most successful drug delivery system for delivering small molecules, monoclonal antibodies, genes, peptides, etc.^[55,56] The success of Doxil in

1995—the first liposome-based cancer nanomedicine, opened a new era of nanomedicine.^[57]

Conventional methods for liposome synthesis rely on first drying lipids to form lipid film followed by subsequent hydration and mechanical dispersion. To make uniform and smaller liposomes, different postprocessing methods are applied, such as sonication or extrusion.^[59] Compared to these conventional methods, microfluidics offers many advantages in fabricating liposomes. It allows one-step fabrication of nearly monodispersed liposomes with tunable and controllable diameters and surface properties.^[61] Also, drug-loaded liposomes produced using microfluidic methods exhibited higher EE, smaller and more uniform size in comparison with those synthesized using the conventional thin-film hydration method.^[62]

Different microfluidic approaches have been developed for making liposomes, including the HFF method, microfluidic jetting technique,^[63] droplet emulsion transfer,^[64] electroformation,^[65] NanoAssemblr (Figure 4b),^[58,66–68] tangential flow filtration device,^[69] and other microfluidic devices.^[70,71] Among

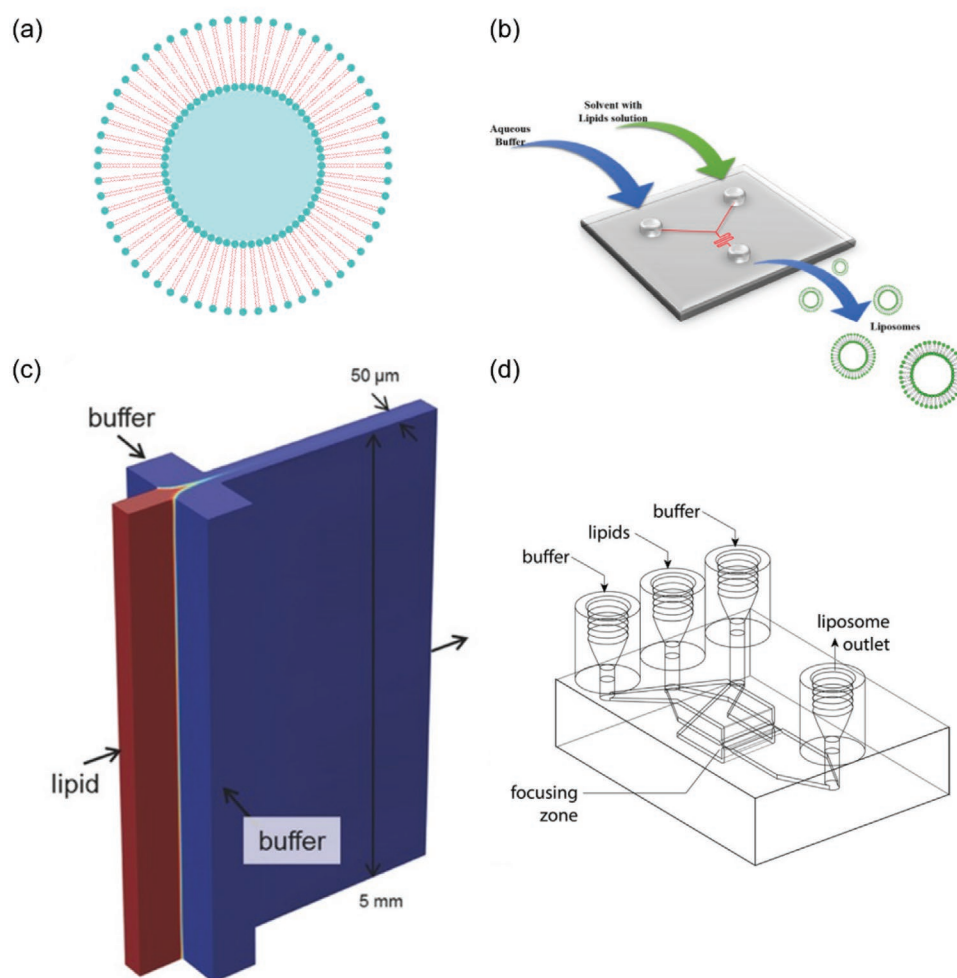


Figure 4. Microfluidic devices for production of liposomes. a) Schematic of liposomes. b) Schematic of NanoAssemblr device for liposome preparation. Reproduced with permission.^[58] Copyright 2016, Elsevier B.V. c) Schematic of microfluidic vertical HFF device. Reproduced with permission.^[59] Copyright 2015, Wiley-VCH. d) Schematic of 3D HFF device. Reproduced with permission.^[60] Copyright 2019, Wiley-VCH.

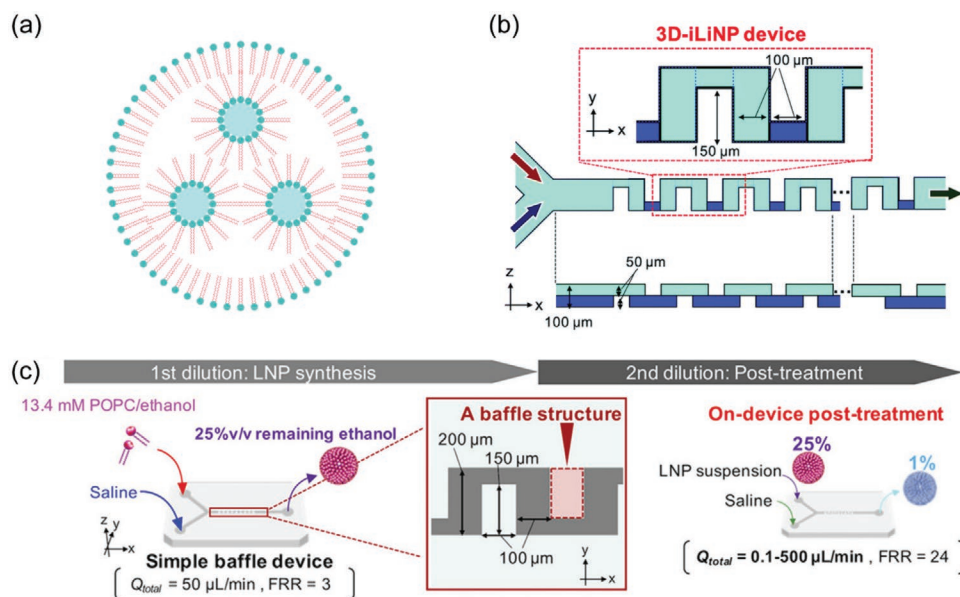


Figure 5. Microfluidic devices for production of lipid NPs. a) Schematic of lipid NPs. b) Schematic of 3D-iLiNP device. Reproduced with permission.^[91] Copyright 2021, The Royal Society of Chemistry. c) Schematic of an integrated baffle device composed of a lipid NP production region and a post-treatment region. Reproduced with permission.^[93] Copyright 2020, American Chemical Society.

these methods, the HFF method is a straightforward method that has been widely used to synthesize nanoliposomes with various compositions and functions.^[59,72] The HFF method is rapid, simple, low-cost, and capable of producing multifunctional liposomes, such as targeted liposomes with PEGylation, single targeting ligand, or dual ligands.^[35,73–75] To improve the mixing, different mixing structures have been incorporated. For example, including serpentine in the main channel can significantly enhance the mixing performance.^[76]

The limited throughput of microfluidics remains a challenge for liposome production, which makes it impractical for large-scale production. A high aspect ratio microfluidic vertical HFF device has been explored as a new method to increase the throughput while keeping the advantages of microfluidics to fabricate monodisperse liposomes. By using this new platform, the throughput was increased to as high as 96 mg h⁻¹ with the size ranging from 80 to 200 nm (Figure 4c).^[59] Additionally, the production rate of liposomes can be increased to 240 mg h⁻¹ by using a single 3D HFF device (Figure 4d).^[60] The resulting liposomes had tunable size, good PDI with a throughput around four orders of magnitude higher than using a traditional 2D HFF device.

2.2.2. Lipid NPs

Lipid NPs have been applied in a wide variety of pharmaceutical applications since the 1990s (Figure 5a).^[77] During the recent SARS-CoV-2 pandemic, two lipid NP-based mRNA vaccines from Pfizer-BioNTech and Moderna have achieved ≈95% efficacy in phase III clinical trials. The success of the two mRNA vaccines using lipid NPs to deliver mRNAs has rightly put lipid NPs in the spotlight.^[78] Lipid NPs, as one of the most widely used NP system, play a critical role in both improving

the stability of mRNAs, but also enhancing their delivery into the cytoplasm of host cells.^[79] Conventional methods for producing lipid NPs often involve ultrasound, high shear or pressure homogenization, microemulsion-based preparations, and solvent evaporation, etc.^[80–84] The emulsion solvent evaporation method is one of the most widely used conventional methods to produce lipid NPs. First, lipophilic material and hydrophobic drugs are dissolved in a water-immiscible organic solvent, which is then mixed with an aqueous phase containing surfactants to offer stability using high-speed homogenization. Finally, lipid NPs are produced by evaporating the organic solvent.^[85] Such conventional methods often suffer problems such as less control over the final lipid NP quality (size and size distribution), harsh conditions (e.g., high energy homogenization, high-temperature evaporation), as well as possible metal contamination from ultrasound. To overcome these disadvantages, microfluidic approaches have been developed to produce lipid NPs with well-controlled size and size distribution.^[84] Microfluidic devices with various structures have been designed to control lipid NP formation including HFF devices, staggered herringbone micromixer,^[86,87] T-shape microfluidic device,^[88] 2D and 3D invasive lipid NP production (iLiNP) device (Figure 5b),^[89–91] and glass capillary-based microfluidic-chip.^[92]

Microfluidic approaches for making lipid NPs are mainly based on nanoprecipitation.^[84] The HFF method is the most widely used microfluidic method for lipid NP synthesis since 2004.^[94] The fast dilution of alcohol using the HFF device facilitates the manufacture of small lipid NPs with a narrow size distribution.^[95] The single-step HFF method was compared with the conventional multistep bulk mixing method for synthesizing transferrin-conjugated lipid NPs for siRNA delivery. It was demonstrated that the HFF method produced smaller lipid NPs with a more uniform structure.^[96] HFF was also combined with passive mixing structures to achieve the self-assembly

of monodisperse lipid-quantum dot NPs with a single-step mixing.^[97] Additionally, it can assist the self-assembly of phospholipids and membrane proteins into polyhedral arrangements for structural analysis of membrane proteins in the presence of transmembrane gradients.^[98] To increase the throughput, Hood et al. designed a 3D glass multicapillary array device comprising of seven small capillaries in one large capillary, which can produce a 3D HFF stream thus improving the throughput (97 and 0.04 mg h⁻¹ for 3D and 2D, respectively) and offering better control over the NP size.^[48] Similarly, comparing to the 2D-iLiNP device, the 3D-iLiNP device produced siRNA-loaded lipid NPs with a more uniform size.^[91]

The SHM has also been used to produce uniform lipid NPs. More specifically, lipids dissolved in a solvent solution are mixed rapidly with an aqueous solution in the SHM to produce NPs continuously with enhanced mixing facilitated by the staggered herringbone mixing structure.^[33] However, lipid NPs fabricated using such nanoprecipitation-based rapid-mixing devices are normally unstable due to Ostwald ripening that could cause the fusion of lipid NPs. For maintaining the good NP quality, it is essential to remove the solvent instantly after synthesis.^[99] An integrated baffle device was designed to address this issue. It consists of a lipid NP production region and a post-treatment region for instant solvent dilution. This design allowed the production of smaller and stable lipid NPs by preventing the unfavorable aggregation (Figure 5c).^[93]

2.2.3. Synthetic Polymer NPs

The production of polymer NPs through self-assembling diblock copolymers has attracted great interest in the past decades for drug delivery and controlled release (Figure 6a). Commonly used synthetic polymers include poly(alkyl cyanoacrylate)

(PACA), poly(lactic-co-glycolic acid) (PLGA), poly-ε-caprolactone (PCL), poly(ethylene oxide) (PEO), polyamidoamine dendrimers, etc. PLGA is one of the most popular biodegradable synthetic polymers due to its excellent biocompatibility and biodegradability, tunable degradation characteristics, long clinical experience. It has been approved by the United States Food and Drug Administration (FDA) for drug delivery.^[100] PLGA can be synthesized with different ratios of glycolic acid and lactic acid to achieve a variety of mechanical strength, degree of crystallinity, and degradation rate, thus controlling its degradation and release kinetics.^[101]

Several conventional methods have been reported for the preparation of synthetic polymer NPs such as PEG–PLGA NPs, including nanoprecipitation (solvent displacement), salting-out, single/double-emulsion solvent evaporation, emulsification-diffusion, and emulsion-diffusion evaporation.^[104] These conventional methods are often based on the “bulk method,” so they often lack control over mixing, nucleation, and particle growth, resulting in the formation of NPs with big size, wide size distribution, and heterogenous NP structure.

The versatile HFF device, staggered herringbone micro-mixer,^[105] two-phase gas–liquid microfluidic mixers (Figure 6b),^[102,106–110] automated microfluidic Asia 320 flow reactor,^[111] the microfluidic coflow capillary device,^[112] and impact-jet micromixers^[113] have been developed to prepare the synthetic polymer NPs in recent years.

Among all the microfluidic methods, the HFF is the most widely used method for synthesizing polymer NPs.^[34,103,114–116] Generally, a middle water-miscible solvent stream with polymers and drugs dissolved is sandwiched by a two-side sheath flow of an antisolvent (water or buffer solutions). The rapid diffusion of the solvent in the aqueous phase leads to the formation of polymer NPs via nanoprecipitation. The properties of final NPs such as size, size distribution, drug loading (DL),

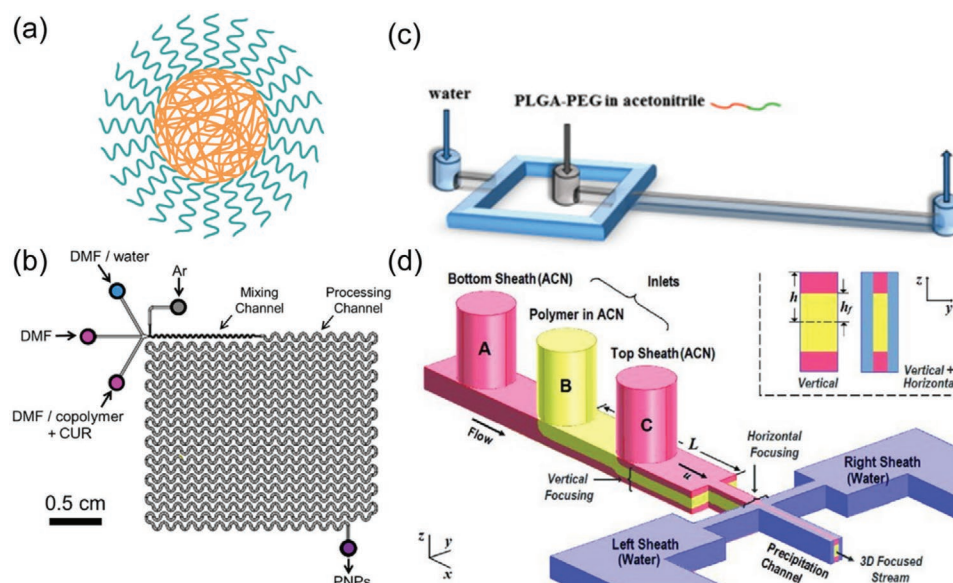


Figure 6. Microfluidic devices for the production of synthetic polymer NPs. a) Schematic of synthetic polymer NPs. b) Schematic of the two-phase gas–liquid microfluidic reactor. Reproduced with permission.^[102] Copyright 2018, American Chemical Society. c) Schematic of a 2D chip-based HFF device. Reproduced with permission.^[6] Copyright 2017, Elsevier Ltd. d) Schematic of 3D HFF device. Reproduced with permission.^[103] Copyright 2011, Wiley-VCH.

and release kinetics, rely on the concentration of polymers or drugs in the solvent solution, flow rate of the solvent and aqueous phases, flow rate ratio, and mixing structure in the HFF device.^[34] Compared to traditional bulk methods, the HFF method allows better control of size, size distribution, and surface properties.^[117] On the other hand, different microfluidic devices have their own advantages and disadvantages in synthesizing polymer NPs. Othman et al. compared the synthesis of PCL NPs using a co-flow and an HFF glass capillary device based on nanoprecipitation. The NP size can be precisely controlled by changing the total flow rate, flow rate ratio, and the orifice size of the inner capillary. Smaller NPs were prepared using the HFF device compared to the co-flow device of the same geometry.^[39] The HFF method can also be combined with electrospray to further improve the size and size distribution of polymer NPs.^[118] Also, the presence of surfactants such as Tween 80 or PVA in the continuous aqueous phase facilitates the formation of smaller NPs with better stability. However, it is worth noting that surfactants could also affect NP structure as it competes with the self-assembly of amphiphilic polymer molecules. Thus, selecting the right type of surfactants with an optimal concentration is important.^[119] Moreover, the HFF device can be used for making hybrid polymer NPs by using different synthetic polymers with different ratios, e.g., hybrid polymer NPs comprised of PCL and poly(trimethylene carbonate) homopolymers, and PLGA/PLGA-PEG NPs.^[120,121]

To increase the throughput of polymer NP production, one way is to increase the polymer concentration or its flow rate.^[47] Baby et al. optimized the HFF device by varying the design parameters such as channel structure, channel depth, channel width, and operating conditions such as flow rate, flow rate ratios, and polymer concentrations. The optimized design can achieve a throughput up to 288 mg h⁻¹ using a single 2D chip-based HFF device, which was more than 100 times higher than the commonly used HFF device having a production rate of 1.8 mg h⁻¹ (Figure 6c).^[6] However, increasing polymer concentration or flow rates could lead to NP deposition and channel clogging, especially when the molecular weight of the PLGA block is higher than 45 kDa.^[122] In addressing this problem, a 3D HFF device was designed. Polymer NPs with a smaller size and improved monodispersity were produced by the 3D HFF compared to 2D HFF devices (Figure 6d).^[103] Furthermore, in contrast to polymer-based HFF devices, 3D HFF devices made of glass provide an inert and stable platform for making polymer NPs.^[123]

2.2.4. Biopolymer NPs

Biopolymer NPs have been investigated as an alternative to synthetic NPs due to their biodegradability, biocompatibility, low cost, and low toxicity,^[124] including chitosan, alginate, shellac, etc.

Chitosan is a biodegradable, biocompatible, nontoxic natural polymer, which is one of the most frequently used natural polymers for drug delivery.^[125] Chitosan is a cationic linear polysaccharide having a positive charge, suitable to load negatively charged therapeutics.^[124] Chitosan NPs can be produced using a range of methods including ionic gelation, chemical

cross-linking, and microfluidic methods.^[126] The staggered herringbone micromixer,^[127,128] microreactor with circular channels and chamber,^[129] and HFF devices have been used to synthesize chitosan NPs. Sodium tripolyphosphate is a commonly used chitosan cross-linker, and the ionic gelation reaction between sodium tripolyphosphate and chitosan can be exploited by microfluidic methods to form chitosan NPs for biomedical applications.^[127,130] The staggered herringbone micromixer was used for the synthesis of curcumin-loaded chitosan NPs via ionic gelation reaction.^[127] The HFF device has also been used to produce chitosan NPs.^[131–133] The key physical properties of the synthesized chitosan NPs such as size, surface charge, and drug release kinetics can be controlled by adjusting the operating conditions of the HFF device.^[134] It was reported that chitosan NPs fabricated by the HFF device were much smaller and more uniform (67 ± 13 nm) than that using the bulk method (452 ± 300 nm).^[135] Similarly, another study reported that the drug-loaded chitosan NPs prepared by the bulk method had irregular structures and non-uniform shapes due to the heterogeneous reaction condition. In contrast, chitosan NPs synthesized by the HFF method were uniform and spherical with an overall diameter of less than 100 nm.^[136] The chitosan-based NPs produced by the HFF method can be exploited for various drug delivery applications. For example, one study used the HFF device to synthesize chitosan-based NPs comprising of poly(*N*-isopropylacrylamide-co-acrylic acid) and cellulose laurate for transdermal multidrug delivery of tretinoin and clindamycin phosphate.^[137] The obtained NPs showed diameters ranging from 200 to 300 nm with a narrow size distribution, and the dual-drug loaded NPs demonstrated a sustained release with a much lower inhibitory and bactericidal concentration compared to the NPs produced by the bulk method. Additionally, the chitosan-modified NPs were able to encapsulate a hydrophobic drug paclitaxel using the HFF method via ionic gelation to avoid the use of chemical crosslinking agents.^[126,138]

Alginate is a natural polymer extracted from brown seaweed, which is an anionic linear unbranched polysaccharide.^[100] As a nonimmunogenic substance, alginate is a random copolymer comprising α -l-guluronic acid and β -d-mannuronic acid via 1,4-glycosidic linkages. Alginate has been approved by the FDA for drug delivery, tissue engineering, and wound healing applications.^[139] Alginate NPs can be produced using microfluidic methods via ionic gelation. For instance, a transforming growth factor-beta 3 (TGF- β 3)-loaded alginate nanogels was fabricated using an HFF device for controlled release of TGF- β 3 during chondrogenic differentiation of mesenchymal stem cells. Basically, an aqueous solution containing alginate and TGF- β 3 in the middle channel was mixed with a CaCl₂ solution in the two side channels for cross-linking.^[140]

Shellac (food additive code: E904) is a natural resin, which is a hydrophobic pH-sensitive polymer that contains a complicated mixture of polyhydroxy polycarboxylic esters, lactones, and anhydrides. Shellac is usually employed as enteric coatings, as it is insoluble around its pKa value ranging between 5.6 and 6.6, but becomes soluble at basic/neutral pH.^[141] Therefore, shellac NPs are exploited for pH-triggered release especially suitable for colon drug delivery. For example, one study reported the development of a 3D tubing microfluidic device for producing curcumin-loaded shellac NPs with tunable DLs

up to 50%. The resulting NPs were stable under acidic conditions for more than 10 d but showed sustained release of curcumin at neutral pH, which was ideal to deliver drugs for colon cancer therapy. A 3D tubing microfluidic device is capable to produce shellac NPs and microparticles, showing several advantages compared to 2D HFF devices, such as no clogging, higher throughput, and better compatibility with most solvents.^[142,143]

2.3. Different Synthesis Mechanisms

2.3.1. Rapid Mixing Induced Nanoprecipitation

Majority of the microfluidic methods for making organic NPs are based on nanoprecipitation through controlling mixing.^[144] Nanoprecipitation, also called solvent displacement, relies on the interfacial disposition of polymer or lipids solubilized in a water-miscible solvent upon mixing with water or a buffer solution.^[145,146] It is a simple and fast method with high reproducibility, and it consumes a low amount of energy and raw materials.^[144,147]

During the nanoprecipitation process, the solvent diffuses into the antisolvent solution first, once reaching a supersaturation state, the nuclei start to form followed by NP growth via molecular deposition of the polymer chain or lipid molecules at their surface.^[148,149] The quality of organic NPs synthesized via nanoprecipitation depends on mixing in microfluidic devices. When the mixing time is shorter than the aggregation time, self-assembly is predominant resulting in the formation of uniform and smaller NPs. The steric stabilization provided by surface stabilizers such as surfactant, surface charge, or the hydrophilic part of the amphiphilic di-block copolymers (e.g., PEG) can reduce NP aggregation.^[148] Therefore, all the microfluidic approaches are designed based on improving or enhancing the mixing of the solvent and anti-solvent solutions in the microfluidic channels.^[150]

Rapid mixing induced nanoprecipitation is ideal for the production of drug-loaded organic NPs. It is a simple, continuous, and controllable method. This method utilizes fast mixing to create homogeneous supersaturation and controlled precipitation of hydrophobic drugs along with the self-assembly of polymers or lipids, leading to the production of precisely controlled organic NPs.^[148,151] When using the rapid mixing induced nanoprecipitation to manufacture NPs with high solute concentration, it requires a mixing time that is less than the nucleation and growth time (τ_{n+g}) of an NP.^[151,152] The rapid mixing induced nanoprecipitation has been widely employed to produce various NPs, such as polymer NPs, lipid NPs, drug NPs, and polyelectrolyte complexes.^[36] While it shares an identical principle with that of bulk nanoprecipitation, the rapid mixing induced microfluidic nanoprecipitation demonstrates numerous advantages, including narrow size distribution, good reproducibility, and easy operation.^[148] The control of NP size is important as it affects NP stability, biological activity, and bio-nanointeractions.^[146]

Many mixing devices, such as HFF, SHM, confined impinging jets (CIJ) mixer and multi-inlet vortex mixer (MIVM), have been commonly used to synthesize NPs based on the rapid mixing induced nanoprecipitation.^[54,152] The CIJ

mixer can control the supersaturation of nanomaterials by adjusting flow rates, consequently controlling the NP size. The MIVM having four streams is designed to overcome the restraint of the need of the same velocity of the opposed jets for CIJ, it can control both the final solvent components and the supersaturation by adjusting the velocity of the stream. Their mixing process is generally controlled by adjusting the Reynolds number of the flow.^[153] These devices allow the flow-based production of a range of nanomaterials such as polymer NPs, inorganic NPs, lipid NPs, liposomes, core-shell NPs, polyplex NPs, etc.^[51,153]

2.3.2. Sequential Nanoprecipitation

Normally, drug-loaded NPs produced using nanoprecipitation especially the rapid mixing induced nanoprecipitation have relatively low DL (lower than 10%), which is mainly due to the different precipitation times of the drugs and nanocarriers.^[34] Precipitation time plays an important role in controlling the DL and the EE based on nanoprecipitation. A combined simulation and experimental approach were used to investigate the fundamental principle that governs the encapsulation of a drug in polymer NPs produced by microfluidic nanoprecipitation. The huge difference in the mixing times of drug and polymer was found to be a key reason leading to very low DL, and a good match between their mixing times is vital for achieving drug-loaded polymer NPs with high DL.^[154] If the nanocarrier precipitates much faster than the drug, it often leads to the production of empty nanocarriers with a large amount of unencapsulated free drug, causing reduced EE as well as low DL.^[155] Therefore, it is critical to make both the drug and nanocarrier precipitate nearly at the same time for the production of high DL NPs, more preferably the drug precipitate firstly followed by the precipitation of nanocarriers leading to the formation of drug-loaded core-shell NPs to further improve the DL.

Sequential nanoprecipitation is a new approach to improve DL. It relies on the sequential precipitation of drug firstly then nanocarriers, thus forming high DL NPs.^[156] In theory, it is achievable. But in practice, it is not trivial as it is challenging to control the sequential precipitation times of drug and nanocarrier to ensure the precipitation time interval between the drug and nanocarrier is short enough thus preventing the aggregation of the firstly precipitated drug NPs.^[36] Sequential nanoprecipitation can be achieved using bulk nanoprecipitation. Liu et al. reported drug-core polymer-shell NPs with a high DL of 58.5% by a bulk sequential nanoprecipitation method using different drugs and polymers.^[157–159] This bulk sequential nanoprecipitation approach used a solvent mixture containing several solvents to regulate the precipitation time of drugs and polymers. Based on the bulk sequential nanoprecipitation method, Baby et al. synthesized curcumin-loaded shellac NPs using a 3D microfluidic tubing device (Figure 7a).^[155] They used the same combination of solvents as the bulk sequential nanoprecipitation method to guarantee the sequential nanoprecipitation. By mixing the solvent-mixture solution containing drugs and polymers with an anti-solvent solution in the 3D microfluidic tubing device, drug NPs could firstly be formed via nanoprecipitation, followed

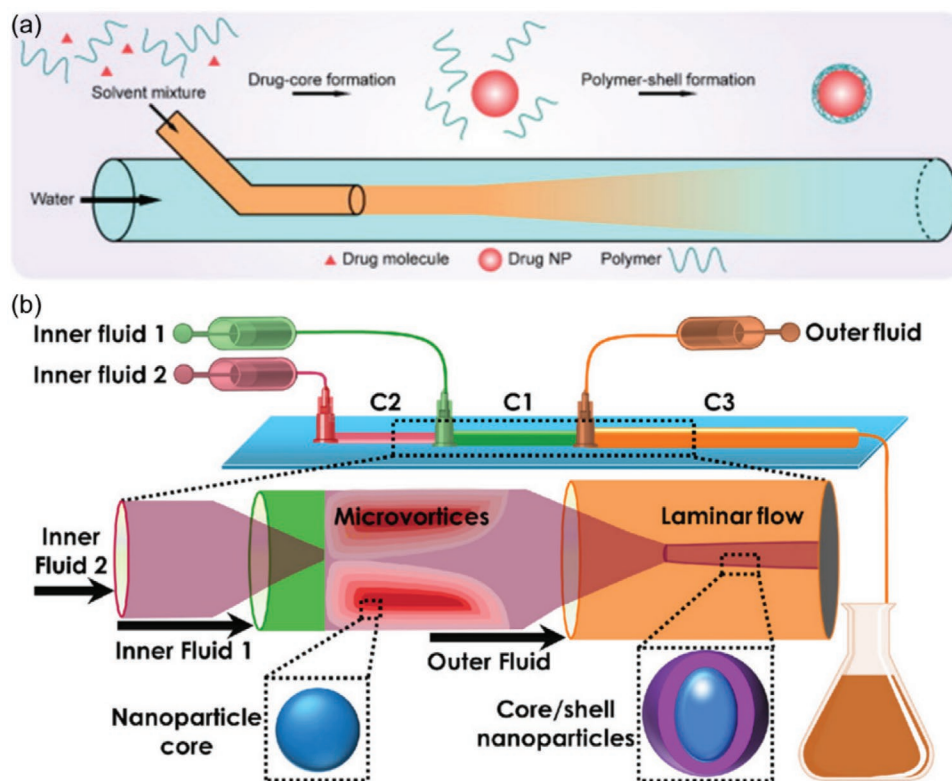


Figure 7. Sequential nanoprecipitation using microfluidic devices. a) Schematic of high drug-loaded curcumin-shellac NP formation in a 3D-HFF microfluidic tubing device through sequential nanoprecipitation. Reproduced with permission.^[155] Copyright 2021, Elsevier Inc. b) Schematic of a 3D glass capillary device to prepare structured core-shell nanocomposites through sequential nanoprecipitation. Reproduced with permission.^[160] Copyright 2017, American Chemical Society.

by deposition of the polymer shellac on the drug NPs. The drug-core shellac-shell NPs had high curcumin loading, excellent stability, and a pH-responsive release profile.

Additionally, sequential nanoprecipitation can also be realized using the unique design of the microfluidic device. A microfluidic platform was designed to produce paclitaxel-loaded hypromellose acetate succinate NPs and achieved a DL of 42.6% (Figure 7b).^[160] The sequential precipitation was achieved by controlling the time intervals between the sequential nanoprecipitation process of the polymer and the drug offered by the device. The solvent phase solubilizing hydrophobic drugs (paclitaxel and sorafenib) and a pH-sensitive polymer, hypromellose acetate succinate, was mixed with a basic antisolvent in a microfluidic device thus drug NPs formed first due to nanoprecipitation. Then an acidic solution was introduced to lower the pH so the pH-responsive polymer was precipitated and coated on the drug NPs, achieving a high DL of 45.2%.

3. Microfluidic Synthesis of Inorganic NPs

Inorganic NPs, such as silica NPs, metal NPs (e.g., Au), metal oxide NPs (e.g., iron oxide), and quantum dots (e.g., CdS and CdSe) generally exhibit superior mechanical and chemical stability, lower polydispersity, richer surface chemistry and surface morphology, and larger surface area (for porous NPs) compared

to organic NPs.^[161–163] Moreover, many inorganic NPs also possess special optical, photothermal, and magnetic properties that can be leveraged for theranostics, thermotherapy and magnetically induced tumor targeting, etc. These unique features render inorganic NPs promising candidates for drug delivery applications, thus they have been widely fabricated via various approaches in the past decades. Among these methods, the microfluidic preparation of inorganic NPs has been attracting increasing attention in recent years due to its efficient mass and heat transfer rate, and the precise and easy control on reaction parameters, which not only dramatically reduce the preparation time of inorganic NPs without sacrificing their quality, but also provide a better insight into reaction mechanisms. Also, the continuous synthesis process offers great potential for future continuous manufacturing industry applications.

Different from the synthesis of organic NPs in microfluidic devices which is based on nanoprecipitation, the preparation of inorganic NPs in microfluidic devices often involves reaction, which requires the addition of reagents, mixing, separation, purification; so different types of microfluidic approaches have been developed. Therefore, instead of summarizing and discussing microfluidic devices, types of organic NPs, and mechanisms separately as we did in Section 2, this Section focuses on providing a wide variety of examples of inorganic NPs, we group them into four subsections including silica NPs, metal NPs, metal oxide NPs, quantum dots.

3.1. Silica NPs

Silica NPs have been widely synthesized and applied as drug delivery vehicles in the past decades due to their good biocompatibility, stability, and ease of surface functionalization.^[164,165] Active components ranging from chemical therapeutics, imaging agents, to siRNA can be covalently or physically loaded on the surface or inside the pores of silica NPs, or entrapped in the interior of a hollow silica shell, while the surface of silica NPs are normally conjugated with antifouling agents and targeting ligands to prolong their blood circulation and selective accumulation at the tumor site.^[166–169] Microfluidics represents an emerging technology for the fabrication of colloidal silica NPs for biomedical applications. Compared to the conventional batch sol–gel processes, the unique advantage of the microfluidic method for silica NPs lies in the more homogeneous reaction by more efficient mixing and the precise control over their size, shape, porosity, composition, and surface modification, while maintaining a high production rate and monodispersity.

In a pioneering work, Khan et al. designed a continuous flow microfluidic device with two inlets leading to a mixing channel (Figure 8a, dotted area) and the following aging section.^[170] Two reactant solutions: 1) diluted ethanol solution of TEOS as silica precursor and 2) a water solution of ammonia and ethanol were pumped into the microfluidic reactor via the inlets to trigger the nucleation and growth of the silica NPs. At a low flow rate that corresponds to a residence time of 16 min, silica NPs with an averaged diameter of 321 nm and a size deviation of 9% were obtained (Figure 8b left). In comparison, at a high flow velocity, the short residence time (3 min) led to smaller NPs (164 nm, Figure 8b right) but with a dramatically higher size deviation of 25% due to the axial dispersion of the growing colloidal particles. This axial dispersion effect was eliminated by using a segmented flow device as all the small segmented batches share the same residence time in the reactor. In another study, both laminar flow (Figure 8c) and segmented flow (Figure 8d) microfluidic reactors were built by connecting commercially available ETFE tubes, fittings, and connectors.^[171] Such a setup effectively attenuated the tube clogging caused by the deposition of NPs on channel walls. By using TMOS as a silicon source and PEI as nucleation catalyst, silica NPs with diameters of less than 100 nm were produced at a yield higher than batch synthesis, and their sizes and size distributions could be readily tuned by adjusting the variables including pH, flow rate, and residence time. Segmented flow microreactor again produced finer particles with narrower size distribution than the continuous flow microreactor, highlighting the importance of eliminating the influence of axial dispersion effect.

Other than solid silica NPs, the production of hollow silica spheres by microfluidics has also been realized. Nie et al. reported the ultrafast fabrication of submicrometer-sized hollow silica particles using a spiral microfluidic channel (Figure 8e-i).^[172] By injecting a silica precursor solution and an aqueous solution containing ammonia and CTAB into the channel separately via the two inlets, two laminar flows were generated to form an interface (Figure 8e-ii) where TEOS emulsions were generated and stabilized by CTAB micelles. Then, the hydrolysis of TEOS occurred in the presence of ammonia, and the condensation of hydrolyzed TEOS generated a silica shell

with the mixing of the two flows (Figure 8e-iii). Different active components including proteins, fluorescent dyes, quantum dots, and magnetic NPs were successfully encapsulated into the hollow silica shells for applications in cell imaging and drug delivery, etc.

Silica NPs with a mesoporous structure can also be prepared using microfluidic flow synthesis. By designing a flow synthesis reactor and using appropriate reactant solutions (Figure 8f), Ng et al. reported the fabrication of mesoporous silica NPs with controllable size (50 to 650 nm) and shapes (spheres and random) using both laminar flow and Taylor flow.^[173] CTAB was added into the aqueous reactant solution and served as a structure-directing agent to create pores in the NPs, and the pore size of the particles could be regulated by controlling mixing quality, different silicon alkoxide precursors, and the addition of a cosolute. Microfluidics has also been exploited to fabricate silica-based hierarchical nanocomposites for combined functionalities. Using two continuously flow microreactors connected in tandem (Figure 8g), fluorescent silica NPs, plasmonic Au NPs, and superparamagnetic NPs were assembled into a multifunctional nanocomposite (Figure 8h).^[174] The fabrication process was highly reproducible and efficient, and can be readily generalized and applied to any type of inorganic NPs. Other than using as-prepared NP suspensions as building blocks, Hao et al. prepared silver–core silica–shell nanocomposites directly from precursor solutions through two spiral-shaped laminar flow microfluidic reactors.^[175] By pumping a NaBH₄ solution and another reactant flow containing AgNO₃, trisodium, and H₂O₂ into the first microreactor (Figure 8i left), triangular-shaped silver nanoplatelets were produced within 250 ms in a large scale. The obtained silver nanoplatelet suspension was then mixed with a silica precursor TEOS (in ethanol) and pumped into one inlet of the second microreactor. By pumping an ammonia solution into the other inlet (Figure 8i right), hierarchical Ag–core silica–shell nanocomposite was produced with a tunable silica shell thickness (Figure 8j). Compared to conventional batch approaches, a salient advantage of flow synthesis lies in the sequential combination of individual reactions (e.g., nucleation, particle growth, and coating) in a single system. Because self-nucleation is suppressed in the microfluidic system, no washing process is required between every reaction step, which dramatically reduces the fabrication time.

3.2. Metal NPs

Metal NPs have been widely applied in various biomedical applications due to their unique optical, mechanical, chemical, and catalytic properties. Among all metals, noble metal NPs such as Au and Ag NPs are of particular interest due to their outstanding biocompatibility and the ease of surface functionalization for conjugating with multiple biomolecules, therapeutics, and targeting ligands, which renders them promising drug delivery vehicles. Moreover, the unique photothermal and plasmonic behavior of noble metal NPs also endows them with potential applications in thermotherapy, biosensing, and theranostics applications. A variety of approaches have been proposed for the generation of metal NPs. For example, an extensively

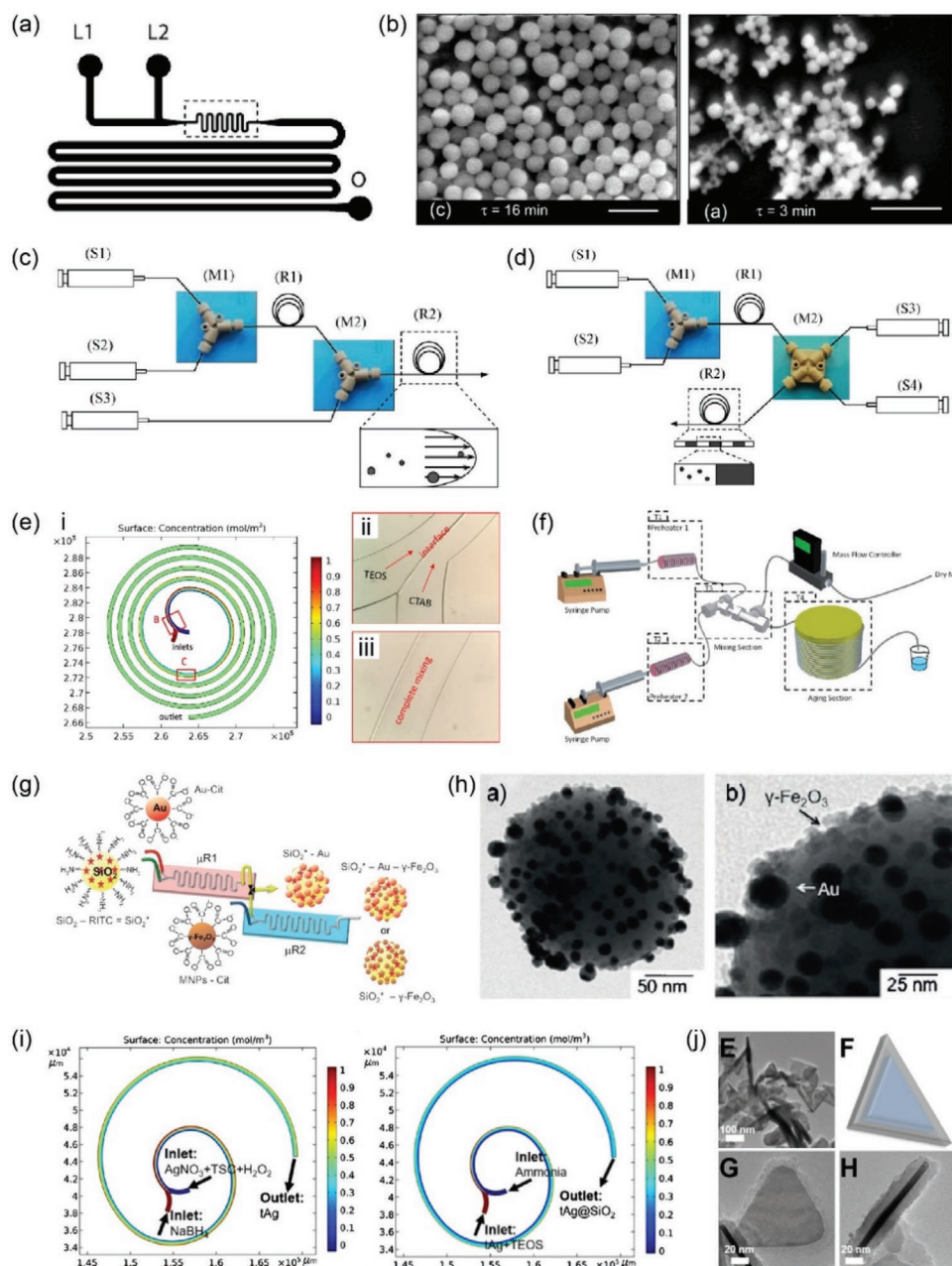


Figure 8. Microfluidic-based synthesis for silica-based nanomaterials. a) Schematic of a microfluidic device with two inlets (L1 and L2) and an outlet (O). Reproduced with permission.^[170] Copyright 2004, American Chemical Society. b) SEM images of silica NPs synthesized using the microfluidic device in (a), with residence times of 16 min (left) and 3 min (right). Reproduced with permission.^[170] Copyright 2004, American Chemical Society. Schematic diagrams of a c) laminar and d) segmented flow-based microreactor for silica NP synthesis. Reproduced with permission.^[171] Copyright 2010, Elsevier B.V. e-i) Simulation results showing the mixing of two flows in the spiral channel; experimental observation of ii) the interface of two reaction flows, and iii) complete mixing. Reproduced with permission.^[172] Copyright 2017, Springer Nature Limited. f) Schematic diagram of the flow synthesis reaction setup for laminar and Taylor flow operations. Reproduced with permission.^[173] Copyright 2015, The Royal Society of Chemistry. g) Schematic of a two-step microfluidic synthetic device for the assembly of multifunctional NPs/fluorescent silica particle assemblies. Reproduced with permission.^[174] Copyright 2013, Wiley-VCH. h) TEM images of $\text{SiO}_2\text{-Au-}\gamma\text{-Fe}_2\text{O}_3$ nanostructures produced using the two-step microfluidic procedure in (g). Reproduced with permission.^[174] Copyright 2013, Wiley-VCH. i) Simulation result of the mixing in the (left) first spiral microchannel, with NaBH_4 and $\text{AgNO}_3+\text{TSC}+\text{H}_2\text{O}_2$ being the two precursor solutions, and triangular Ag NPs (tAg) obtained from the outlet; simulation result of the mixing in the (right) second spiral microchannel, with ammonia and tAg+TEOS being the two precursor solutions, and TiO_2 -coated triangular Ag (tAg@ SiO_2) NPs obtained from the outlet. Reproduced with permission.^[175] Copyright 2019, Elsevier Inc. j) TEM images and schematic drawing (upper right) of tAg@ SiO_2 NPs produced using the devices in (i). Reproduced with permission.^[175] Copyright 2019, Elsevier Inc.

used method is the chemical reduction route by which the aqueous metal ionic precursors are reduced by reducing agents such as ascorbic acid, sodium citrate, and sodium borohydride, etc., and stabilized by polymeric capping agents or surfactants to avoid aggregation. Conventionally, metal NPs were mostly produced through a batch process in bulk solutions. However, the microfluidic route has recently emerged as a promising tool for metal NP synthesis as it greatly improves the production yield and reliability, and offers more precise and facile control on the characteristics of the NPs. Moreover, compared to the batch process, it is easier to fabricate and functionalize NPs in microfluidic reactors through a single step.

By using 12 nm sized, citrate-stabilized Au NPs as seeds, Wagner et al. successfully synthesized larger Au NPs of diameters ranging from 15 to 24 nm using a continuous flow microfluidic reactor (Figure 9a), wherein HAuCl₄ was reduced by ascorbic acid, leading to the growth of Au NPs, which was further stabilized using polyvinyl pyrrolidone (PVP).^[176] The size and size distribution of the particles could be altered by adjusting the flow rate and the concentration ratio of the reactants. The same authors also reported the synthesis of ultrasmall Au NPs (4 to 7 nm) directly from precursor solutions under continuous flow conditions.^[177] Rather than using smaller Au NPs seeds, an Au salt (HAuCl₄) solution, a reducing agent (NaBH₄), and a ligand were pumped separately from different inlets into a glass-silicon microreactor system consisting of three static chip micromixers (Figure 9b), which led to the formation and direct surface modification with thiol ligands of Au NPs. Two approaches: 1) the hydrophobic treatment of the reactor and 2) the elevation of pH were adopted to suppress the Au nucleation at the inner channel surface, which can potentially cause channel clogging. The channel blockage issue can also be eliminated by using microfluidic coaxial flow reactors, in which the nucleation and growth of NPs are confined at the interface of the inner and outer flows away from the channel walls. For example, by using an ETFE T-piece connector, Baber et al. successfully prepared Ag NPs with AgNO₃ and NaBH₄ being the inner and outer streams, respectively, in the presence of trisodium citrate as the surfactant (Figure 9c).^[178]

In addition to single-phase NPs, binary composed noble metal NPs can also be fabricated using microfluidics. Knauer et al. synthesized Ag-shell Au-core NPs using a segment flow microreactor system (Figure 9d), wherein Ag was reduced from its precursor salt solution and uniformly grew on Au NP seeds to form a homogeneous 1.1–6.1 nm layer.^[179] The inherent wide particle size distribution, which is a common issue of conventional wet-chemical synthesis, is dramatically suppressed by the microfluidic reactor owing to its effective mixing condition. Using a continuous flow microreactor with multiple inlets at different locations (Figure 9e), star-like and core-shell structured Au/Ag NPs have been prepared by directly reducing Au and Ag salts with ascorbic acid (Figure 9f).^[180] By controlling the concentration of the reducing agent, the relative nucleation rate of Au and Ag can be adjusted, leading to the different spatial distribution of elements inside the NPs.

In addition to noble metals, researchers have also realized the microfluidic preparation of other metal NPs including Cu,^[181] Pd,^[182] and Gd,^[183] etc. For example, Cu NPs were prepared by reducing CuSO₄ with NaBH₄ under a segmented flow

condition using a T-shaped microfluidic chip (Figure 9g).^[181] By using PVP as dispersant and antioxidant, Cu NPs possessing a uniform size distribution and an oxidation resistance were prepared, with their diameter, morphology, and size distribution and elemental compositions regulated by the flow rates. The synthesis of liquid metal NPs using microfluidics has also been reported recently. Due to the large surface tension of liquid metals relative to water, it is challenging to create fine liquid metal NPs merely by the shear force provided by a T-junction. In this regard, Tang et al. embedded the T-shaped PDMS microfluidic channel into a sonication bath to break the eutectic gallium indium (EGaIn) liquid metal microparticles into NPs using acoustic wave (Figure 9h).^[184] By adopting a solution of brushed PEG polymer with trithiocarbonate end groups as the aqueous phase, the generated EGaIn NPs with a diameter ranging from tens to a few hundreds of nanometers can be directly coated and stabilized in the channel.

3.3. Metal Oxide NPs

Metal oxide NPs represent another important subclass of inorganic nanomaterials that have found various biomedical applications including tissue engineering, immunotherapy, biosensing, dentistry, diagnosis, and drug delivery owing to their unique physical and chemical features, such as high stability, biocompatibility, and ease of functionalization, etc. Besides, different types of oxide NPs possess unique properties that can be leveraged for specific applications. For example, TiO₂ is well known for its outstanding biocompatibility and cell adhesion ability, thus suitable for regenerative tissue engineering; the superparamagnetic behavior of iron oxide NPs has been extensively exploited for MRI, magnetically guided drug delivery and hyperthermia, etc. Given these merits, metal oxide NPs have been widely prepared during the past decades. Among the various synthetic strategies, microfluidics is emerging as a powerful platform for the fabrication of metal oxide NPs that are superior in monodispersity and quality control compared to other conventional procedures.

Iron oxide NPs have been prepared using both tubular and chip-based microreactors via the coprecipitation mechanism, which relies on the pH-dependent solubility of iron oxides. At a pH above 10, iron salt solutions become supersaturated, triggering the nucleation and growth of the iron oxide NPs in the solution.^[185] Using a continuous flow microreactor, iron oxide NPs with sizes between 26.5 and 34 nm were synthesized through the oxidative hydrolysis of Fe²⁺ salts in just 3 min by controlling the variables (e.g., temperature, flow pattern, etc.) in the flow system, which was much more efficient than batch synthesis.^[186] The two modular unit design allowed the control on the type of gas dissolved in the solution (Figure 10a), and it was found that the presence of H₂ in the reaction solution promoted the formation of magnetic phase, while dissolving CO in the solution resulted in smaller NPs. In another case, magnetic iron oxide NPs were fabricated using a 3D hydrodynamic flow focusing microreactor, which effectively eliminated the fouling of channels and provided good control on the average particle sizes.^[187] Notably, a miniaturized NMR relaxometer was integrated into the microfluidic system to allow a facile online

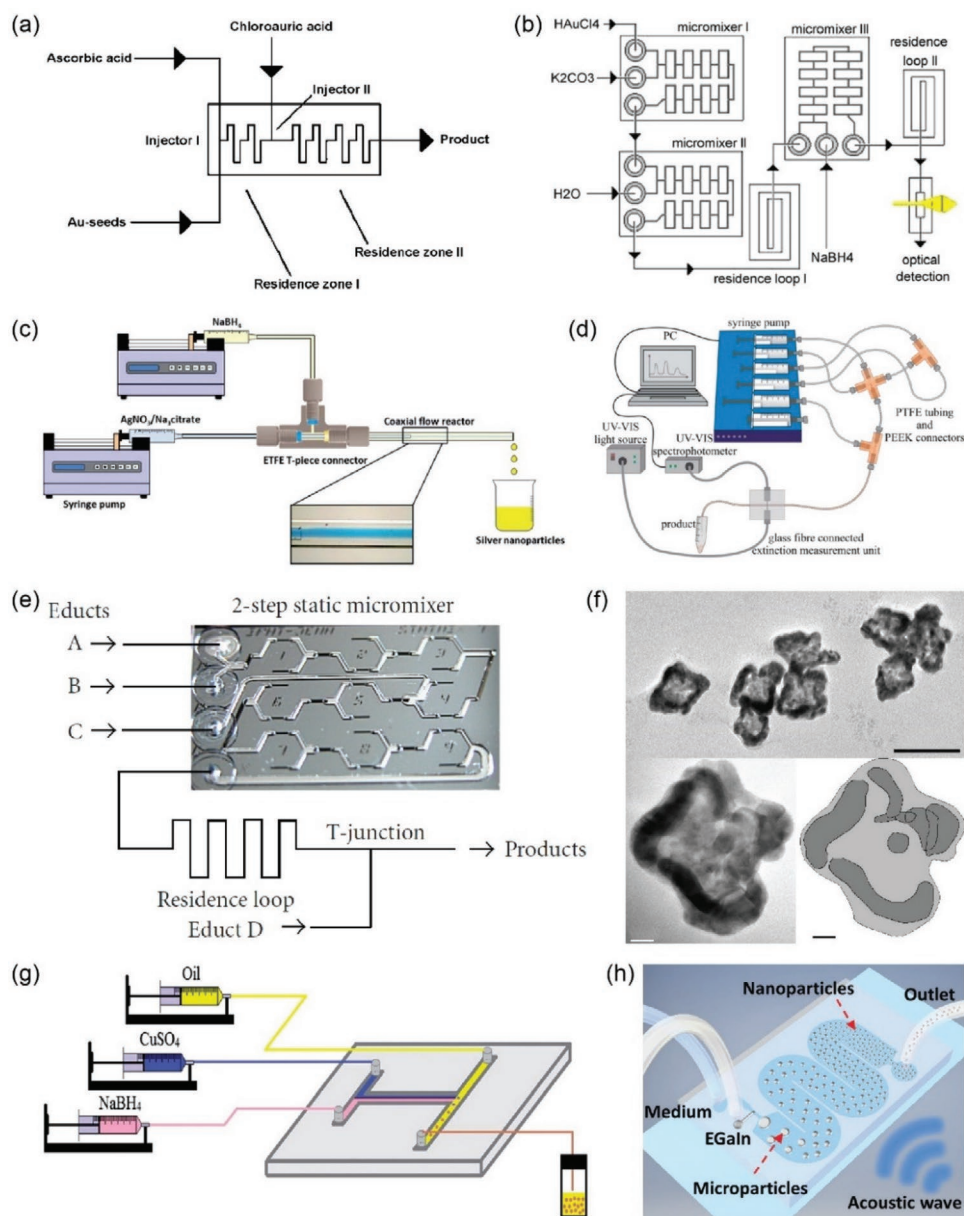


Figure 9. Microfluidic-based synthesis of metal nanomaterials. a) Schematic illustration of the experimental set-up and the connectivity of a microfluidic reactor for Au NP synthesis. Reproduced with permission.^[176] Copyright 2003, Elsevier B.V. b) Schematic diagram of a modular microreactor arrangement for the flow-based synthesis of Au NPs. Reproduced with permission.^[177] Copyright 2007, Elsevier B.V. c) Schematic diagram of the coaxial flow reactor setup. Inset displays flow visualization of laminar flow inside the coaxial flow reactor. Reproduced with permission.^[178] Copyright 2015, The Royal Society of Chemistry. d) Schematic diagram of the experimental arrangement for the combinatorial synthesis screening for Ag-shell Au-core NPs. Reproduced with permission.^[179] Copyright 2014, The Royal Society of Chemistry. e) Schematic illustration of the experimental arrangement for the microflow-based synthesis of core-shell NPs (A, B, C, D, ... inlet ports for educt solutions). Reproduced with permission.^[180] Copyright 2007, Hindawi. f) TEM images and an interpretation scheme (bottom right) of star-like Au/Ag NPs. Reproduced with permission.^[180] Copyright 2007, Hindawi. g) Schematic of the synthetic processes of Cu NPs by T-shaped microflow chip at room temperature. Reproduced with permission.^[181] Copyright 2014, The Royal Society of Chemistry. h) Schematic representation illustrating the working mechanism of liquid metal NP formation, where liquid metal microdroplets formed at the T-junction are later gradually broken into NPs in the presence of acoustic waves. Reproduced with permission.^[184] Copyright 2018, Wiley-VCH.

process monitoring of NP formation, size optimization, and final characterization by their transverse and longitudinal relaxivity data. Iron oxide nanocrystals with sizes ranging from 23 to 70 nm have also been prepared via segmented flow using a gas slug microfluidic reactor (Figure 10b), in which the mixing

and reaction stages of the reactants are segregated for the fast mixing of precursor solutions as well as precise control over the reaction temperature and atmosphere to adjust the characteristics of the NP products.^[188] The type of gas slug was demonstrated to play an important role in regulating the morphology

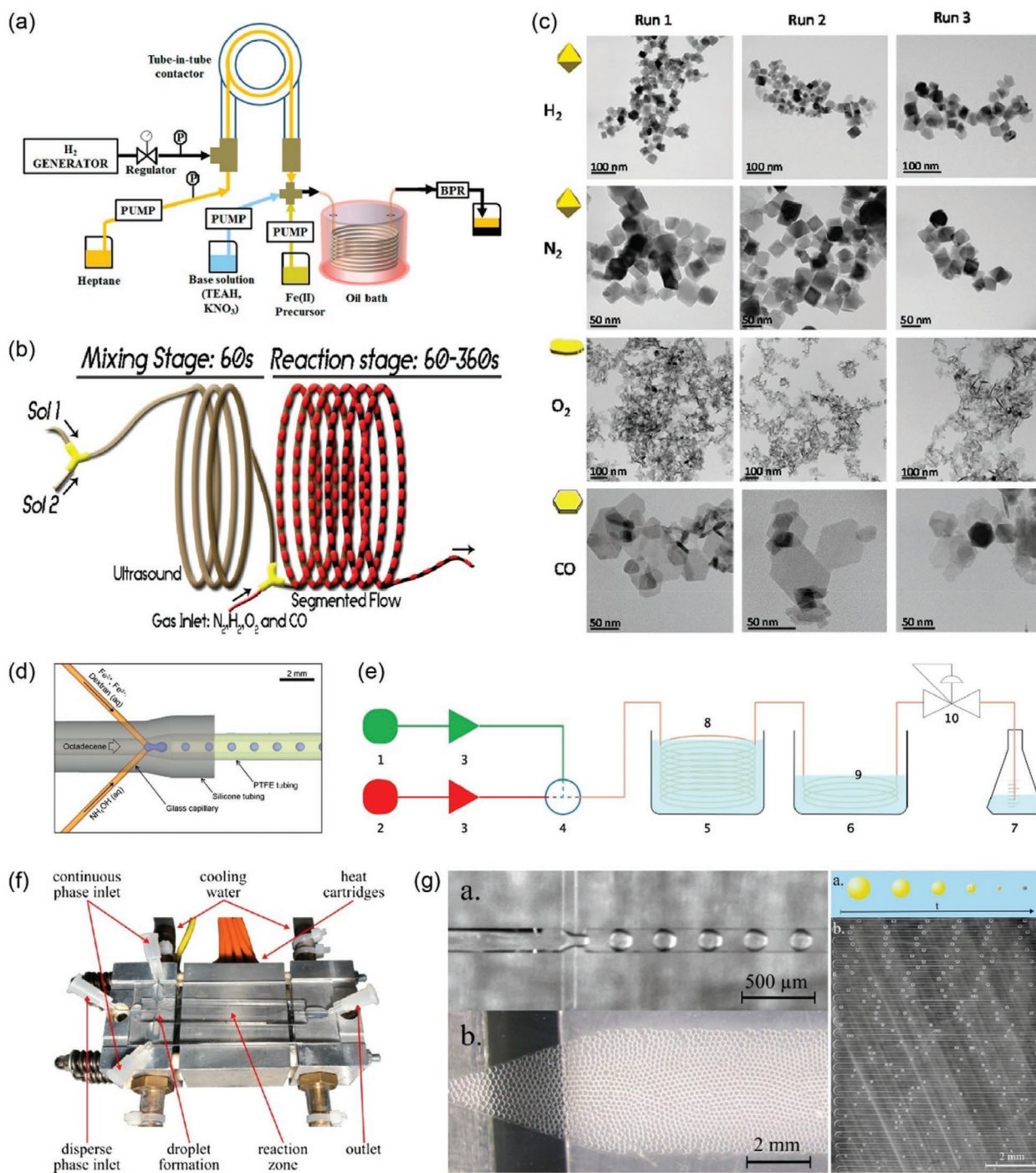


Figure 10. Microfluidic-based synthesis of metal oxide nanomaterials. a) Schematic of the experimental setup with H₂-saturated heptane for flow synthesis of iron oxide NPs. Reproduced with permission.^[186] Copyright 2020, MDPI. b) Schematic diagram of the microfluidic setup designed to produce magnetic NPs in gas-liquid segmented flow. Reproduced with permission.^[188] Copyright 2015, American Chemical Society. c) TEM images of magnetic NPs obtained using the microfluidic setup in (b) at different runs and under different gas environments (H₂, N₂, O₂, and CO). Reproduced with permission.^[188] Copyright 2015, American Chemical Society. d) Schematic of the capillary-based segmented flow reactor showing the injection of precursor solutions of Fe²⁺/Fe³⁺/dextran and NH₄OH into a continuous octadecene stream for the synthesis of iron oxide NPs. Reproduced with permission.^[189] Copyright 2012, The Royal Society of Chemistry. e) Schematic diagram of the experimental setup for the preparation of TiO₂ NPs (1—CO(NH)₂ solution, 2—TiOSO₄ solution, 3—advection pumps, 4—micromixer, 5—oil bath, 6—water bath, 7—triangle beaker, 8—steel tube for heating, 9—steel tube for cooling, 10—back-pressure regulator). Reproduced with permission.^[190] Copyright 2021, Chinese Society of Particology and Institute of Process Engineering, Chinese Academy of Sciences. Published by Elsevier B.V. f) Photograph of the temperature controlling module mounting with a microfluidic chip. Reproduced with permission.^[192] Copyright 2018, Elsevier Ltd. g) Droplet formation of precursor and benzyl alcohol in Fluoronox inside the microfluidic device (left) and the dissolution of benzyl alcohol in the continuous phase causing droplet shrinkage over time (right). Reproduced with permission.^[192] Copyright 2018, Elsevier Ltd.

of the iron oxide NPs, with H₂ and N₂ slugs leading to cubic NPs, O₂ and CO slugs resulting in the formation of spherical/rod and hexagonal NPs, respectively (Figure 10c). Iron oxide NPs coated with a polymer layer have also been prepared using microfluidic devices. By using aqueous solutions of Fe²⁺/Fe³⁺/dextran and NH₄OH as the two precursor solutions to induce the coprecipitation of iron oxide in a capillary-based droplet reactor (Figure 10d), Kumar et al. successfully obtained dextran-coated superparamagnetic iron oxide NPs with a mean diameter of 3.6 nm and narrow size distribution.^[189] The dextran layer not only stabilized the NPs but also improved their biocompatibility for biomedical applications.

TiO₂ NPs have been extensively fabricated through a hydrothermal process, in which the TiO₂ precursors crystalizes at high pressure and relatively low temperature, thus leading to low agglomeration, finer particle sizes, and narrower size distribution compared to other conventional procedures that require calcination, such as liquid-phase precipitation and sol-gel methods.^[190] However, a long reaction time is normally required for the preparation of TiO₂ due to the low thermal transmission rate and the slow hydrolysis of organic titanium reagents. This problem can be addressed by preparing TiO₂ NPs using a microfluidic reactor, which features a high mass and heat transmission and a more uniform mixing compared to batch processes. For example, Deng et al. successfully synthesized superfine anatase TiO₂ NPs with an averaged size of 5.3 nm using a microcurved-tube system (Figure 10e).^[190] In the study, TiOSO₄ and urea solutions were pumped into the microreactor and mixed in the tube. No reaction occurred until the mixed solution was heated at 120–200 °C to allow the hydrolysis of urea into NH₄OH and react with TiOSO₄ to form the TiO₂ precursor, which then undergoes a fluidic hydrothermal process in the hot tube to yield TiO₂ NPs. The whole fabrication process finished in 3.5 min, as compared to the conventional batch hydrothermal process that normally requires hours or even days. The authors have also reported the hydrothermal synthesis of CeO₂ NPs by using the same microfluidic experimental setup.^[191] In this case, the reagent solutions, NaOH and Ce(NO₃)₃, were pumped into the T-shaped mixer via the two inlets separately. The mixed solution was then led to a helical microreactor heated at a temperature ranging from 100 to 230 °C to generate CeO₂ NPs. Compared to the time-consuming traditional batch hydrothermal method that generally takes days to synthesize ceria NPs, a reaction time of only 8 min is needed for the microfluidic approach. Moreover, the addition of PVP as a capping agent into the reaction system was found to promote the conversion of ceria nanorods to nanocubes. By utilizing a droplet-based segment flow microfluidic reactor integrated with a computer-controlled heating and cooling system (Figure 10f,g), Stolzenburg et al. reported the synthesis of multiple types of metal oxide NPs.^[192] For example, zinc acetylacetonate hydrate and cerium trichloride solutions, which are the precursors for ZnO and CeO₂, respectively, were supplied to the microfluidic device to form segmented droplets dispersed in a fluorocarbon oil via flow focusing. By subsequently heating the device at a temperature ranging from 100 to 200 °C and precisely controlling the residence time of droplets, ZnO and CeO₂ NPs with diameters of 150 nm and 100 nm were produced.

3.4. Quantum Dots

Quantum dots (QDs) are 5–20 nm sized semiconductor nanocrystals with their excitons confined in all three dimensions.^[193] Due to this discrete energy level, QDs exhibit outstanding electronic and optical performances such as high fluorescence brightness, long fluorescence lifetime and good stability, etc. As a result, QDs have found various applications in the biomedical fields such as bioimaging, biosensing, and drug delivery,^[194,195] and their laboratory and industrial production has also been arousing increasingly more interests during the past decades. Compared to traditional batch procedures, microfluidics represents a relatively new but powerful platform for the precise production of QDs. The nucleation and growth of QDs can also be accurately regulated in microfluidic devices by adjusting the reaction parameters to control their size and composition, which are critical in determining their emission bands and width. As such, various QDs and QD-doped nanomaterials have been produced using microfluidics.

As the most numerous family of QDs, semiconductor QDs have been widely synthesized using microfluidics. Semiconductor QDs can be roughly classified into II–VI group (e.g., CdSe, Cds, CdTe, ZnS, ZnSe, ZnTe), III–V group (e.g., InP, InAs), IV–VI group (e.g., PbS, PbSe, SnS, SnSe), I–III–VI group (e.g., CuInS₂, CuInSe₂), IV group (Si, Ge), etc., by the groups of their constituent elements. In a pioneering work in 2002, Yen et al. reported the microfluidic preparation of CdSe, which is the most well-characterized colloidal semiconductor nanocrystal.^[196] Two precursor liquids: cadmium oleate and tri-*n*-octylphosphine selenide in a high-boiling solvent system were delivered into a continuous flow microreactor and combined in a mixing chamber (Figure 11a), before the mixture was led to a heat glass reaction channel (180–320 °C) to form CdSe QDs. By changing the precursor concentration, it was able to control the nucleation rate of the CdSe nanocrystals, therefore their sizes correspond to a wide spectral range. By developing a two-phase oscillatory segmented flow microprocessor integrated with a spectral detecting module (Figure 11b), Abolhasani et al. fabricated both II–VI and III–V group semiconductor QDs and studied the kinetics and mechanism of their nucleation and growth stages via in situ spectral characterizations.^[197] The effect of reaction time, precursor ratio, and temperature on obtained QDs was systematically investigated, providing valuable insights into the optimal conditions that can be potentially transferred to the large-scale manufacturing of semiconductor nanocrystals with reproducible quality. QDs with heterogeneous structures such as core–shell architecture can also be prepared using the flow-based approach. Beak et al. reported the synthesis of multiple III–V core–shell semiconductor QDs including InP/ZnS, InP/ZnSe, InP/CdS, and InAs/InP QDs using a continuous chip microreactor-based multistage platform (Figure 11c).^[198] The microreactor system consisted of six cascaded high-temperature and high-pressure silicon-pyrex microchip reactors that allow the sequential occurrence of six consecutive reactions including mixing, aging, growth, two shell formation steps, and an annealing process. Such a configuration allows the fabrication of core–shell QDs of comparable quality with those obtained from batch processes but in a much shorter reaction time. Besides, the reaction parameters can be

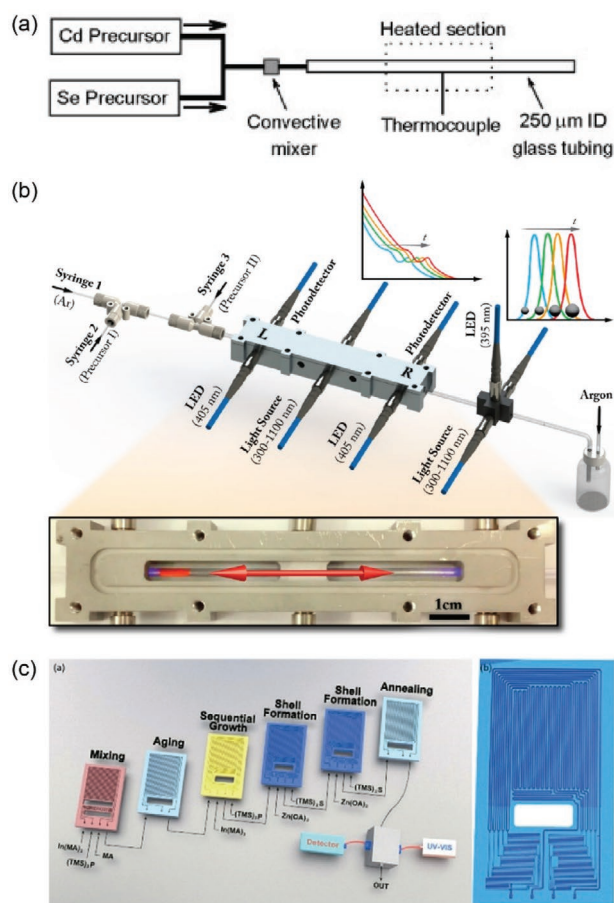


Figure 11. Microfluidic-based reactors for the synthesis of quantum dots. a) Schematic of the capillary microreactor for the synthesis of CdSe nanocrystals. Reproduced with permission.^[196] Copyright 2003, Wiley-VCH. b) Schematic of the oscillatory microprocessor for the synthesis of II–VI and III–V group semiconductor quantum dots. The Inset shows an image of a droplet oscillating inside the tubular fluorinated ethylene propylene reactor embedded within the aluminum chuck. Reproduced with permission.^[197] Copyright 2015, American Chemical Society. c) Schematic of the multistage microfluidic platform for the synthesis of InP/ZnS core-shell quantum dots. The first three stages are used for the synthesis of InP cores and the following three stages for the core-shell morphology (left). The ten subchannel design of the shell-formation microreactor (right). Reproduced with permission.^[198] Copyright 2018, Wiley-VCH.

easily screened using the flow-based platform to figure out the optimized conditions for QD nucleation and growth.

Carbon QDs, such as graphene QDs and multiple-graphene layered QDs, represent another important subclass of QDs. Compared to traditional semiconductor QDs, carbon QDs do not contain any metal elements, thus generally demonstrating better biocompatibility and lower toxicity, which are preferable for biomedical applications.^[199] Carbon QDs have also been synthesized using microfluidic approaches to improve the synthetic efficiency and quantum yields. By utilizing a continuous flow microreactor and anhydrous citric acid/ethylene-diamine as precursors, Rao et al. realized the rapid production of carbon QDs in less than 5 min, which was faster than most of previously reported methods.^[200] The additive concentration, flow rate, and reaction temperature were screened using the microreactor

to determine the optimal conditions, leading to the preparation of carbon QDs with a high quantum yield of 60.1%, which is comparable to or even greater than those obtained via hydrothermal approaches. Shao et al. synthesized carbon QDs with full-spectrum emission fluorescence from citric acid and urea solutions as precursors using a continuous flow microreactor.^[201] The microflow-based reaction greatly reduced the conventional reaction time from 12 to 24 h to 20 min, while the uniform and rapid mass transfer facilitated the production of smaller (average diameter of 2.88 nm) and more uniform carbon QDs than those synthesized in the autoclave.

4. Microfluidic Synthesis of Hybrid NPs

4.1. Polymer–Lipid NPs

Polymer–lipid hybrid NPs usually have a polymer core coated by lipid layers. The polymer core allows the encapsulation of drugs or imaging agents for high drug encapsulation, good stability, and sustained release properties, while the lipid surface takes advantage of the unique properties of lipids such as their excellent biocompatibility and biomimicking properties, and chemical tunability.^[202] Therefore, the combination of polymer and lipid in a hybrid NP makes good use of the attractive features of both polymer NPs and liposomes.^[203] Furthermore, they can encapsulate two therapeutic agents having different hydrophobicity by loading the hydrophobic one in the polymer core and the hydrophilic one in the lipid envelope to achieve the controlled release of both agents.^[97] Polymer–lipid hybrid NPs have great potential for drug delivery due to their attractive properties including high stability, high EE, efficient cellular uptake, and prolonged circulation.^[204] Microfluidics offers a powerful platform to precisely manipulate and control hybrid NP properties. Two approaches are available for making polymer–lipid hybrid NPs, that is, two-step or one-step methods. The two-step method makes polymer NPs first followed by a lipid bilayer or lipid multilayer coating.^[205,206] Alternatively, the one-step method synthesizes hybrid NPs by self-assembling polymer and lipid simultaneously.^[207]

Various microfluidic devices such as HFF, multistage microfluidic chip,^[208] parallelized swirling microvortex reactors,^[209] glass capillary-based microfluidic chips (Figure 12a),^[210] three-inlet microfluidic chips,^[211,212] and Tesla micromixer^[213] have been deployed for making polymer–lipid NPs. Sorafenib-loaded polymer–lipid NPs were synthesized using PLGA, lecithin, and DSPE–PEG 2000 in a glass capillary microfluidic device.^[210] Two immiscible solutions were injected into the capillary to co-flow and mix rapidly in the outer glass capillary leading to nanoprecipitation and formation of polymer–lipid NPs in one step. Hybrid NPs with a core–shell structure were observed. Also, they exhibited comparatively higher EE and better-controlled release of sorafenib compared to those NPs prepared using a bulk method.

Polymer–lipid NPs have been fabricated in an HFF device using either a two-step or one-step method. Uniform temperature-sensitive polymer–lipid hybrid NPs were synthesized via the two-step method by controlling the convective-diffusive mixing of two miscible NP precursor solutions, that is, a lipid

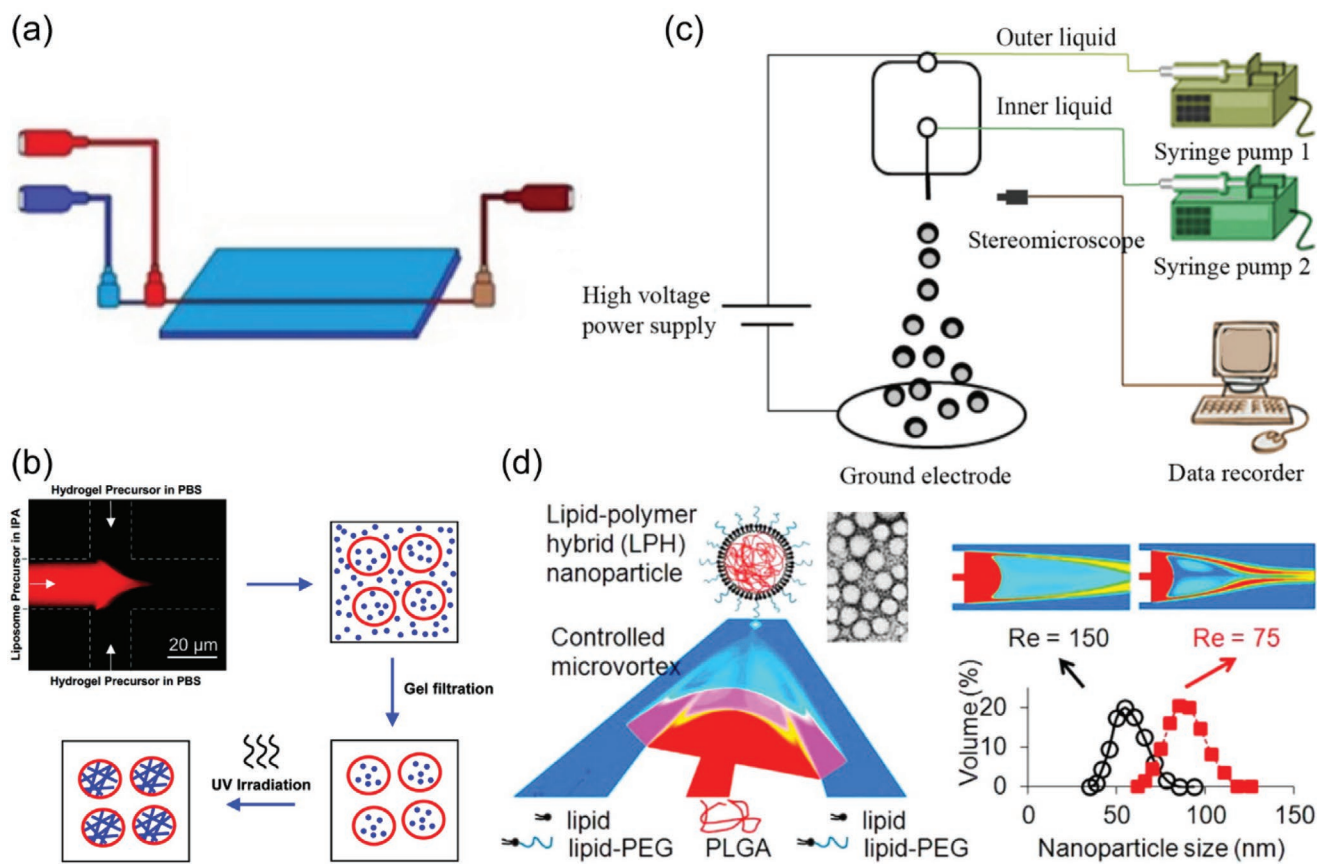


Figure 12. Synthesis of polymer–lipid NPs using microfluidic approaches. a) Schematic of glass capillary microfluidic device. Reproduced with permission.^[210] Copyright 2020, Elsevier B.V. b) Schematic of two-step fabrication of polymer–lipid hybrid NPs. Reproduced with permission.^[214] Copyright 2010, American Chemical Society. c) Schematic of the electro spray integrated with a microfluidic chip. Reproduced with permission.^[118] Copyright 2021, IOP Publishing. d) Schematic of a three-inlet microfluidic platform. Reproduced with permission.^[211] Copyright 2012, American Chemical Society.

mixture in isopropanol and a photopolymerizable polymer mixture in an aqueous buffer, thus forming lipid nanovesicles encapsulating the hydrogel precursors. The synthesized NPs collected from microfluidic synthesis were then irradiated with UV light to polymerize the hydrogel precursors into polymer cores (Figure 12b).^[214] Another study produced polymer–lipid NPs via a one-step HFF method for siRNA delivery. PEI-800 and cationic lipids were mixed in the HFF forming polymer–lipid hybrid NPs loaded with VEGF siRNA, and the resulting NPs achieved high gene silencing efficiency.^[215,216] Basically, the lipid/polymer solution was introduced from the middle channel while the siRNA solution was injected from two side channels and then mixed in an S-style channel. The final NPs synthesized were smaller with a narrower size distribution compared to the bulk method.

Polymer–lipid hybrid NPs have also been fabricated combining HFF with other active modules. For instance, drug-loaded PLGA/DPPG NPs were produced using an HFF device combined with electro spraying (Figure 12c).^[118] DPPG is a charged surfactant that can increase the stability of NPs. A mixture of DPPG and PLGA solution was introduced into the microfluidic device as an outer phase. DPPG spontaneously covers the surface of the PLGA core through electrostatic repulsion under an electric field, consequently forming a shell to

improve the stability of the hybrid NPs. HFF devices have been used in the production of polymer–lipid NPs for both RNA-based drug and vaccine delivery. Polymer–lipid hybrid NPs loaded with VEGF siRNA had an average smaller mean diameter and PDI when compared to those NPs produced using the bulk mixing method. The HFF produced NPs also exhibited higher cytotoxicity, more efficient cellular uptake and greater inhibition of tumor growth when compared to bulk mixing produced NPs, demonstrating the advantages of using microfluidic HFF devices for making NPs for drug delivery.^[215,216]

In addition to glass capillary microfluidic devices and HFF devices, a three-inlet microfluidic chip was developed for the one-step fabrication of polymer–lipid hybrid NPs with increased production throughput. Langer's group reported the synthesis of polymer–lipid hybrid NPs with enhanced productivity up to 0.3 g h^{-1} using a controllable microvortex platform with the three-inlet microfluidic chip. They used a highly diluted polymer solution (5 mg mL^{-1}) to avoid aggregation (Figure 12d).^[211]

Similarly, TPGS–PLGA hybrid NPs were also synthesized using the three-inlet microfluidic chip by microvortex-induced fast mixing, with PLGA dissolved in an organic solvent in the inner channel and an FDA-approved polymer d- α -tocopheryl polyethylene glycol 1000 succinate (TPGS) in the outer

channels.^[217] Compared to conventional microfluidic methods, microvortex can increase productivity significantly. The microvortex pattern can be controlled by changing the Reynolds number and the flow rate ratio of the outer solution to the inner solution.^[211,212]

In addition to polymer–lipid hybrid NPs, chitosan,^[213,218] and polycation polyethyleneimine (PEI)^[216] have also been used to form hybrid NPs. Chitosan/polymer hybrid NPs were synthesized using an HFF device to produce the chitosan NPs firstly, followed by the Eudragit FS 30D coating via a Tesla micro-mixer.^[213] On the other hand, liposomes can be first produced and then coated with chitosan, where both steps used the microfluidic device.¹⁸⁶ By utilizing the electrostatic interaction between positively charged polymer PEI and negatively charged siRNA, hybrid polymer-lipid NPs encapsulating siRNA can be fabricated by one step using a three-inlet HFF device.^[216]

4.2. Metal-Organic Frameworks (MOFs)

MOFs have been exploited as a new class of crystalline nanoporous materials in recent years.^[219] Extensive attention has been paid to expanding the microfluidics method beyond organic or inorganic NPs to more advanced materials such as MOFs.^[220] Compared to traditional porous materials, MOFs demonstrate many unique characteristics such as biodegradability, biocompatibility, flexible or tailorable pore size, and high surface area. With the careful selection of organic linkers and metal-based building blocks, it is possible to fine-tune the size, functionality, and geometry of the porous structures of MOFs, which makes MOFs a good candidate for drug delivery applications especially when the size of MOFs is reduced to the nanoscale.^[220,221]

Microfluidics is able to make MOFs with controlled morphology using a one-step continuous method.^[221,222] Lymph node and tumor-targeting aptamer-modified biozeolitic imidazolate framework (BioZIF-8) were synthesized using a one-step microfluidic method (Figure 13a).^[223] ZIF-8 loaded with different molecules (doxorubicin (DOX), small interfering ribonucleic acid (siRNA), and bovine serum albumin) were fabricated first, followed by aptamer modification of the BioZIF-8 surface in a microfluidic chip. This microfluidic method not only reduced the total production time from 15 h (using the conventional two-step method) to about 10 min but also increased the biomolecule loadings.

Microfluidic methods can also be used to control the structure of MOFs for further improving their performance in bio-applications. For example, enzyme–MOF composites were made in a microfluidic mixing device with a significantly improved enzyme activity (Figure 13b).^[222] The precise control of diffusion-based mixing was realized in a microfluidic laminar flow system containing a three-way mixing scheme, which created structural defects in the enzyme–MOF composites, resulting in enhanced enzyme activity due to increased substrate accessibility.

5. Drug Delivery Applications

5.1. Key Physicochemical Properties

Identifying the key physicochemical properties of NPs is important for engineering efficient drug delivery applications. Precise control over the identified key physicochemical properties plays a critical role in dictating the nano-bio interactions.^[151] Microfluidics offers a powerful tool for making NPs with tunable and controlled physicochemical properties by using different microfluidic devices and controlling their operation conditions.^[224]

One of the key physicochemical properties is the particle size of NPs, affecting their *in vivo* fate.^[87] More specifically, larger NPs (>200 nm) have been demonstrated to accumulate in the spleen and liver.^[225] While NPs under 150 nm can cross the endothelial barrier.^[66] Compared to NPs of 100 nm, NPs of 50 nm demonstrated superior penetration in cells *in vitro*, tumor spheroids *ex vivo*, and tumor xenografts *in vivo*.²¹² NPs of 30 nm were demonstrated to be ideal for the effective outcome of an immune response.^[226] Extremely small NPs of 6 nm can transfer quickly from lungs to lymph nodes and bloodstream, eventually being cleared by kidneys.²¹¹

Microfluidic methods are very effective at controlling the size of NPs, especially to produce NPs between 10 and 200 nm, which is the size range most related to systematic drug delivery.^[227] Fast mixing achieved by microfluidic methods enables the synthesis of NPs with small size and excellent stability.^[89] For example, liposomes with particle sizes ranging from 31 to 277 nm could be prepared using the microfluidic HFF devices.^[61,228] Bigger liposomes above 105 nm were observed to be excluded from deeper skin layers past the stratum corneum, while smaller liposomes between 31 and

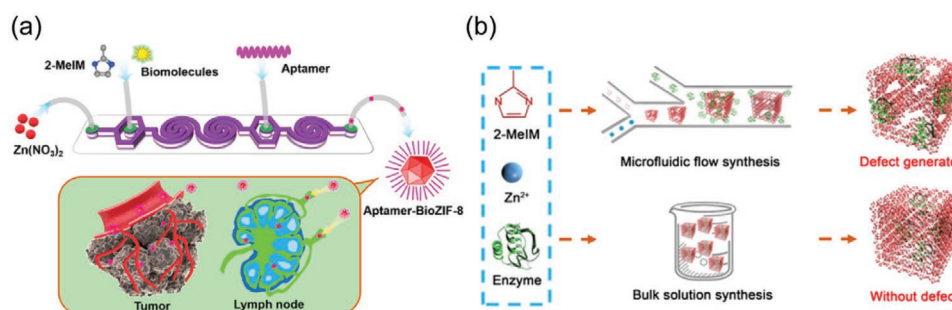


Figure 13. Synthesis of MOFs in microfluidic devices. a) Schematic of the fabrication of ZIF-8 MOFs via double spiral microfluidic devices. Reproduced with permission.^[223] Copyright 2021, American Chemical Society. b) Schematic of microfluidic laminar flow synthesis and bulk solution synthesis of enzyme–MOF composites. Reproduced with permission.^[222] Copyright 2020, The Authors, Published by American Association for the Advancement of Science.

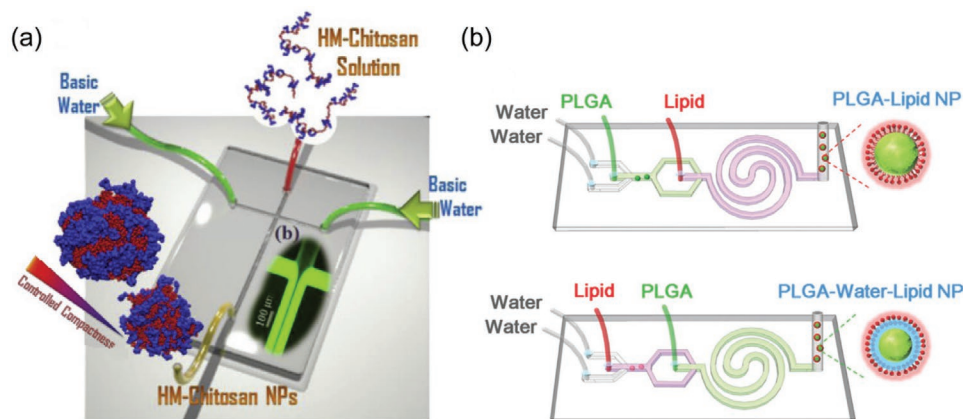


Figure 14. Microfluidic approaches for controlling NPs' mechanical properties. a) Schematic of the HFF device used for the synthesis of polymer NPs with controlled compactness. Reproduced with permission.^[234] Copyright 2013, Elsevier Ltd. b) Schematic of the two-stage microfluidic platforms for assembling polymer-lipid hybrid NPs with controlled rigidity. Reproduced with permission.^[204] Copyright 2014, Wiley-VCH.

41 nm exhibited considerably increased penetration. Similarly, the size of polymer NPs can also be controlled via the HFF device by varying flow rate, solvent, surfactant, and polymer composition and concentration.^[229] Considering the wide range of drug delivery applications of NPs, it is important and necessary to develop a microfluidic method that is able to produce NPs with tunable and reproducible particle size, so an NP library could be established to screen the optimal NP size tailored for a particular drug delivery application.

In addition to NP size, particle shape, surface properties, and mechanical properties play a critical role in regulating nano-bio interactions. NPs directly interact with biological systems on their surface when they are administered. The shape and rigidity of NPs affect their cellular uptake,^[230–232] release kinetics of the encapsulated drugs, and *in vivo* fate. Microfluidic methods allow tuning of size and shape of the generated droplets as well as producing NPs with desired surface textures.^[233] Microfluidic methods can also be used to control the NPs' mechanical properties such as compactness and rigidity (Figure 14a).^[234] For instance, a two-stage microfluidic platform was developed to produce polymer–lipid hybrid NPs with tunable stiffness by changing the amounts of interfacial water between the lipid shell and PLGA core through controlling the injection order of the PLGA and PEGylated lipid solutions. Polymer–lipid hybrid NPs with different rigidity were synthesized while keeping other properties the same, including surface properties, size, and chemical composition, for investigating the influences of rigidity of NPs on their cellular uptake (Figure 14b).^[204] Additionally, size-tunable monodisperse lipid–PLGA hybrid NPs can also be generated using this two-stage microfluidic chip by varying the flow rates.^[235]

5.2. Drug Encapsulation

5.2.1. Chemotherapy Drugs

It was reported that 40% of drugs currently on the market and approximately 90% of new drug candidates under development have poor water solubility especially chemotherapy drugs,

small inhibitors.^[236] To increase their water solubility, improve their bioavailability and reduce their side effects, chemotherapy drugs are commonly formulated using NPs. However, DL of these NPs is normally very low (less than 5% or even as low as 1%), which means that majority of NPs are the nanocarrier material which could lead to undesirable toxicity or adverse immune responses.^[237] Although most nanoformulations on the market or in clinical trials are based on liposomes with low DL ($\leq 10\%$) suggesting that low DL is not necessarily a hindrance to success, increasing numbers of recent studies indicate that high DL is beneficial for improved antitumor efficacy and favorable pharmacokinetics, especially for solid NPs other than soft liposomes.^[157,238] High DL can help to reduce the required administration volumes of NPs and reduce the toxicity from the nanocarrier itself, thus improving adherence.^[157,239,240] Microfluidic methods have been exploited to load various chemotherapy drugs in different NPs with enhanced EE and DL compared to bulk methods.

Paclitaxel is a commonly used antitumor drug against a broad spectrum of tumors, such as ovarian cancer, lung cancer, breast cancer, and glioma, but its poor water solubility makes it challenging for applications. Microfluidic methods have been used to make paclitaxel-loaded NPs with improved drug loading and encapsulation efficiency. One study developed a microfluidic HFF platform for the synthesis of paclitaxel-loaded nanocapsules via controlled self-assembly. The resulting nanocapsules comprised of a Pluronic copolymer shell and dendritic polyethylene core with uniform sizes of 50–200 nm. These nanocapsules achieved a relatively high loading of paclitaxel (9.9%) while providing a sustained release profile with high tunability.^[241] Moreover, the application of external forces within a microfluidic device can facilitate the control of morphology, size, and internal crystallinity of polymer NPs for drug delivery.^[242] It was reported that the encapsulation efficiency and release rate of paclitaxel-loaded polymer NPs prepared by a two-phase microfluidic reactor were strongly dependent on both the flow rate and the block copolymer composition (Figure 15a).^[243] In another study, a microfluidic chip combined with an electric field was used to produce paclitaxel-loaded polymer NPs with a core–shell structure having an encapsulation efficiency of above

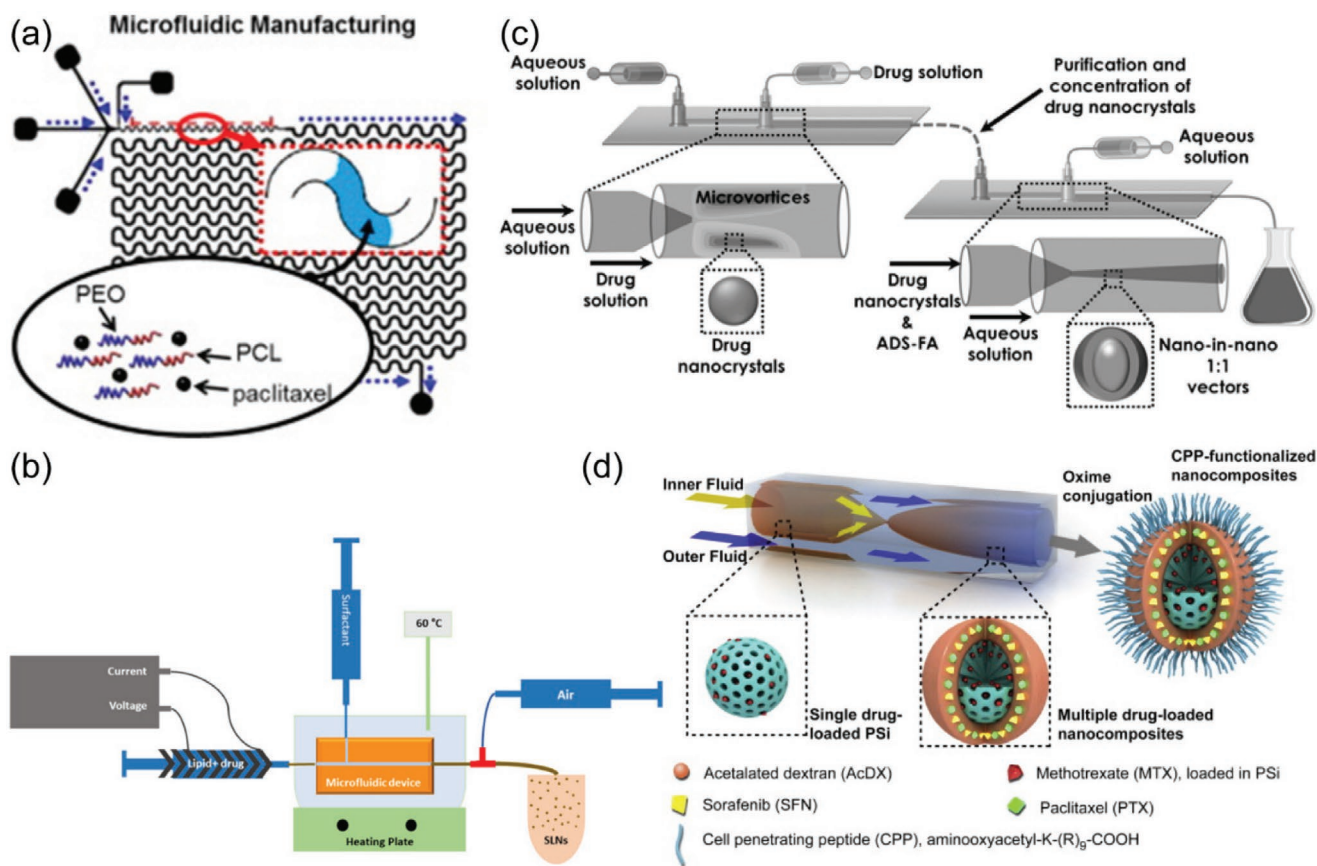


Figure 15. Synthesis of chemotherapy drug-loaded NPs using microfluidic methods. a) Schematic of paclitaxel-loaded polymer NPs prepared by a two-phase microfluidic reactor. Reproduced with permission.^[243] Copyright 2017, Elsevier Inc. b) Schematic of the production of paclitaxel-loaded solid lipid NPs via glass capillary-based microfluidic chip. Reproduced with permission.^[92] Copyright 2020, Acta Materialia Inc., Published by Elsevier Ltd. c) Schematic of the multistep microfluidic nanoprecipitation of sorafenib-core polymer-shell NPs. Reproduced with permission.^[112] Copyright 2017, Wiley-VCH. d) Schematic of the process to synthesize CPP-functionalized multidrug-loaded PSI@AcDX-CPP. Reproduced with permission.^[244] Copyright 2014, Elsevier Ltd.

90% and drug loading of 7.5%.^[118] The morphology, size, and encapsulation efficiency of NPs can be easily optimized through the precise control of operating parameters including flow rate ratio, PLGA concentration, and working voltage of the electric field. The obtained NPs showed a slow-release profile, which improved the bioavailability of paclitaxel and reduced its toxicity.^[118] Additionally, paclitaxel can be loaded in lipid NPs using a glass capillary-based microfluidic chip with an encapsulation efficiency of 54% and drug loading of 1.4% (Figure 15b).^[92] The obtained paclitaxel-loaded lipid NPs showed a sustained release and higher cytotoxic effect in 2D and 3D cell models compared to free paclitaxel.

Besides paclitaxel, doxorubicin,^[245] 5-fluorouracil,^[116] and sorafenib (SFN)^[210] have also been widely used as anticancer drugs for making drug-loaded NPs using microfluidic methods. Generally, microfluidic nanoprecipitation produces NPs with drug loading lower than 10%. The sorafenib-loaded lipid NPs with encapsulation efficiency of 79% and drug loading of 1.04% were produced using a glass capillary-based microfluidic chip.^[92] The simultaneous precipitation of polymer/lipid and hydrophobic drugs limited the space in the polymer/lipid matrix to incorporate hydrophobic drugs. In contrast, core-shell

spermine-functionalized dextran NPs with sorafenib-loaded and folic-acid-conjugated (SFN@ADS-FA) were generated with a very high sorafenib drug loading of 58.4% via a microfluidic sequential nanoprecipitation (Figure 15c).^[112] The synthesized SFN@ADS-FA NPs consisted of a sorafenib drug core and a polymer shell at a ratio of 1:1, showing high drug loading, high stability in serum, pH-responsive fast dissolution, and good biodegradability. Basically, the drug nanocrystals were produced first, then the ADS-FA precipitated and deposited onto the surface of drug nanocrystals upon mixing the solvent and antisolvent fluids, resulting in the formation of the sorafenib-core polymer-shell NPs. Their half-maximal inhibitory concentration was approximately 54 times lower than the low drug loading NPs, indicating the higher efficacy of the high drug loading NPs.^[112]

Intrinsic or acquired multidrug resistance (MDR) remains a main cause of the failure of cancer chemotherapy, presenting a big challenge for current chemotherapies.^[246] Encapsulation of chemotherapeutics and MDR modulators concurrently in NPs offers a new strategy to overcome the MDR.^[225] Moreover, combination therapy of multiple drugs for synergistic effects benefits the treatment of complicated diseases, such as cancer.^[247]

For instance, the combination therapy of cisplatin and irinotecan, two routinely used drugs, showed synergistic effects with improved anticancer efficacy.^[248] Microfluidics provides an ideal platform for the synthesis of NPs encapsulating multiple drugs with a ratiometric control. Although cisplatin and irinotecan have different chemical and physical properties, they were effectively co-loaded into the same polymer NP. The more hydrophilic drug cisplatin was conjugated to the backbone of a polymer followed by the encapsulation of the hydrophobic irinotecan via a single-step nanoprecipitation in a microfluidic device.^[249] The obtained two drug-loaded NPs were around 55 nm with a low polydispersity index of about 0.04 owing to the fast mixing in the microfluidic devices. Their strong synergistic cytotoxicity was observed when incubating with cancer cells. Additionally, a nanocomposite comprising of an encapsulated PSi NP and an acid-degradable acetalated dextran (AcDX) matrix was synthesized using a one-step microfluidic self-assembly approach. The obtained PSi@AcDX composites can be simultaneously loaded with multiple chemotherapy drugs having different physicochemical properties with a ratiometric control, including paclitaxel, sorafenib, and methotrexate. The release kinetics of these three drugs was mainly controlled by the disintegration rate of the outer AcDX matrix (Figure 15d).^[244] The HFF device was able to produce multiple cargos-loaded NPs as well, for instance, the synthesis of multifunctional targeting nanocarriers for cancer drug delivery, diagnostic imaging, and hyperthermia treatment simultaneously.^[250] The nanocarriers comprised of PLGA chains conjugating with radioactive bisphosphonate tracer molecules as the bone-targeting moiety, followed by loading with paclitaxel and superparamagnetic iron oxide NPs as an MRI contrast agent using the HFF device. The obtained NPs have potential for theranostic applications in bone cancers treatment.

5.2.2. Gene Therapeutics

Gene therapy employs genetic materials such as DNA or RNA as therapeutics for genetic, acquired, and infectious diseases. Although gene therapy has great potential, the lack of efficient and safe gene delivery methods limits its clinical applications. Gene delivery often uses recombinant viruses as delivery vectors and nanocarriers as delivery vehicles. The nonviral gene delivery method using nanocarriers such as liposomes, lipid NPs, polypeptides, and polymers NPs are able to protect the genetic material from nucleolytic enzymes, extending their lifetime in the blood, and delivering the genetic material to a specific tissue or cell.^[251] Compared to viral delivery vehicles, inert nanocarriers are normally much safer but suffer insufficient delivery efficiency.^[252] Among the wide variety of genetic materials, small interfering RNA (siRNA) and messenger RNA (mRNA) have broad potential as therapeutics.^[226] Recently, the clinical translation of mRNA and siRNA therapeutics has been improved significantly as a result of the developments of NPs.^[253] However, delivery of siRNA and mRNA in vivo remains challenging due to their poor stability. Compared to liposomes, lipid NPs show improved stability, and their rigid structure also assists deeper cellular penetration.^[79] Therefore, lipid NPs represent the most clinically advanced mRNA delivery vehicles.

The two approved SARS-CoV-2 mRNA vaccines both employ lipid NPs consisting of cationic or ionizable lipids, which have been studied extensively to deliver siRNA and mRNA due to their high encapsulation efficiency, effective cytosolic delivery as well as simple industrial production.^[226]

While cationic lipids can preserve their charges despite changes in pH, ionizable lipids only display positive charges via protonation of amines when the pH is decreased. Positively charged polymers such as polycation polyethylenimine (PEI) have also been used for mRNA and siRNA delivery.^[216] In addition, polyamidoamine (PAMAM) or polypropylenimine-based dendrimers, cell-penetrating peptides (CPPs), and other materials have been investigated for their potential as vehicles for intracellular delivery of gene materials.^[253]

Conventional methods for synthesis of siRNA or mRNA-loaded NPs are based on bulk mixing of cationic components and RNA solutions, which is an uncontrolled process typically including multiple steps, leading to poor reproducibility. In contrast, microfluidic methods with improved mixing can produce high-quality siRNA or mRNA-loaded NPs with improved biological efficiency than the bulk method.^[254] The success of lipid NPs for mRNA and siRNA drug delivery has set a milestone for microfluidics to produce NPs in a commercial context. Patisiran, a lipid NP-based siRNA drug, was the first siRNA drug approved by the FDA, which was prepared using a pH-sensitive cationic lipid based on a microfluidic approach. Furthermore, production on an industrial scale can be achieved using microfluidic continuous synthesis.^[255] HFF method has been usually used to produce siRNA-loaded NPs. In one study, VEGF siRNA-loaded hybrid polymer–lipid NPs were prepared in an HFF device with a smaller size and a narrower size distribution compared to the NPs synthesized using the bulk method.^[256] They showed low vehicle cytotoxicity and potent tumor cell inhibition in vitro and exhibited prolonged blood circulation and greater down-regulation of VEGF mRNA and protein levels as well as greater tumor inhibition in a xenograft tumor model compared to free VEGF siRNA.^[216] Similarly, another study reported the synthesis of small (≈ 38 nm) nucleic acid-loaded lipid NPs using a HFF device, which exhibited higher encapsulation efficiency, a narrower size distribution, and higher stability in blood plasma and serum compared to those NPs synthesized using the bulk mixing method.^[257]

Lipid NPs have also shown numerous advantages for mRNA delivery in biocompatibility, simplicity of formulation, and better stability. During the SARS-CoV-2 pandemic, the emergency use authorization (EUA) by the FDA for two mRNA-based vaccines BNT162b2 (Pfizer-BioNTech) and mRNA-1273 (Moderna) has been a significant milestone for NP drug delivery.^[78] The success of the BNT162b2 vaccine with about 95% efficacy in phase III clinical trials would not have been possible without the use of lipid NPs.^[79] Furthermore, the BNT162b2 vaccine also benefited from its continuous production with parallelization of 100 static mixers, named an impingement jet mixer (IJM), which have been used to increase vaccine productivity at their site in Kalamazoo (US) to 100 million doses/month.^[258] Lipid NPs were used to improve the stability of mRNA by protecting it from ribonucleases and enabling the delivery of undamaged mRNA to the target site. Typically, purified mRNA is mixed with lipids in an IJM microfluidic device to form

mRNA-loaded lipid NPs. Fast mixing provided by a microfluidic device induces the precipitation and self-assembly of lipid NPs while encapsulating mRNA instantly during self-assembly.^[78]

5.3. Drug Delivery Applications

5.3.1. Cancer Drug Delivery

A wide variety of NPs have been developed for cancer drug delivery. Compared to bulk methods, microfluidic approaches are so versatile, robust, reproducible, and scalable that can be used to synthesize NP libraries with precisely controlled and systematically varied properties (e.g., size, charge, and surface properties) for screening the optimal formulations for cancer drug delivery.^[259] Moreover, microfluidic approaches have been developed to synthesize NPs with tunable compactness thus controlling the release property of drug-loaded NPs,^[234] and to tune the rigidity of lipid-polymer hybrid NPs to improve their therapeutic efficiency.^[204]

Microfluidics provides a facile strategy to develop libraries of nanocarriers with designed surface properties, which have been recognized to play a vital role in affecting NP pharmacokinetics and biodistribution. For example, anionic NPs usually show considerably prolonged circulating half-lives. In contrast, highly cationic NPs are quickly cleared from circulation. However, the presence of cationic surface charge facilitates the disruption of endo/lysosomal membranes, thus improving the endo/lysosomal escape of NPs after cellular uptake.^[225] This intricate interplay between NP charge and their nano-bio interactions makes it important to design NPs purposely for particular cancer drug delivery application.

Long blood circulation time is a prerequisite for cancer drug delivery to achieve enhanced tumor accumulation. NPs are often modified with polyethylene glycol (PEG) or coated with cell or vesicle membranes to prolong the circulation time for cancer drug delivery applications.^[260] Additionally, NPs can be decorated with targeting ligand to improve targeted drug delivery. For example, surface coating of natural cellular or exosomal membranes (EMs) onto polymer NPs can extend their circulation time by evading immune surveillance (**Figure 16a**). A one-step microfluidic sonication method was used to break the structure of natural EM while reassembling EM over PLGA cores to form core-shell structured EM-coated PLGA NPs. The resulting NPs showed not only a prolonged *in vivo* circulation time due to the surface coating of EM but also a high tumor targeting efficiency benefiting from the surface binding of AS1411 aptamers that targeted nucleolin on cancer cells membrane.^[261] However, it was observed that the introduction of targeting ligands to some nanocarriers such as PEG-PCL polymer micelles, was not effective because most of the micelles were rapidly disassembled in the bloodstream after *in vivo* administration. Therefore, the stability of surface-functionalized nanocarriers is vital.^[262]

In addition to the combination of two different surface modification strategies, the synergistic effect from two targeting ligands, or one targeting ligand combined with a cell-penetrating ligand can improve cancer drug delivery as well. However, the dual-ligand targeting strategy remains controversial

because of the complicated interplay between numerous factors including the selection of two ligands, their ratios, densities, and length matching, etc. Microfluidics makes it simple and straightforward. A one-step microfluidic technology was exploited to produce libraries of PLGA NPs with diverse properties such as ligand density, ratio, and length to screen their targeting efficiency (**Figure 16b**).^[259] A series of single- and dual-ligand targeted polymer NPs with hyaluronic acid and acid folic as the two targeting ligands were designed and successfully manufactured using an HFF device. All the synthesized NPs had sizes of 70–90 nm, low PDI (0.053–0.221), and negative charges (-25.9–7.8 mV). The optimal dual-ligand targeted NPs showed the highest targeting specificity both *in vitro* and *in vivo*. Similarly, Ran et al. reported the production of a library of single- and dual-ligand liposomes with systematically varied properties including size, zeta potential, targeting ligand, ligand ratio, and ligand density using the HFF method. A targeting ligand folic acid and a cell-penetrating peptide transactivating transcriptional activator (TAT) were utilized to obtain the best synergistic targeting effect.^[35,74] These two studies demonstrated the versatility of microfluidic methods in engineering libraries of multifunctional NPs with controlled properties.

Drug release solely relying on slow diffusion and degradation is generally insufficient in cancer drug delivery applications. The ideal release profile of drug-loaded nanocarriers is a minimal release during circulation and in healthy tissues but a quick release at targeting sites.^[263] In addition to targeted drug delivery strategies, stimuli-responsive drug release is highly desirable for improving the efficacy of cancer drug delivery. The stimuli-responsive property of NPs relies primarily on the microenvironments in cells, tissues, or organs within the human body, e.g., different pH in stomach and colon, different glutathione concentrations in normal and cancer cells, different temperature in healthy and inflammable tissues, etc. Among the different types of stimuli, pH is one of the earliest and widely studied stimuli for cancer drug delivery applications, due to the very different pH from organs to compartments in a cell.^[155] For instance, the pH gradients in the tumor microenvironment (pH 5.7–7.0 in tumor tissues, compared to pH around 7.4 in normal tissues) have been exploited to design pH-responsive NPs to achieve higher drug concentrations in cancer cells.^[264]

Taking advantage of the capability of microfluidic methods in controlling the key properties of drug-loaded NPs, Baby et al. used a 3D tubing microfluidic device to synthesize curcumin-loaded shellac NPs with tunable DL from 20% to 57% and high encapsulation efficiency, through a sequential nanoprecipitation process.^[155] These curcumin-loaded shellac NPs remained very stable under acidic conditions (pH 4.5) for at least 10 days but released the curcumin at neutral pH in a sustained manner due to the pH-responsive property of shellac. Therefore, these stable curcumin-loaded shellac NPs have potential in oral drug delivery for colon cancers. Additionally, the pH-responsive release property can be achieved by controlling the compactness of nanocarriers via microfluidic synthesis. For example, the hydrophobically modified chitosan (HMCS) via N-palmitoyl groups can be used to encapsulate hydrophobic anticancer drugs such as paclitaxel using an HFF device with

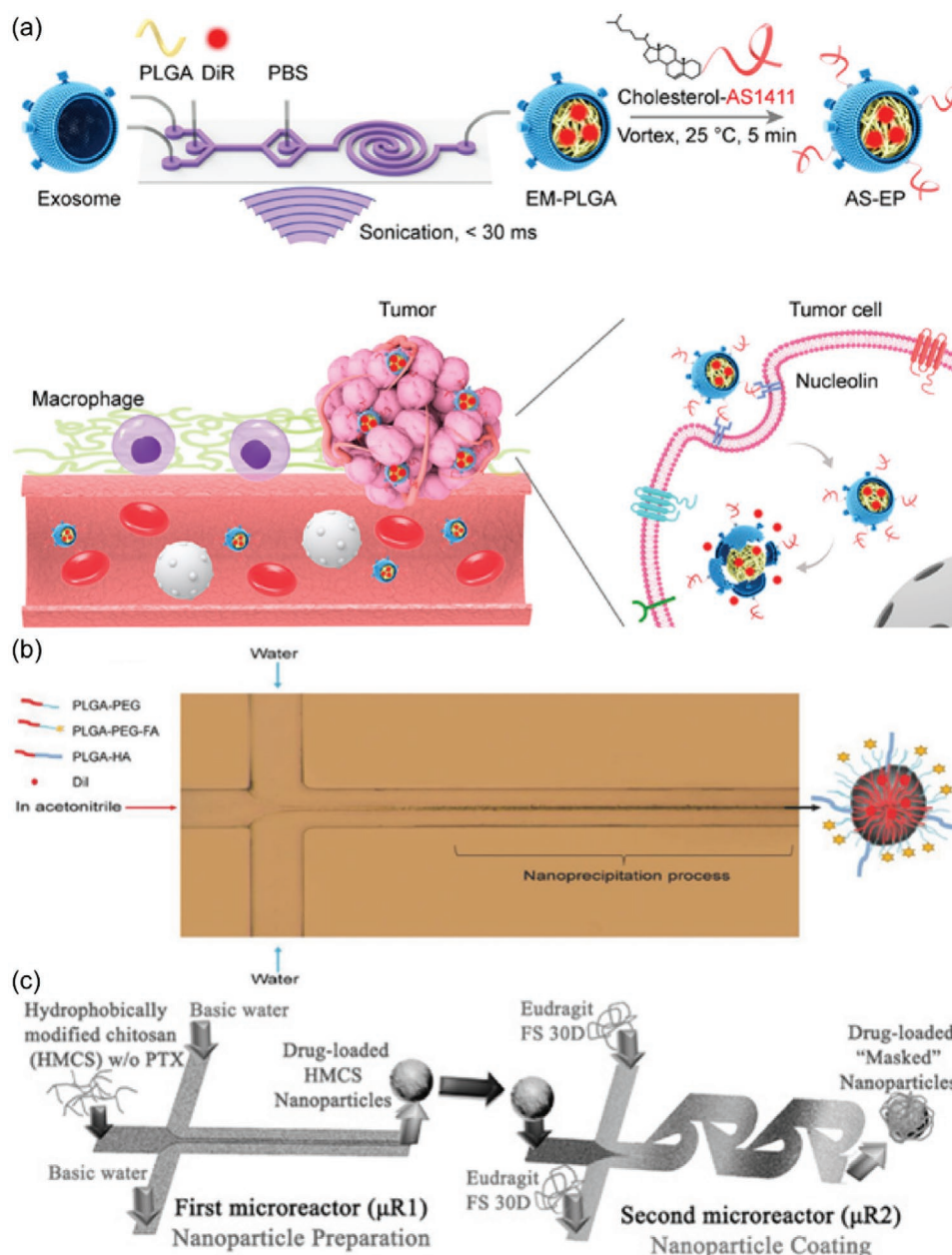


Figure 16. Microfluidic production of NPs for cancer drug delivery. a) Schematic of EM-coated PLGA NPs conjugated with AS1411 aptamers for extended circulation in the blood and improved tumor targeting. Reproduced with permission.^[261] Copyright 2020, American Chemical Society. b) Schematic of the HFF device for synthesizing a combinatorial library of single and dual-ligand NPs. Reproduced with permission.^[259] Copyright 2018, Wiley-VCH. c) Schematic of the dual microfluidic platform used to synthesis pH-responsive paclitaxel-loaded HMCS NPs. Reproduced with permission.^[213] Copyright 2016, Wiley-VCH.

an encapsulation efficiency of above 95%. These microfluidic manufactured paclitaxel-loaded HMCS NPs showed a low release rate at pH 7.4 due to their compact nanostructures, which was attractive for long-term circulation stability. However, when these paclitaxel-loaded HMCS NPs were exposed to pH 5.5, the NPs released the paclitaxel over an order of magnitude faster.^[126] Their paclitaxel release profile was observed to be effectively controlled by the compactness of the NPs.^[234] Moreover, microfluidics provides an alternative strategy to achieve pH stimuli-responsive release by coating a pH-sensitive

layer onto the prefabricated drug-loaded NPs to tailor the pH-responsive range (Figure 16c).^[213] A HFF device was used to synthesize paclitaxel-loaded HMCS NPs, and basic water was employed to induce the NP self-assembly. Then, a Tesla micro-mixer was used to make a pH-sensitive Eudragit FS 30D layer coating onto the paclitaxel-loaded HMCS NPs for colon drug delivery application. The paclitaxel-loaded HMCS NPs manufactured and coated via the dual microfluidic platform demonstrated improved cellular uptake during pH changes compared to those produced by a bulk method.

5.3.2. Other Diseases

In addition to cancer drug delivery, microfluidic methods have been exploited widely to deliver other drugs such as coenzyme Q10 for the prevention and treatment of ischemic diseases,^[265] efavirenz for the treatment of human immunodeficiency virus (HIV),^[266] Mithramycin A for the treatment of hematological diseases,^[267] dexamethasone for regulating osteogenic differentiation of mesenchymal stem cells,^[134] metformin hydrochloride (MET) for diabetes therapy,^[136] streptokinase for thrombolysis disease therapy,^[135] hydromorphone and ketamine for pain relief,^[206] azithromycin (a macrolide antibiotic) against biofilm-forming,^[212] etc.

Based on the different physicochemical properties of these drugs, liposomes, PLGA NPs, chitosan NPs, and hybrid lipid-polymer NPs have been frequently used to formulate drug-loaded NPs via various microfluidic methods. A microfluidic device incorporating a baffled mixer named invasive lipid NP (iLiNP) production device was used to load the coenzyme Q10 in liposomes, which allowed the production of small-sized homogenous coenzyme Q10-loaded liposomes with good reproducibility (Figure 17a).^[265] The efavirenz-loaded PLGA NPs produced through microfluidics showed reduced size, comparable polydispersity, less negative zeta-potential, higher encapsulation efficiency of above 80%, and higher drug loading of 10.8% compared to the NPs synthesized using a bulk method. The efavirenz-loaded PLGA NPs produced by the microfluidic method also demonstrated a sustained in vitro efavirenz release (Figure 17b).^[266] A HFF device was used to load the DNA-binding drug, mithramycin, in Pluronic block copolymers based polymer NPs,^[267] to load streptokinase in chitosan NPs,^[135] as well as to synthesize crosslinked carboxymethyl chitosan NPs containing MET.^[136] The size of MET-loaded chitosan

NPs was around 77 nm with a narrow size distribution. These NPs showed a high encapsulation efficiency of around 90% and controlled drug release properties. Moreover, the in vivo assessments of MET-loaded chitosan NPs illustrated a decreased blood glucose level of 43.58% and an increased body weight up to 7.94% for diabetic rats when compared to the free MET.^[136] Besides the HFF device, a two-stage microfluidic method was used to fabricate hydromorphone/ketamine-loaded hybrid lipid-polymeric NPs.^[206] Furthermore, ultrasmall azithromycin-loaded TPGS-PLGA hybrid NPs were fabricated using a trident-shaped microfluidic chip, demonstrating its capability in overcoming multiple barriers, and achieved sustained release of antibiotics in the surrounding area of biofilm-forming bacteria (Figure 17c).^[212]

6. Conclusions and Outlook

Significant research interests have been drawn to both microfluidics and NPs for more than two decades. However, microfluidics has been mainly directed toward analytical applications such as analysis, diagnosis, due to its unique characteristics such as using samples of picoliter (or less) scale, rapid mixing, precise control over the addition of reagent and reaction conditions, and cost-effectiveness, as its application in synthesis and production has been limited by its production scale. On the other hand, the concept of NPs for drug delivery applications has been around for more than two decades since the first clinical approval of Doxil using nanosized liposomes for cancer therapy, but nanomedicine has never really lived up to its promise. Until COVID-19, the success of the first nanotechnology-enabled mRNA vaccine has really put both microfluidics and nanomedicine in the spotlight, highlighting the great

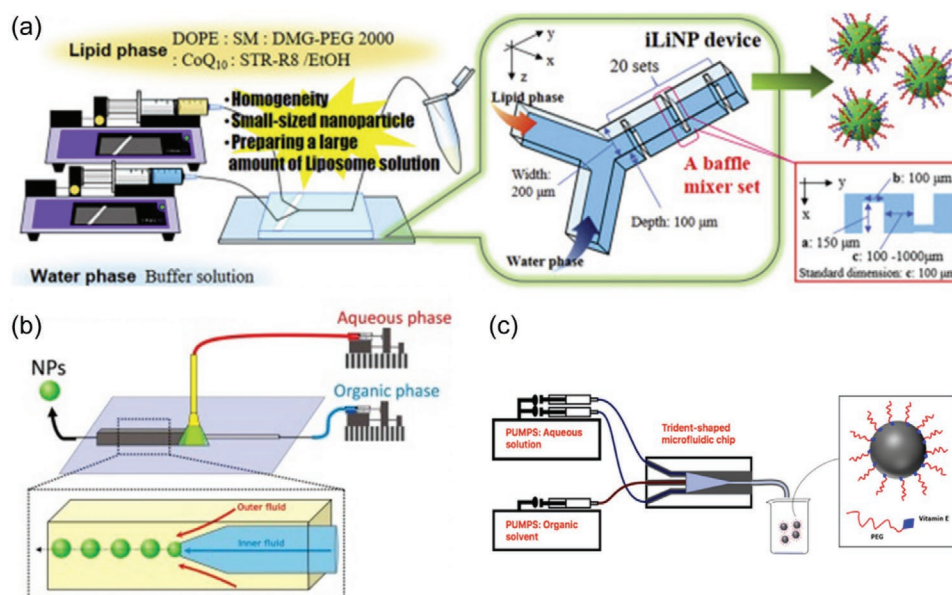


Figure 17. Microfluidic synthesis of NPs for other drugs delivery. a) Schematic of the preparation of the coenzyme Q10-loaded liposomes. Reproduced with permission.^[265] Copyright 2019, Published by Elsevier Inc. on behalf of the American Pharmacists Association. b) Schematic of production of efavirenz-loaded PLGA NPs. Reproduced with permission.^[266] Copyright 2018, Elsevier B.V. c) Schematic of preparation of ultrasmall azithromycin-loaded TPGS-PLGA hybrid NPs prepared by the trident-shaped microfluidic chip. Reproduced with permission.^[212] Copyright 2019, American Chemical Society.

potential of using microfluidics for making NPs for pharmaceutical applications.

Microfluidics holds great promise in making various kinds of NPs, especially for those based on single-step synthesis mechanisms. For example, most organic NPs are synthesized in microfluidic devices based on mixing-induced nanoprecipitation. It is a single-step, easy and facile process. More importantly, such a simple microfluidic method can be used for making multifunctional NPs depending on the composition of the initial precursor solution. For example, lipid or polymer NP libraries with systematically varied properties (charge, surface properties) can be produced by using PEGylated, targeting ligand conjugated lipid or polymers at different ratios. Furthermore, the size and size distribution can be tuned by varying the operating conditions such as flow rate, flow rate ratio, lipid or polymer concentrations. Therefore, microfluidics offers a very powerful tool to synthesize NP libraries with systematically varied properties which allow the screening and identification of the optimal formulation for drug delivery applications.

To make it viable for large-scale production, instead of scaling it up by using bigger volume, microfluidic devices can be replicated to achieve parallelization (or numbering-up) of hundreds or thousands of the exact same devices, allowing the continuous synthesis and the increase of productivity. This capability of microfluidics really revolutionizes the traditional concept of process scaling up and large-scale production, and significantly shortens the translational development from laboratory-scale synthesis to industrial-scale manufacturing. Furthermore, with the rapid development of new technologies, such as atomization, digitization, machine learning for optimization, the whole manufacturing process using microfluidics can be automated, ensuring precise control over the qualities of NPs for drug delivery applications.

The continuing progress in microfluidics and nanomedicine promises to create unparalleled opportunities for microfluidic synthesis of NPs for various drug delivery applications. Based on the experiences and lessons from previous laboratory and clinical studies, microfluidic nanomedicine can be further improved in several aspects. Firstly, the NP concentration synthesized using microfluidic approaches needs to be further increased. Many new microfluidic approaches have been developed to improve production throughput, but not the NP concentration of the final product. On the other hand, high NP concentration may compromise the mobility of NPs in microfluidic devices, resulting in NP deposition and sedimentation on the microchannel then fouling and clogging of the microchannel.^[268] Therefore, the development of new coatings with low nonspecific binding and high solvent resistance, and the introduction of non-invasive external fields (e.g., acoustic focusing,^[269] microwave,^[270] ultrasonic,^[271] magnetic,^[272] electrical fields,^[273] etc.) may provide new opportunities for microfluidic approaches in producing NPs with increased concentrations. Second, the integration of multiple processes in a single microchip could be further developed to include NP synthesis, purification, sample concentration, online analysis, etc. Most of the current NPs synthesized using microfluidic devices need further off-chip purification, concentration steps, and off-line NP quality control. Integrated multi-process microfluidic systems will allow short processing time, continuous production as well as strong automation potential. Third, despite the wide

application of microfluidics for the synthesis of inorganic NPs, their real application in drug delivery is quite limited. Although most of the clinical translation efforts focus on organic NPs, the immense potential of inorganic NPs for future biomedicine is undisputed, which is evidenced by the fact that more than 25 inorganic nanomedicines have been approved since the success of the first inorganic nanomedicine CosmoFer in 1974.^[274] Therefore, there are enormous opportunities for the continuous and large-scale production of inorganic NPs for future clinical translation. Finally, although microfluidics offers various advantages for making NPs for drug delivery, it requires expertise and iterative process optimization to achieve the successful synthesis of NPs with desirable properties. The convergence of microfluidics and machine learning will enable the prediction of NP properties based on the design parameters of microfluidic devices, it will also eliminate expensive design iteration and process optimization. More importantly, accurate NP property prediction will facilitate the design of automatic control tools for NP synthesis.

Acknowledgements

Y.L. and G.Y. contributed equally to this work. This work was supported by Australian Research Council Discovery project (DP200101238, DP210103079) and National Health and Medical Research Council Investigator grant (APP2008698).

Open access publishing facilitated by The University of Adelaide, as part of the Wiley - The University of Adelaide agreement via the Council of Australian University Librarians.

Conflict of Interest

The authors declare no conflict of interest.

Keywords

drug delivery, lipids, microfluidics, nanomedicine, nanoparticles, polymers

Received: October 27, 2021

Revised: December 20, 2021

Published online: April 9, 2022

- [1] J. Shi, P. W. Kantoff, R. Wooster, O. C. Farokhzad, *Nat. Rev. Cancer* **2017**, *17*, 20.
- [2] R. J. Wilson, Y. Li, G. Yang, C.-X. Zhao, *Particuology* **2021**, *64*, 85.
- [3] C.-X. Zhao, L. He, S. Z. Qiao, A. P. Middelberg, *Chem. Eng. Sci.* **2011**, *66*, 1463.
- [4] S. Marre, K. F. Jensen, *Chem. Soc. Rev.* **2010**, *39*, 1183.
- [5] A. Yaghmur, A. Ghazal, R. Ghazal, M. Dimaki, W. E. Svendsen, *Phys. Chem. Chem. Phys.* **2019**, *21*, 13005.
- [6] T. Baby, Y. Liu, A. P. J. Middelberg, C. X. Zhao, *Chem. Eng. Sci.* **2017**, *169*, 128.
- [7] R. Ran, Q. Sun, T. Baby, D. Wibowo, A. P. J. Middelberg, C. X. Zhao, *Chem. Eng. Sci.* **2017**, *169*, 78.
- [8] A. Sealy, Manufacturing moonshot: How Pfizer makes its millions of Covid-19 vaccine doses, <https://edition.cnn.com/2021/03/31/health/pfizer-vaccine-manufacturing/index.html> (accessed: October 2021).

- [9] I. U. Khan, C. A. Serra, N. Anton, T. F. Vandamme, *Expert Opin. Drug Delivery* **2015**, *12*, 547.
- [10] M. Yang, Y. Gao, Y. Liu, G. Yang, C.-X. Zhao, K.-J. Wu, *Chem. Eng. Sci.* **2021**, *234*, 116450.
- [11] C.-Y. Lee, W.-T. Wang, C.-C. Liu, L.-M. Fu, *Chem. Eng. J.* **2016**, *288*, 146.
- [12] K. Ward, Z. H. Fan, *J. Micromech. Microeng.* **2015**, *25*, 094001.
- [13] D. Khoeni, T. F. Scott, A. Neild, *Lab Chip* **2021**, *21*, 1661.
- [14] B. Dincau, E. Dressaire, A. Sauret, *Small* **2020**, *16*, 1904032.
- [15] H. Cho, J. Kim, K. Suga, T. Ishigami, H. Park, J. W. Bang, S. Seo, M. Choi, P. S. Chang, H. Umakoshi, S. Jung, K. Y. Suh, *Lab Chip* **2015**, *15*, 373.
- [16] I. O. de Solorzano, L. Uson, A. Larrea, M. Miana, V. Sebastian, M. Arruebo, *Int. J. Nanomed.* **2016**, *11*, 3397.
- [17] M. Lu, A. Ozcelik, C. L. Grigsby, Y. Zhao, F. Guo, K. W. Leong, T. J. Huang, *Nano Today* **2016**, *11*, 778.
- [18] N. Kamaly, G. Fredman, J. J. R. Fojas, M. Subramanian, W. I. Choi, K. Zepeda, C. Vilos, M. Y. Yu, S. Gadde, J. Wu, J. Milton, R. C. Leitao, L. R. Fernandes, M. Hasan, H. Y. Gao, V. Nguyen, J. Harris, I. Tabas, O. C. Farokhzad, *ACS Nano* **2016**, *10*, 5280.
- [19] E. Lallana, R. Donno, D. Magri, K. Barker, Z. Nazir, K. Treacher, M. J. Lawrence, M. Ashford, N. Tirelli, *Int. J. Pharm.* **2018**, *548*, 530.
- [20] S. Hoang, S. Olivier, S. Cuenot, A. Montillet, J. Bellettre, E. Ishow, *ChemPhysChem* **2020**, *21*, 2502.
- [21] A. D. Stroock, S. K. Dertinger, A. Ajdari, I. Mezic, H. A. Stone, G. M. Whitesides, *Science* **2002**, *295*, 647.
- [22] E. Kastner, R. Kaur, D. Lowry, B. Moghaddam, A. Wilkinson, Y. Perrie, *Int. J. Pharm.* **2014**, *477*, 361.
- [23] A. Gdowski, K. Johnson, S. Shah, I. Gryczynski, J. Vishwanatha, A. Ranjan, *J. Nanobiotechnol.* **2018**, *16*, 12.
- [24] K. Abstiens, A. M. Goepferich, *J. Drug Delivery Sci. Technol.* **2019**, *49*, 433.
- [25] C. C. L. Cheung, W. T. Al-Jamal, *Int. J. Pharm.* **2019**, *566*, 687.
- [26] F. Bongiovi, C. Fiorica, F. S. Palumbo, G. Pitarresi, G. Giammona, *Int. J. Pharm.* **2020**, *573*, 118851.
- [27] C. B. Roces, D. Christensen, Y. Perrie, *Drug Delivery Transl. Res.* **2020**, *10*, 582.
- [28] N. H. A. Le, H. V. Phan, J. Q. Yu, H. K. Chan, A. Neild, T. Alan, *Int. J. Nanomed.* **2018**, *13*, 1353.
- [29] P. H. Huang, S. G. Zhao, H. Bachman, N. Nama, Z. S. Li, C. Y. Chen, S. J. Yang, M. X. Wu, S. P. Zhang, T. J. Huang, *Adv. Sci.* **2019**, *6*, 1970113.
- [30] J. Seaberg, S. Kaabipour, S. Hemmati, J. D. Ramsey, *Eur. J. Pharm. Biopharm.* **2020**, *154*, 127.
- [31] N. H. A. Le, H. Deng, C. Devendran, N. Akhtar, X. M. Ma, C. Pouton, H. K. Chan, A. Neild, T. Alan, *Lab Chip* **2020**, *20*, 582.
- [32] A. Pourabed, T. Younas, C. Liu, B. K. Shanbhag, L. Z. He, T. Alan, *J. Colloid Interface Sci.* **2021**, *585*, 229.
- [33] M. Maeki, T. Saito, Y. Sato, T. Yasui, N. Kaji, A. Ishida, H. Tani, Y. Baba, H. Harashima, M. Tokeshi, *RSC Adv.* **2015**, *5*, 46181.
- [34] R. Karnik, F. Gu, P. Basto, C. Cannizzaro, L. Dean, W. Kyei-Manu, R. Langer, O. C. Farokhzad, *Nano Lett.* **2008**, *8*, 2906.
- [35] R. Ran, H. F. Wang, Y. Liu, Y. Hui, Q. Sun, A. Seth, D. Wibowo, D. Chen, C. X. Zhao, *Eur. J. Pharm. Biopharm.* **2018**, *130*, 1.
- [36] Y. Liu, G. Yang, D. Zou, Y. Hui, K. Nigam, A. P. J. Middelberg, C.-X. Zhao, *Ind. Eng. Chem. Res.* **2020**, *59*, 4134.
- [37] M. V. Bandulasena, G. T. Vladislavjević, O. G. Odunmbaku, B. Benyahia, *Chem. Eng. Sci.* **2017**, *171*, 233.
- [38] R. Othman, G. T. Vladislavjević, H. C. Hemaka Bandulasena, Z. K. Nagy, *Chem. Eng. J.* **2015**, *280*, 316.
- [39] R. Othman, G. T. Vladislavjevic, Z. K. Nagy, *Chem. Eng. Sci.* **2015**, *137*, 119.
- [40] S. J. Shepherd, D. Issadore, M. J. Mitchell, *Biomaterials* **2021**, *274*, 120826.
- [41] C. Walsh, K. Ou, N. M. Belliveau, T. J. Leaver, A. W. Wild, J. Huft, P. J. Lin, S. Chen, A. K. Leung, J. B. Lee, in *Drug Delivery System* (Ed: K. K. Jain), Springer, Berlin **2014**, pp. 109–120.
- [42] A. W. Leung, C. Amador, L. C. Wang, U. V. Mody, M. B. Bally, *Pharmaceutics* **2019**, *11*, 124.
- [43] T. Van de Vyver, B. Bogaert, L. De Backer, F. Joris, R. Guagliardo, J. Van Hoeck, P. Mercckx, S. Van Calenbergh, S. Ramishetti, D. Peer, *ACS Nano* **2020**, *14*, 4774.
- [44] J. Vogler, R. Böttger, N. A. Fayez, W. Zhang, Z. Qin, L. Hohenwarter, P.-H. Chao, E. Rouhollahi, N. Bilal, N. Chen, *J. Controlled Release* **2021**, *333*, 151.
- [45] M. N. Vu, H. G. Kelly, H. X. Tan, J. A. Juno, R. Esterbauer, T. P. Davis, N. P. Truong, A. K. Wheatley, S. J. Kent, *Adv. Healthcare Mater.* **2021**, *10*, 2002142.
- [46] J.-M. Lim, N. Bertrand, P. M. Valencia, M. Rhee, R. Langer, S. Jon, O. C. Farokhzad, R. Karnik, *Nanomedicine* **2014**, *10*, 401.
- [47] K. I. Min, D. J. Im, H. J. Lee, D. P. Kim, *Lab Chip* **2014**, *14*, 3987.
- [48] R. R. Hood, D. L. DeVoe, J. Atencia, W. N. Vreeland, D. M. Omiatek, *Lab Chip* **2014**, *14*, 2403.
- [49] D. Di, X. Qu, C. Liu, L. Fang, P. Quan, *Int. J. Pharm.* **2019**, *572*, 118831.
- [50] S. M. D'Addio, R. K. Prud'homme, *Adv. Drug Delivery Rev.* **2011**, *63*, 417.
- [51] G. Bovone, E. A. Guzzi, M. W. Tibbitt, *AIChE J.* **2019**, *65*, e16840.
- [52] J. Han, Z. Zhu, H. Qian, A. R. Wohl, C. J. Beaman, T. R. Hoye, C. W. Macosko, *J. Pharm. Sci.* **2012**, *101*, 4018.
- [53] C. E. Markwalter, R. K. Prud'homme, *J. Pharm. Sci.* **2018**, *107*, 2465.
- [54] Y. Liu, C. Cheng, Y. Liu, R. K. Prud'homme, R. O. Fox, *Chem. Eng. Sci.* **2008**, *63*, 2829.
- [55] R. Molinaro, M. Evangelopoulos, J. R. Hoffman, C. Corbo, F. Taraballi, J. O. Martinez, K. A. Hartman, D. Cosco, G. Costa, I. Romeo, M. Sherman, D. Paolino, S. Alcaro, E. Tasciotti, *Adv. Mater.* **2018**, *30*, 1702749.
- [56] S. Shah, V. Dhawan, R. Holm, M. S. Nagarsenker, Y. Perrie, *Adv. Drug Delivery Rev.* **2020**, *154*, 102.
- [57] Y. C. Barenholz, *J. Controlled Release* **2012**, *160*, 117.
- [58] M. G. S. Correia, M. L. Briuglia, F. Niosi, D. A. Lamprou, *Int. J. Pharm.* **2017**, *516*, 91.
- [59] R. R. Hood, D. L. DeVoe, *Small* **2015**, *11*, 5790.
- [60] Z. Chen, J. Y. Han, L. Shumate, R. Fedak, D. L. DeVoe, *Adv. Mater. Technol.* **2019**, *4*, 1800511.
- [61] A. U. Andar, R. R. Hood, W. N. Vreeland, D. L. DeVoe, P. W. Swaan, *Pharm. Res.* **2014**, *31*, 401.
- [62] H. Elsana, T. O. B. Olusanya, J. Carr-Wilkinson, S. Darby, A. Faheem, A. A. Elkordy, *Sci. Rep.* **2019**, *9*, 15120.
- [63] J. C. Stachowiak, D. L. Richmond, T. H. Li, A. P. Liu, S. H. Parekh, D. A. Fletcher, *Proc. Natl. Acad. Sci. USA* **2008**, *105*, 4697.
- [64] T. Hamada, Y. Miura, Y. Komatsu, Y. Kishimoto, M. d. Vestergaard, M. Takagi, *J. Phys. Chem. B* **2008**, *112*, 14678.
- [65] M. L. Berre, A. Yamada, L. Reck, Y. Chen, D. Baigl, *Langmuir* **2008**, *24*, 2643.
- [66] J. R. Hoffman, E. Tasciotti, R. Molinaro, in *Multiple Myeloma: Methods and Protocols*, Vol. 1792 (Eds: C. Heuck, N. Weinhold), Humana, New York, NY **2018**, pp. 205–214.
- [67] M. X. Zheng, T. M. Fyles, *Eur. J. Lipid Sci. Technol.* **2018**, *120*, 1700347.
- [68] G. Charest, T. Tippayamontri, M. H. Shi, M. Wehbe, M. Anantha, M. Bally, L. Sanche, *Int. J. Mol. Sci.* **2020**, *21*, 4848.
- [69] N. Dimov, E. Kastner, M. Hussain, Y. Perrie, N. Szita, *Sci. Rep.* **2017**, *7*, 12045.
- [70] F. Yanar, A. Mosayyebi, C. Nastruzzi, D. Carugo, X. L. Zhang, *Pharmaceutics* **2020**, *12*, 1001.
- [71] J. Kim, A. Dey, A. Malhotra, J. B. Liu, S. I. Ahn, Y. J. Sei, A. M. Kenney, T. J. MacDonald, Y. Kim, *Proc. Natl. Acad. Sci. USA* **2020**, *117*, 24205.

- [72] M. Mijajlovic, D. Wright, V. Zivkovic, J. X. Bi, M. J. Biggs, *Colloids Surf., B* **2013**, *104*, 276.
- [73] R. R. Hood, C. R. Shao, D. M. Omiatek, W. N. Vreeland, D. L. DeVoe, *Pharm. Res.* **2013**, *30*, 1597.
- [74] R. Ran, A. P. J. Middelberg, C. X. Zhao, *Colloids Surf., B* **2016**, *148*, 402.
- [75] R. Ran, H. F. Wang, F. Hou, Y. Liu, Y. Hui, N. Petrovsky, F. Zhang, C. X. Zhao, *Adv. Healthcare Mater.* **2019**, *8*, 1900015.
- [76] E. Bottaro, A. Mosayyebi, D. Carugo, C. Nastruzzi, *Micromachines* **2017**, *8*, 209.
- [77] M. B. De Jesus, I. S. Zuhorn, *J. Controlled Release* **2015**, *201*, 1.
- [78] N. Chaudhary, D. Weissman, K. A. Whitehead, *Nat. Rev. Drug Discovery* **2021**, *20*, 817.
- [79] A. Khurana, P. Allawadhi, I. Khurana, S. Allwadh, R. Weiskirchen, A. K. Banothu, D. Chhabra, K. Joshi, K. K. Bharani, *Nano Today* **2021**, *38*, 101142.
- [80] B. Sjöström, B. Bergenstahl, *Int. J. Pharm.* **1992**, *88*, 53.
- [81] P. Ahlin, J. Kristl, J. Smid-Korbar, *Acta Pharm.* **1998**, *48*, 259.
- [82] A. zur Mühlen, C. Schwarz, W. Mehnert, *Eur. J. Pharm. Biopharm.* **1998**, *45*, 149.
- [83] W. Mehnert, K. Mäder, *Adv. Drug Delivery Rev.* **2012**, *64*, 83.
- [84] M. Maeki, N. Kimura, Y. Sato, H. Harashima, M. Tokeshi, *Adv. Drug Delivery Rev.* **2018**, *128*, 84.
- [85] A. Garud, D. Singh, N. Garud, *Int. Curr. Pharm. J.* **2012**, *1*, 384.
- [86] M. Maeki, Y. Fujishima, Y. Sato, T. Yasui, N. Kaji, A. Ishida, H. Tani, Y. Baba, H. Harashima, M. Tokeshi, *PLoS One* **2017**, *12*, e0187962.
- [87] Y. Sato, N. Okabe, Y. Note, K. Hashiba, M. Maeki, M. Tokeshi, H. Harashima, *Acta Biomater.* **2020**, *102*, 341.
- [88] X. N. Zhang, W. Zong, Y. Hu, N. Luo, W. L. Cheng, X. J. Han, *J. Microencapsulation* **2016**, *33*, 663.
- [89] N. Kimura, M. Maeki, Y. Sato, Y. Note, A. Ishida, H. Tani, H. Harashima, M. Tokeshi, *ACS Omega* **2018**, *3*, 5044.
- [90] M. A. Younis, I. A. Khalil, Y. H. A. Elewa, Y. Kon, H. Harashima, *J. Controlled Release* **2021**, *331*, 335.
- [91] N. Kimura, M. Maeki, K. Sasaki, Y. Sato, A. Ishida, H. Tani, H. Harashima, M. Tokeshi, *RSC Adv.* **2021**, *11*, 1430.
- [92] I. Arduino, Z. H. Liu, A. Rahikkala, P. Figueiredo, A. Correia, A. Cutrignelli, N. Denora, H. A. Santos, *Acta Biomater.* **2021**, *121*, 566.
- [93] N. Kimura, M. Maeki, Y. Sato, A. Ishida, H. Tani, H. Harashima, M. Tokeshi, *ACS Appl. Mater. Interfaces* **2020**, *12*, 34011.
- [94] A. Jahn, W. N. Vreeland, M. Gaitan, L. E. Locascio, *J. Am. Chem. Soc.* **2004**, *126*, 2674.
- [95] A. Jahn, S. M. Stavis, J. S. Hong, W. N. Vreeland, D. L. DeVoe, M. Gaitan, *ACS Nano* **2010**, *4*, 2077.
- [96] Y. J. Li, R. J. Lee, X. Q. Huang, Y. H. Li, B. C. Lv, T. P. Wang, Y. H. Qi, F. Hao, J. H. Lu, Q. F. Meng, L. R. Teng, Y. L. Zhou, J. Xie, L. S. Teng, *Nanomedicine* **2017**, *13*, 371.
- [97] P. M. Valencia, P. A. Basto, L. F. Zhang, M. Rhee, R. Langer, O. C. Farokhzad, R. Karnik, *ACS Nano* **2010**, *4*, 1671.
- [98] T. Basta, H. J. Wu, M. K. Morphew, J. Lee, N. Ghosh, J. Lai, J. M. Heumann, K. Wang, Y. C. Lee, D. C. Rees, M. H. B. Stowell, *Proc. Natl. Acad. Sci. USA* **2014**, *111*, 670.
- [99] K. M. Pustulka, A. R. Wohl, H. S. Lee, A. R. Michel, J. Han, T. R. Hoye, A. V. McCormick, J. Panyam, C. W. Macosko, *Mol. Pharmaceutics* **2013**, *10*, 4367.
- [100] W. Zhang, A. Mehta, Z. Tong, L. Esser, N. H. Voelcker, *Adv. Sci.* **2021**, *8*, 2003937.
- [101] H. K. Makadia, S. J. Siegel, *Polymers* **2011**, *3*, 1377.
- [102] R. Y. Chen, J. E. Wulff, M. G. Moffitt, *Mol. Pharmaceutics* **2018**, *15*, 4517.
- [103] M. Rhee, P. M. Valencia, M. I. Rodriguez, R. Langer, O. C. Farokhzad, R. Karnik, *Adv. Mater.* **2011**, *23*, H79.
- [104] I. Bala, S. Hariharan, M. N. V. R. Kumar, *Crit. Rev. Ther. Drug Carrier Syst.* **2004**, *21*, 387.
- [105] Y. Morikawa, T. Tagami, A. Hoshikawa, T. Ozeki, *Biol. Pharm. Bull.* **2018**, *41*, 899.
- [106] Z. Q. Xu, B. Yan, J. Riordon, Y. Zhao, D. Sinton, M. G. Moffitt, *Chem. Mater.* **2015**, *27*, 8094.
- [107] A. Bains, Y. M. Cao, M. G. Moffitt, *Macromol. Rapid Commun.* **2015**, *36*, 2000.
- [108] Z. Q. Xu, C. H. Lu, C. Lindenberger, Y. M. Cao, J. E. Wulff, M. G. Moffitt, *ACS Omega* **2017**, *2*, 5289.
- [109] Y. M. Cao, L. Silverman, C. H. Lu, R. Hof, J. E. Wulff, M. G. Moffitt, *Mol. Pharmaceutics* **2019**, *16*, 96.
- [110] Y. H. Huang, A. M. Jazani, E. P. Howell, L. A. Reynolds, J. K. Oh, M. G. Moffitt, *ACS Biomater. Sci. Eng.* **2020**, *6*, 5069.
- [111] J. M. R. De La Rosa, A. Spadea, R. Donno, E. Lallana, Y. Lu, S. Puri, P. Caswell, M. J. Lawrence, M. Ashford, N. Tirelli, *Sci. Rep.* **2020**, *10*, 14505.
- [112] D. F. Liu, C. R. Bernuz, J. Fan, W. Li, A. Correia, J. Hirvonen, H. A. Santos, *Adv. Funct. Mater.* **2017**, *27*, 1604508.
- [113] N. Anton, F. Bally, C. A. Serra, A. Ali, Y. Arntz, Y. Mely, M. J. Zhao, E. Marchioni, A. Jakhmola, T. F. Vandamme, *Soft Matter* **2012**, *8*, 10628.
- [114] L. Capretto, D. Carugo, W. Cheng, M. Hill, X. L. Zhang, *J. Colloid Interface Sci.* **2011**, *357*, 243.
- [115] M. H. M. Leung, A. Q. Shi, *Langmuir* **2018**, *34*, 3961.
- [116] M. G. Toudeshkchouei, P. Zahedi, A. Shavandi, *Materials* **2020**, *13*, 1483.
- [117] A. Perez, R. Hernandez, D. Velasco, D. Voicu, C. Mijangos, *J. Colloid Interface Sci.* **2015**, *441*, 90.
- [118] W. X. Zeng, P. H. Guo, P. Jiang, W. F. Liu, T. T. Hong, C. P. Chen, *Nanotechnology* **2020**, *31*, 145301.
- [119] F. Heshmatnezhad, A. R. S. Nazar, *Chem. Eng. Technol.* **2020**, *43*, 2073.
- [120] R. Song, C. Peng, X. Xu, J. Wang, M. Yu, Y. Hou, R. Zou, S. Yao, *ACS Appl. Mater. Interfaces* **2018**, *10*, 14312.
- [121] M. Brzezinski, M. Socka, T. Makowski, B. Kost, M. Cieslak, K. Krolewska-Golinska, *Colloids Surf., B* **2021**, *201*, 111598.
- [122] E. M. Chan, A. P. Alivisatos, R. A. Mathies, *J. Am. Chem. Soc.* **2005**, *127*, 13854.
- [123] T. Lorenz, S. Bojko, H. Bunjes, A. Dietzel, *Lab Chip* **2018**, *18*, 627.
- [124] D. Zhao, S. Yu, B. Sun, S. Gao, S. Guo, K. Zhao, *Polymers* **2018**, *10*, 462.
- [125] C. W. Chen, Y. X. Liu, H. Wang, G. P. Chen, X. W. Wu, J. A. Ren, H. D. Zhang, Y. J. Zhao, *ACS Nano* **2018**, *12*, 10493.
- [126] F. S. Majedi, M. M. Hasani-Sadrabadi, J. J. VanDersarl, N. Mokarram, S. Hojjati-Emami, E. Dashtimoghadam, S. Bonakdar, M. A. Shokrgozar, A. Bertsch, P. Renaud, *Adv. Funct. Mater.* **2014**, *24*, 432.
- [127] E. Chiesa, A. Greco, F. Riva, E. M. Tosca, R. Dorati, S. Pisani, T. Modena, B. Conti, I. Genta, *Int. J. Mol. Sci.* **2019**, *20*, 6212.
- [128] N. Escareno, N. Hassan, M. J. Kogan, J. Juarez, A. Topete, A. Daneri-Navarro, *J. Colloid Interface Sci.* **2021**, *591*, 440.
- [129] V. Kamat, I. Marathe, V. Ghormade, D. Bodas, K. Paknikar, *ACS Appl. Mater. Interfaces* **2015**, *7*, 22839.
- [130] V. Adibnia, M. Mirbagheri, P. L. Latreille, J. Faivre, B. Cecyre, J. Robert, J. F. Bouchard, V. A. Martinez, T. Delair, L. David, D. K. Hwang, X. Banquy, *Acta Biomater.* **2019**, *99*, 211.
- [131] S. Chen, H. J. Zhang, X. T. Shi, H. K. Wu, N. Hanagata, *Lab Chip* **2014**, *14*, 1842.
- [132] F. Moradikhah, M. Doosti-Telgerd, I. Shabani, S. Soheili, B. Dolatyar, E. Seyedjafari, *Life Sci.* **2020**, *254*, 117768.
- [133] S. Soheili, E. Mandegar, F. Moradikhah, M. Doosti-Telgerd, H. A. Javar, *J. Drug Delivery Sci. Technol.* **2021**, *61*, 102268.
- [134] M. M. Hasani-Sadrabadi, S. P. Hajrezaei, S. H. Emami, G. Bahlakeh, L. Daneshmandi, E. Dashtimoghadam, E. Seyedjafari, K. I. Jacob, L. Tayebi, *Nanomedicine* **2015**, *11*, 1809.

- [135] M. Shamsi, P. Zahedi, *J. Pharm. Sci.* **2017**, *106*, 3623.
- [136] A. S. Lari, P. Zahedi, H. Ghourchian, A. Khatibi, *Carbohydr. Polym.* **2021**, *261*, 117889.
- [137] M. Shamsi, P. Zahedi, H. Ghourchian, S. Minaeian, *Int. J. Biol. Macromol.* **2017**, *99*, 433.
- [138] F. S. Majedi, M. M. Hasani-Sadrabadi, S. H. Emami, M. A. Shokrgozar, J. J. VanDersarl, E. Dashtimoghadam, A. Bertsch, P. Renaud, *Lab Chip* **2013**, *13*, 204.
- [139] A. Sosnik, *Int. Scholarly Res. Not.* **2014**, 2014.
- [140] Z. Mahmoudi, J. Mohammadnejad, S. R. Bazaz, A. A. Mehri, M. Saidijam, R. Dinarvand, M. E. Warkiani, M. Soleimani, *Carbohydr. Polym.* **2020**, *229*, 115551.
- [141] D. Chen, C.-X. Zhao, C. Lagoin, M. Hai, L. R. Arriaga, S. Koehler, A. Abbaspourrad, D. A. Weitz, *R. Soc. Open Sci.* **2017**, *4*, 170919.
- [142] L. Kong, R. Chen, X. Wang, C.-X. Zhao, Q. Chen, M. Hai, D. Chen, Z. Yang, D. A. Weitz, *Lab Chip* **2019**, *19*, 2089.
- [143] B. Wu, C. Yang, B. Li, L. Feng, M. Hai, C. X. Zhao, D. Chen, K. Liu, D. A. Weitz, *Small* **2020**, *16*, 2002716.
- [144] C. J. M. Rivas, M. Tarhini, W. Badri, K. Miladi, H. Greige-Gerges, Q. A. Nazari, S. A. G. Rodríguez, R. Á. Román, H. Fessi, A. Elaissari, *Int. J. Pharm.* **2017**, *532*, 66.
- [145] H. Fessi, F. Puisieux, J. P. Devissaguet, N. Ammoury, S. Benita, *Int. J. Pharm.* **1989**, *55*, R1.
- [146] C. G. Barreras-Urbina, B. Ramírez-Wong, G. A. López-Ahumada, S. E. Burruel-Ibarra, O. Martínez-Cruz, J. A. Tapia-Hernández, F. Rodríguez Felix, *Int. J. Food Prop.* **2016**, *19*, 1912.
- [147] U. Bilati, E. Allémann, E. Doelker, *Eur. J. Pharm. Sci.* **2005**, *24*, 67.
- [148] W. S. Saad, R. K. Prud'homme, *Nano Today* **2016**, *11*, 212.
- [149] S. Y. Cao, X. Xu, X. X. Wang, *China Pet. Process. Petrochem. Technol.* **2017**, *19*, 32.
- [150] S. Ding, N. Anton, T. F. Vandamme, C. A. Serra, *Expert Opin. Drug Delivery* **2016**, *13*, 1447.
- [151] J. W. Hickey, J. L. Santos, J. M. Williford, H. Q. Mao, *J. Controlled Release* **2015**, *219*, 536.
- [152] B. K. Johnson, R. K. Prud'homme, *AIChE J.* **2003**, *49*, 2264.
- [153] J.-M. Lim, A. Swami, L. M. Gilson, S. Chopra, S. Choi, J. Wu, R. Langer, R. Karnik, O. C. Farokhzad, *ACS Nano* **2014**, *8*, 6056.
- [154] W. Li, Q. L. Chen, T. Baby, S. Jin, Y. Liu, G. Z. Yang, C. X. Zhao, *Chem. Eng. Sci.* **2021**, *235*, 116468.
- [155] T. Baby, Y. Liu, G. Yang, D. Chen, C.-X. Zhao, *J. Colloid Interface Sci.* **2021**, *594*, 474.
- [156] Y. Liu, G. Yang, S. Jin, L. Xu, C.-X. Zhao, *ChemPlusChem* **2020**, *85*, 2143.
- [157] Y. Liu, G. Yang, T. Baby, D. Chen, D. A. Weitz, C. X. Zhao, *Angew. Chem., Int. Ed.* **2020**, *132*, 4750.
- [158] Y. Liu, G. Yang, S. Jin, R. Zhang, P. Chen, L. Wang, D. Chen, D. A. Weitz, C. X. Zhao, *Angew. Chem., Int. Ed.* **2020**, *59*, 20065.
- [159] F. Y. Han, Y. Liu, V. Kumar, W. Xu, G. Yang, C.-X. Zhao, T. M. Woodruff, A. K. Whittaker, M. T. Smith, *Int. J. Pharm.* **2020**, *581*, 119291.
- [160] D. Liu, H. Zhang, S. Cito, J. Fan, E. Mäkilä, J. Salonen, J. Hirvonen, T. M. Sikanen, D. A. Weitz, H. A. Santos, *Nano Lett.* **2017**, *17*, 606.
- [161] G. Yang, Y. Liu, S. Jin, C. X. Zhao, *ChemBioChem* **2020**, *21*, 2871.
- [162] Tengji, Y. Hui, G. Yang, C. Fu, Y. Liu, C.-X. Zhao, *J. Colloid Interface Sci.* **2021**, *581*, 185.
- [163] C. X. Zhao, A. P. J. Middelberg, *RSC Adv.* **2013**, *3*, 21227.
- [164] C. Bharti, U. Nagaich, A. K. Pal, N. Gulati, *Int. J. Pharm. Invest.* **2015**, *5*, 124.
- [165] G. Yang, Y. Liu, H. Wang, R. Wilson, Y. Hui, L. Yu, D. Wibowo, C. Zhang, A. K. Whittaker, A. P. Middelberg, *Angew. Chem., Int. Ed.* **2019**, *131*, 14495.
- [166] J. Wen, K. Yang, F. Liu, H. Li, Y. Xu, S. Sun, *Chem. Soc. Rev.* **2017**, *46*, 6024.
- [167] R. K. Kankala, Y. H. Han, J. Na, C. H. Lee, Z. Sun, S. B. Wang, T. Kimura, Y. S. Ok, Y. Yamauchi, A. Z. Chen, *Adv. Mater.* **2020**, *32*, 1907035.
- [168] G. Yang, Y. Liu, C.-X. Zhao, *Colloids Surf., B* **2021**, 111923.
- [169] Y. Hui, Y. Fan, D. Zou, G. H. Talbo, G. Yang, C.-X. Zhao, *J. Colloid Interface Sci.* **2022**, *606*, 1737.
- [170] S. A. Khan, A. Günther, M. A. Schmidt, K. F. Jensen, *Langmuir* **2004**, *20*, 8604.
- [171] P. He, G. Greenway, S. J. Haswell, *Chem. Eng. J.* **2011**, *167*, 694.
- [172] Y. Nie, N. Hao, J. X. J. Zhang, *Sci. Rep.* **2017**, *7*, 12616.
- [173] T. N. Ng, X. Q. Chen, K. L. Yeung, *RSC Adv.* **2015**, *5*, 13331.
- [174] N. Hassan, V. Cabuil, A. Abou-Hassan, *Angew. Chem., Int. Ed.* **2013**, *52*, 1994.
- [175] N. Hao, Y. Nie, Z. Xu, J. X. J. Zhang, *J. Colloid Interface Sci.* **2019**, *542*, 370.
- [176] J. Wagner, T. Kirner, G. Mayer, J. Albert, J. M. Köhler, *Chem. Eng. J.* **2004**, *101*, 251.
- [177] J. Wagner, T. R. Tshikhudo, J. M. Köhler, *Chem. Eng. J.* **2008**, *135*, S104.
- [178] R. Baber, L. Mazzei, N. T. K. Thanh, A. Gavriilidis, *RSC Adv.* **2015**, *5*, 95585.
- [179] A. Knauer, A. Eisenhardt, S. Krischok, J. M. Koehler, *Nanoscale* **2014**, *6*, 5230.
- [180] J. M. Köhler, H. Romanus, U. Hübner, J. Wagner, *J. Nanomater.* **2007**, *2007*, 098134.
- [181] L. Xu, J. Peng, C. Srinivasakannan, L. Zhang, D. Zhang, C. Liu, S. Wang, A. Q. Shen, *RSC Adv.* **2014**, *4*, 25155.
- [182] A. Pekkari, Z. Say, A. Susarrey-Arce, C. Langhammer, H. Härelind, V. Sebastian, K. Moth-Poulsen, *ACS Appl. Mater. Interfaces* **2019**, *11*, 36196.
- [183] X. Li, Q. Feng, X. Jiang, *Adv. Healthcare Mater.* **2019**, *8*, 1900672.
- [184] S.-Y. Tang, R. Qiao, S. Yan, D. Yuan, Q. Zhao, G. Yun, T. P. Davis, W. Li, *Small* **2018**, *14*, 1800118.
- [185] Z. Li, B. Tan, M. Allix, A. I. Cooper, M. J. Rosseinsky, *Small* **2008**, *4*, 231.
- [186] L. Panariello, G. Wu, M. O. Besenhard, K. Loizou, L. Storozhuk, N. T. K. Thanh, A. Gavriilidis, *Materials* **2020**, *13*, 1019.
- [187] J. Bemetz, A. Wegemann, K. Saatchi, A. Haase, U. O. Häfeli, R. Niessner, B. Gleich, M. Seidel, *Anal. Chem.* **2018**, *90*, 9975.
- [188] A. Larrea, V. Sebastian, A. Ibarra, M. Arruebo, J. Santamaria, *Chem. Mater.* **2015**, *27*, 4254.
- [189] K. Kumar, A. M. Nightingale, S. H. Krishnadasan, N. Kamaly, M. Wylenzinska-Arridge, K. Zeissler, W. R. Branford, E. Ware, A. J. deMello, J. C. deMello, *J. Mater. Chem.* **2012**, *22*, 4704.
- [190] N. Deng, Y. Wang, G. Luo, *Particuology* **2022**, *60*, 61.
- [191] H. Yao, Y. Wang, Y. Jing, G. Luo, *Ind. Eng. Chem. Res.* **2018**, *57*, 7525.
- [192] P. Stolzenburg, T. Lorenz, A. Dietzel, G. Garnweitner, *Chem. Eng. Sci.* **2018**, *191*, 500.
- [193] Y. Cheng, S. D. Ling, Y. Geng, Y. Wang, J. Xu, *Nanoscale Adv.* **2021**, *3*, 2180.
- [194] D. Bera, L. Qian, T.-K. Tseng, P. H. Holloway, *Materials* **2010**, *3*, 2260.
- [195] A. M. Wagner, J. M. Knipe, G. Orive, N. A. Peppas, *Acta Biomater.* **2019**, *94*, 44.
- [196] B. K. H. Yen, N. E. Stott, K. F. Jensen, M. G. Bawendi, *Adv. Mater.* **2003**, *15*, 1858.
- [197] M. Abolhasani, C. W. Coley, L. Xie, O. Chen, M. G. Bawendi, K. F. Jensen, *Chem. Mater.* **2015**, *27*, 6131.
- [198] J. Baek, Y. Shen, I. Lignos, M. G. Bawendi, K. F. Jensen, *Angew. Chem., Int. Ed.* **2018**, *57*, 10915.
- [199] N. Azam, M. Najabat Ali, T. Javaid Khan, *Front. Mater.* **2021**, *8*, 272.
- [200] L. Rao, Y. Tang, Z. Li, X. Ding, G. Liang, H. Lu, C. Yan, K. Tang, B. Yu, *Mater. Sci. Eng. C* **2017**, *81*, 213.

- [201] M. Shao, Q. Yu, N. Jing, Y. Cheng, D. Wang, Y.-D. Wang, J.-H. Xu, *Lab Chip* **2019**, *19*, 3974.
- [202] A. E. Nel, L. Mädler, D. Velegol, T. Xia, E. M. Hoek, P. Somasundaran, F. Klaessig, V. Castranova, M. Thompson, *Nat. Mater.* **2009**, *8*, 543.
- [203] L. Zhang, J. M. Chan, F. X. Gu, J.-W. Rhee, A. Z. Wang, A. F. Radovic-Moreno, F. Alexis, R. Langer, O. C. Farokhzad, *ACS Nano* **2008**, *2*, 1696.
- [204] J. S. Sun, L. Zhang, J. L. Wang, Q. Feng, D. B. Liu, Q. F. Yin, D. Y. Xu, Y. J. Wei, B. Q. Ding, X. H. Shi, X. Y. Jiang, *Adv. Mater.* **2015**, *27*, 1402.
- [205] J. Thevenot, A.-L. Troutier, L. David, T. Delair, C. Ladavière, *Bio-macromolecules* **2007**, *8*, 3651.
- [206] M. Z. Zhu, A. K. Whittaker, X. Y. Jiang, R. P. Tang, X. Y. Li, W. Z. Xu, C. K. Fu, M. T. Smith, F. Y. Han, *Pharm. Res.* **2020**, *37*, 1.
- [207] L. Zhang, Q. Feng, J. L. Wang, S. Zhang, B. Q. Ding, Y. J. Wei, M. D. Dong, J. Y. Ryu, T. Y. Yoon, X. H. Shi, J. S. Sun, X. Y. Jiang, *ACS Nano* **2015**, *9*, 9912.
- [208] L. Zhang, Q. Feng, J. L. Wang, J. S. Sun, X. H. Shi, X. Y. Jiang, *Angew. Chem., Int. Ed.* **2015**, *54*, 3952.
- [209] M. J. Toth, T. Kim, Y. Kim, *Lab Chip* **2017**, *17*, 2805.
- [210] N. Tahir, A. Madni, W. Li, A. Correia, M. M. Khan, M. A. Rahim, H. A. Santos, *Int. J. Pharm.* **2020**, *581*, 119275.
- [211] Y. Kim, B. Lee Chung, M. Ma, W. J. Mulder, Z. A. Fayad, O. C. Farokhzad, R. Langer, *Nano Lett.* **2012**, *12*, 3587.
- [212] F. Wan, S. S. R. Bohr, S. N. Klodzinska, H. Jumaa, Z. Huang, T. Nylander, M. B. Thygesen, K. K. Sorensen, K. J. Jensen, C. Sternberg, N. Hatzakis, H. M. Nielsen, *ACS Appl. Mater. Interfaces* **2020**, *12*, 380.
- [213] M. M. Hasani-Sadrabadi, S. Taranejoo, E. Dashtimoghdam, G. Bahlakeh, F. S. Majedi, J. J. VanDersarl, M. Janmaleki, F. Sharifi, A. Bertsch, K. Hourigan, L. Tayebi, P. Renaud, K. I. Jacob, *Adv. Mater.* **2016**, *28*, 4134.
- [214] J. S. Hong, S. M. Stavis, S. H. D. Lacerda, L. E. Locascio, S. R. Raghavan, M. Gaitan, *Langmuir* **2010**, *26*, 11581.
- [215] Y. J. Li, X. Q. Huang, R. J. Lee, Y. H. Qi, K. K. Wang, F. Hao, Y. Zhang, J. H. Lu, Q. F. Meng, S. Li, J. Xie, L. S. Teng, *Molecules* **2016**, *21*, 1314.
- [216] X. Q. Huang, R. J. Lee, Y. H. Qi, Y. J. Li, J. H. Lu, Q. F. Meng, L. S. Teng, J. Xie, *Oncotarget* **2017**, *8*, 96826.
- [217] C. Yang, T. Wu, Y. Qi, Z. Zhang, *Theranostics* **2018**, *8*, 464.
- [218] A. Dalmoro, S. Bochicchio, S. F. Nasibullin, P. Bertoncin, G. Lamberti, A. A. Barba, R. I. Moustafine, *Eur. J. Pharm. Sci.* **2018**, *121*, 16.
- [219] D. Zou, L. Yu, Q. Sun, Y. Hui, Y. Liu, G. Yang, D. Wibowo, C.-X. Zhao, *Colloids Surf., B* **2020**, *193*, 111108.
- [220] M. X. Wu, Y. W. Yang, *Adv. Mater.* **2017**, *29*, 1606134.
- [221] J. Cui, N. Gao, X. Yin, W. Zhang, Y. Liang, L. Tian, K. Zhou, S. Wang, G. Li, *Nanoscale* **2018**, *10*, 9192.
- [222] C. Hu, Y. Bai, M. Hou, Y. Wang, L. Wang, X. Cao, C.-W. Chan, H. Sun, W. Li, J. Ge, *Sci. Adv.* **2020**, *6*, eaax5785.
- [223] Y. L. Balachandran, X. Y. Li, X. Y. Jiang, *Nano Lett.* **2021**, *21*, 1335.
- [224] L. Capretto, W. Cheng, D. Carugo, O. L. Katsamenis, M. Hill, X. Zhang, *Nanotechnology* **2012**, *23*, 375602.
- [225] E. Blanco, H. Shen, M. Ferrari, *Nat. Biotechnol.* **2015**, *33*, 941.
- [226] T. Nakamura, H. Harashima, *Adv. Drug Delivery Rev.* **2020**, *167*, 78.
- [227] T. F. Abelha, T. W. Phillips, J. H. Bannock, A. M. Nightingale, C. A. Dreiss, E. Kemal, L. Urbano, J. C. deMello, M. Green, L. A. Dailey, *Nanoscale* **2017**, *9*, 2009.
- [228] R. R. Hood, E. L. Kendall, M. Junqueira, W. N. Vreeland, Z. Quezado, J. C. Finkel, D. L. Devoe, *PLoS One* **2014**, *9*, e92978.
- [229] B. Amoyav, O. Benny, *Appl. Nanosci.* **2018**, *8*, 905.
- [230] Y. Hui, X. Yi, D. Wibowo, G. Yang, A. P. J. Middelberg, H. Gao, C. X. Zhao, *Sci. Adv.* **2020**, *6*, eaaz4316.
- [231] Y. Hui, X. Yi, F. Hou, D. Wibowo, F. Zhang, D. Zhao, H. Gao, C. X. Zhao, *ACS Nano* **2019**, *13*, 7410.
- [232] Y. Hui, D. Wibowo, Y. Liu, R. Ran, H. F. Wang, A. Seth, A. P. J. Middelberg, C. X. Zhao, *ACS Nano* **2018**, *12*, 2846.
- [233] N. R. Visaveliya, C. W. Leishman, K. Ng, N. Yehya, N. Tobar, D. M. Eisele, J. M. Kohler, *Adv. Mater. Interfaces* **2017**, *4*, 1700929.
- [234] E. Dashtimoghdam, H. Mirzadeh, F. A. Taromi, B. Nystrom, *Polymer* **2013**, *54*, 4972.
- [235] Q. Feng, L. Zhang, C. Liu, X. Y. Li, G. Q. Hu, J. S. Sun, X. Y. Jiang, *Biomicrofluidics* **2015**, *9*, 052604.
- [236] T. Loftsson, M. E. Brewster, *J. Pharm. Pharmacol.* **2010**, *62*, 1607.
- [237] M. H. Stenzel, *Angew. Chem., Int. Ed.* **2021**, *60*, 2202.
- [238] Z. He, X. Wan, A. Schulz, H. Bludau, M. A. Dobrovolskaia, S. T. Stern, S. A. Montgomery, H. Yuan, Z. Li, D. Alakhova, *Bio-materials* **2016**, *101*, 296.
- [239] D. Reker, S. M. Blum, C. Steiger, K. E. Anger, J. M. Sommer, J. Fanikos, G. Traverso, *Sci. Transl. Med.* **2019**, *11*, eaau6753.
- [240] D. Reker, Y. Rybakova, A. R. Kirtane, R. Cao, J. W. Yang, N. Navamajiti, A. Gardner, R. M. Zhang, T. Esfandiary, J. L'Heureux, *Nat. Nanotechnol.* **2021**, *16*, 725.
- [241] M. M. Hasani-Sadrabadi, V. Karimkhani, F. S. Majedi, J. J. Van Dersarl, E. Dashtimoghdam, F. Afshar-Taromi, H. Mirzadeh, A. Bertsch, K. I. Jacob, P. Renaud, F. J. Stadler, I. Kim, *Adv. Mater.* **2014**, *26*, 3118.
- [242] A. Bains, Y. Cao, S. Kly, J. E. Wulff, M. G. Moffitt, *Mol. Pharmaceutics* **2017**, *14*, 2595.
- [243] A. Bains, M. G. Moffitt, *J. Colloid Interface Sci.* **2017**, *508*, 203.
- [244] D. F. Liu, H. B. Zhang, E. Makila, J. Fan, B. Herranz-Blanco, C. F. Wang, R. Rosa, A. J. Ribeiro, J. Salonen, J. Hirvonen, H. A. Santos, *Biomaterials* **2015**, *39*, 249.
- [245] L. J. C. Albuquerque, V. Sincari, A. Jager, R. Konefal, J. Panek, P. Cernoch, E. Pavlova, P. Stepanek, F. C. Giacomelli, E. Jager, *Langmuir* **2019**, *35*, 8363.
- [246] Q. Feng, J. P. Liu, X. Y. Li, Q. H. Chen, J. S. Sun, X. H. Shi, B. Q. Ding, H. J. Yu, Y. P. Li, X. Y. Jiang, *Small* **2017**, *13*, 1603109.
- [247] H. Zhang, G. Wang, H. Yang, *Expert Opin. Drug Delivery* **2011**, *8*, 171.
- [248] P. G. Tardi, N. Dos Santos, T. O. Harasym, S. A. Johnstone, N. Zisman, A. W. Tsang, D. G. Bermudes, L. D. Mayer, *Mol. Cancer Ther.* **2009**, *8*, 2266.
- [249] P. M. Valencia, E. M. Pridgen, B. Perea, S. Gadde, C. Sweeney, P. W. Kantoff, N. H. Bander, S. J. Lippard, R. Langer, R. Karnik, O. C. Farokhzad, *Nanomedicine* **2013**, *8*, 687.
- [250] M. M. Hasani-Sadrabadi, E. Dashtimoghdam, G. Bahlakeh, F. S. Majedi, H. Keshvari, J. J. Van Dersarl, A. Bertsch, A. Panahifar, P. Renaud, L. Tayebi, M. Mahmoudi, K. I. Jacob, *Nanomedicine* **2015**, *10*, 3431.
- [251] D. W. Pack, A. S. Hoffman, S. Pun, P. S. Stayton, *Nat. Rev. Drug Discovery* **2005**, *4*, 581.
- [252] S. C. De Smedt, J. Demeester, W. E. Hennink, *Pharm. Res.* **2000**, *17*, 113.
- [253] P. S. Kowalski, A. Rudra, L. Miao, D. G. Anderson, *Mol. Ther.* **2019**, *27*, 710.
- [254] C. Liu, Q. Feng, J. S. Sun, *Adv. Mater.* **2019**, *31*, 1804788.
- [255] T. Nakamura, M. Kawai, Y. Sato, M. Maeki, M. Tokeshi, H. Harashima, *Mol. Pharmaceutics* **2020**, *17*, 944.
- [256] S. H. Kim, J. H. Jeong, S. H. Lee, S. W. Kim, T. G. Park, *J. Controlled Release* **2008**, *129*, 107.
- [257] R. Krzysztos, B. Salem, D. J. Lee, G. Schwake, E. Wagner, J. O. Radler, *Nanoscale* **2017**, *9*, 7442.
- [258] Chemtrix Pfizer Showcase Industrial-scale Continuous Manufacturing!, <https://chemtrix.com/news/pfizer-showcase-industrial-scale-continuous-manufacturing> (accessed: January 2022).

- [259] Y. Liu, Y. Hui, R. Ran, G. Z. Yang, D. Wibowo, H. F. Wang, A. P. Middelberg, C. X. Zhao, *Adv. Healthcare Mater.* **2018**, *7*, 1800106.
- [260] H.-F. Wang, Y. Liu, G. Yang, C.-X. Zhao, *Mater. Today Sustainable* **2020**, *11*, 100055.
- [261] Z. W. Han, W. X. Lv, Y. K. Li, J. Q. Chang, W. Zhang, C. Liu, J. S. Sun, *ACS Appl. Bio. Mater.* **2020**, *3*, 2666.
- [262] X. R. Sun, G. W. Wang, H. Zhang, S. Q. Hu, X. Liu, J. B. Tang, Y. Q. Shen, *ACS Nano* **2018**, *12*, 6179.
- [263] M. Huo, J. Yuan, L. Tao, Y. Wei, *Polym. Chem.* **2014**, *5*, 1519.
- [264] L. E. Gerweck, S. Vijayappa, S. Kozin, *Mol. Cancer Ther.* **2006**, *5*, 1275.
- [265] M. Hibino, Y. Yamada, N. Fujishita, Y. Sato, M. Maeki, M. Tokeshi, H. Harashima, *J. Pharm. Sci.* **2019**, *108*, 2668.
- [266] C. Martins, F. Araujo, M. J. Gomes, C. Fernandes, R. Nunes, W. Li, H. A. Santos, F. Borges, B. Sarmiento, *Eur. J. Pharm. Biopharm.* **2019**, *138*, 111.
- [267] L. Capretto, S. Mazzitelli, E. Brognara, I. Lampronti, D. Carugo, M. Hill, X. L. Zhang, R. Gambari, C. Nastruzzi, *Int. J. Nanomed.* **2012**, *7*, 307.
- [268] S. Colombo, M. Beck-Broichsitter, J. P. Bøtker, M. Malmsten, J. Rantanen, A. Bohr, *Adv. Drug Delivery Rev.* **2018**, *128*, 115.
- [269] N. Ota, Y. Yalikun, T. Suzuki, S. W. Lee, Y. Hosokawa, K. Goda, Y. Tanaka, *R. Soc. Open Sci.* **2019**, *6*, 181776.
- [270] J. Macioszczyk, O. Rac-Rumijowska, P. Słobodzian, H. Teterycz, K. Malecha, *Micromachines* **2017**, *8*, 318.
- [271] F. Castro, S. Kuhn, K. Jensen, A. Ferreira, F. Rocha, A. Vicente, J. A. Teixeira, *Chem. Eng. J.* **2013**, *215*, 979.
- [272] J. Sun, Z. Shi, M. Li, S. Chen, M. Zhong, X. Liu, J. Sha, S. Jia, *J. Phys. D: Appl. Phys.* **2021**, *54*, 325004.
- [273] D. Chen, H. Du, *Microfluid. Nanofluid.* **2010**, *9*, 281.
- [274] H. Huang, W. Feng, Y. Chen, J. Shi, *Nano Today* **2020**, *35*, 100972.



Yun Liu is currently a postdoctoral research fellow in Australian Institute for Bioengineering and Nanotechnology (AIBN), the University of Queensland (UQ). She received her Ph.D. from AIBN, UQ, in 2020. She obtained her Master's degree in food studies from UQ in 2015, and her Bachelor's degree from Tianjin University in 2010. Her research focuses on the design, manufacture, and drug delivery applications of multifunctional high drug-loaded polymer and lipid nanoparticles as well as the development of the corresponding microfluidic platform technology.



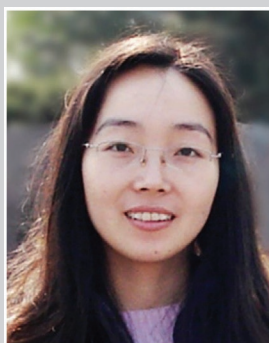
Guangze Yang is currently a postdoctoral research fellow in Australian Institute for Bioengineering and Nanotechnology (AIBN), the University of Queensland (UQ). He received his Ph.D. from AIBN, UQ, in 2020. He obtained his Master's degree in Engineering Science from UQ in 2014, and his Bachelor's degree from Tianjin University in 2012. His research focuses on the rational design and fabrication of functional peptides-, proteins-, and polymers- based nanomaterials for drug delivery, imaging, and mining applications.



Yue Hui is currently a postdoctoral fellow in School of Engineering at the Westlake University, China. He received his Ph.D. in Biomedical Engineering from Australian Institute for Bioengineering and Nanotechnology, the University of Queensland, in 2019, and his Bachelor's degree in Materials Science and Engineering from Xi'an Jiaotong University in 2014. His current research interests are rooted in the manufacturing of hydrogel electronics by 3D printing techniques. His Ph.D. work was focused on the effects of nanoparticles' mechanical properties on their cancer drug delivery performances.



Supun Akash Ranaweera is a Ph.D. student at the University of Queensland (UQ). His project focuses on developing a microfluidic organ chips for nanovaccine evaluation. During his Bachelor of Biotechnology (Honours, UQ), his research focused on developing a tumor-on-chip for evaluating drug transport and efficacy against tumor targets.



Chun-Xia Zhao is currently a professor at the School of Chemical Engineering and Advanced Materials, The University of Adelaide (UofA), and honorary professor at the Australian Institute for Bioengineering and Nanotechnology (AIBN), the University of Queensland (UQ). Before she joined UofA in mid-2021, she was a group leader, UQ amplify fellow, ARC future fellow at AIBN, UQ. She leads a research team focusing on the development of bioinspired micro/nanostructures for drug delivery and bioinspired devices (e.g., organs-on-a-chip models) for drug screening and evaluation.